

Analysis and Development of Stochastic Multigrid Methods in Lattice Field Theory

Martin Grabenstein*

II. Institut für Theoretische Physik, Universität Hamburg,
Luruper Chaussee 149, 22761 Hamburg, Germany,
internet i02gra@dsyibm.desy.de

preprint DESY 94-007, hep-lat/9401024

Abstract

We study the relation between the dynamical critical behavior and the kinematics of stochastic multigrid algorithms. The scale dependence of acceptance rates for nonlocal Metropolis updates is analyzed with the help of an approximation formula. A quantitative study of the kinematics of multigrid algorithms in several interacting models is performed. We find that for a critical model with Hamiltonian $\mathcal{H}(\phi)$ absence of critical slowing down can only be expected if the expansion of $\langle \mathcal{H}(\phi + \psi) \rangle$ in terms of the shift ψ contains no relevant term (mass term). The predictions of this rule are verified in a multigrid Monte Carlo simulation of the Sine Gordon model in two dimensions.

Our analysis can serve as a guideline for the development of new algorithms: We propose a new multigrid method for nonabelian lattice gauge theory, the time slice blocking. For $SU(2)$ gauge fields in two dimensions, critical slowing down is almost completely eliminated by this method, in accordance with the theoretical prediction. The generalization of the time slice blocking to $SU(2)$ in four dimensions is investigated analytically and by numerical simulations. Compared to two dimensions, the local disorder in the four dimensional gauge field leads to kinematical problems.

*supported by Deutsche Forschungsgemeinschaft

Contents

1	Introduction	1
2	Multigrid Monte Carlo algorithms	5
2.1	Local Metropolis updating	5
2.2	Nonlocal multigrid updating	5
2.3	The average Metropolis acceptance rate $\Omega(s)$	7
2.4	Unigrid versus recursive multigrid	8
2.5	Multigrid cycles	8
3	An approximation formula for $\Omega(s)$	10
4	Coarse-to-fine interpolation	11
4.1	Optimal interpolation kernels	11
4.2	Truncation of the support of the optimal kernel	11
4.2.1	Kernels with support on a block and its nearest neighbors	11
4.2.2	Kernels with support on a single block	12
4.3	Other kernels with support on the block	12
4.3.1	Piecewise constant interpolation	12
4.3.2	Piecewise linear interpolation	12
4.3.3	Ground state projection	13
4.4	Results for $\alpha = (\psi, -\Delta\psi)$ in two and four dimensions	13
5	Acceptance rates in free field theory	15
5.1	Massless free field theory	15
5.2	Scale dependence of the Metropolis step size	15
5.3	Intuitive random walk picture of the W-cycle	17
5.4	Massive free field theory	17
5.5	Behavior of a term $\sum_x \psi_x^4$	18
5.6	Degree of relevance	19
6	Acceptance rates for interacting models	20
6.1	The two dimensional Sine Gordon model	20
6.2	The two dimensional XY model	22
6.3	The ϕ^4 theory in d dimensions	23
6.4	The two dimensional $O(N)$ nonlinear σ -model	26
6.5	The two dimensional CP^{N-1} model	27
6.6	Summary	29
7	Multigrid Simulation of the Sine Gordon model	31
7.1	Motivation	31

7.2	The multigrid algorithm	32
7.3	Simulation and results	33
7.4	Summary	35
8	Multigrid algorithms for lattice gauge fields in two dimensions	38
8.1	Abelian gauge fields: $U(1)$ in two dimensions	38
8.1.1	The algorithm of Laursen, Smit and Vink	38
8.1.2	Comments and possible modifications	40
8.2	Nonabelian gauge fields: $SU(2)$ in two dimensions	41
8.2.1	The nonabelian character of the gauge field	42
8.2.2	Gauge covariant time slice blocking algorithm	43
8.2.3	Acceptance analysis of the proposal	44
8.3	Summary	45
9	Multigrid Monte Carlo simulation of $SU(2)$ lattice gauge fields in two dimensions	46
9.1	Implementation of the time slice blocking	46
9.1.1	Smooth nonlocal heat bath updates in $U(1)$ subgroups	46
9.1.2	Sequence of updates	47
9.1.3	Axial gauge	47
9.2	Simulation and results	47
9.2.1	Observables	47
9.2.2	Run parameters and results	48
9.3	Summary	49
10	Multigrid methods for lattice gauge fields in four dimensions	51
10.1	The abelian case	51
10.2	The nonabelian case: gauge group $SU(2)$	52
10.2.1	Covariant time slice blocking for $SU(2)$ in four dimensions	52
10.2.2	Acceptance analysis for nonlocal $SU(2)$ -updates	54
10.2.3	Monte Carlo study of m_D	56
10.2.4	Digression: Monte Carlo study of m_D in two dimensions	58
10.2.5	Comparison of volume and surface effects in four dimensions	60
10.2.6	Maximally abelian gauge	62
10.3	Summary	63
11	Multigrid Monte Carlo simulation of $SU(2)$ lattice gauge fields in four dimensions	64
11.1	Implementation of the time slice blocking	64
11.1.1	Organization of a basic time slice blocking step	64
11.1.2	Sequence of basic time slice blocking steps	66

11.2 Simulation and Results	67
11.2.1 Observables	67
11.2.2 Run parameters and static results	67
11.2.3 Autocorrelation times	68
11.3 Summary	69
12 Summary and Outlook	73
Acknowledgements	75
A Details of the acceptance analysis for gauge theories	76
A.1 Abelian gauge fields	76
A.2 Nonabelian gauge fields	77
B Exact results for $SU(2)$ lattice gauge theory in two dimensions	79
C Gauge conditions on the lattice	80
C.1 The Landau gauge	80
C.2 The Coulomb gauge	81
C.3 An alternative formulation of the Landau gauge condition	81
References	83

1 Introduction

Monte Carlo simulations have become an important tool for the study of critical phenomena in statistical mechanics [1] and for nonperturbative calculations in Euclidian lattice field theory close to the continuum limit [2].

However, the method has limitations. In the vicinity of a critical point the phenomenon of critical slowing down (CSD) is a serious problem: For conventional local algorithms the autocorrelation time - that is, roughly speaking, the time needed to generate a new, “statistically independent” configuration on a computer - grows rapidly as the system approaches criticality. More precisely, the autocorrelation time τ behaves like $\tau \sim \xi^z$, where ξ denotes the spatial correlation length, and z is the dynamical critical exponent. For conventional local algorithms, $z \approx 2$. Thus, when the critical point is approached, there is a dramatic increase of computer time needed to calculate observables to a given accuracy. It is therefore important to find Monte Carlo algorithms that have reduced CSD.

Accelerated algorithms that are still local, such as overrelaxation or the optimized hybrid Monte Carlo algorithm, can sometimes reduce the dynamical critical exponent to $z \approx 1$ [3, 4].

For the complete elimination of CSD in the sense of $z \approx 0$, nonlocal update algorithms are needed. Heuristic arguments based on the picture that in simulations with local algorithms “information” propagates through the lattice in the form of a random walk lead to a value of $z = 2$. Therefore it is natural to use nonlocal update schemes that perform changes of the configuration not only on the scale of the lattice spacing but create fluctuations on all length scales, in analogy to the physical fluctuations at a critical point.

Stochastic cluster algorithms are very successful in reducing CSD in spin models: The first cluster algorithm was developed by Swendsen and Wang for discrete spin variables in Ising and Potts models [5]. This method could be successfully extended to continuous spin variables in $O(N)$ nonlinear σ -models by Wolff [6] and Hasenbusch [7]. However, the generalization to $SU(N) \times SU(N)$ principal chiral models with $N > 2$, which are models with the same type of variables as QCD, seems to be difficult [8]. There are arguments that cluster algorithms will not be efficient if the spin variables take values in manifolds other than spheres, products of spheres or the quotient of such a space by a discrete group [9].

An alternative method to overcome CSD in the simulation of models with continuous variables is multigrid Monte Carlo: Multigrid methods are well established tools for the solution of discretized partial differential equations [10, 11]. Their generalization to Monte Carlo simulations was proposed by Parisi [12]. Early ideas for nonlocal updating schemes were formulated by H. Meyer-Ortmanns [13]. Goodman and Sokal generalized deterministic multigrid methods to multigrid Monte Carlo in the ϕ^4 theory in two dimensions [14]. Mack presented a stochastic multigrid approach that was inspired by constructive quantum field theory and renormalization group considerations [15].

In the present thesis, every algorithm that performs stochastic updates of predesigned shape on a hierarchy of length scales is called multigrid Monte Carlo algorithm.

There are examples, e.g. the $SU(3) \times SU(3)$ principal chiral model, where no fast cluster algorithms have been found whereas multigrid Monte Carlo algorithms could reduce CSD considerably [8, 16].

Presently, the only generally applicable method to study the dynamical critical behavior of Monte Carlo algorithms for interacting models is numerical experiment. For some models experiments show that the dynamical critical exponent z can be substantially reduced by a

multigrid algorithm [16, 17, 18, 19]. For other models, still $z = 2$ is found [14, 20]. Theoretical insight into the critical dynamics of multigrid Monte Carlo algorithms is therefore desirable.

We present a method that can help to judge which algorithm will have a chance to overcome CSD in the simulation of a given model *before* performing the simulation: We study the kinematics of multigrid Monte Carlo algorithms. By kinematics we mean the study of the scale (block size) dependence of the Metropolis acceptance rates for nonlocal update proposals. We do not address the more difficult problem of analytically calculating the dynamical critical behavior from the stochastic evolution of the system. However, we are able to find a heuristic relation between the kinematical and the critical dynamical behavior of multigrid Monte Carlo methods. This relation is based on the fact that sufficiently high acceptance rates are necessary to overcome CSD.

We derive an approximation formula for the block size dependence of acceptance rates for nonlocal Metropolis updates. The influence of the coarse-to-fine interpolation kernel (shape function) on the kinematics in free field theory, where the formula is exact, is investigated in detail.

The formula is then applied to several interacting models and turns out to be a very good approximation. By comparison with free field theory, where CSD is eliminated by a multigrid algorithm, we can formulate a necessary criterion for a given multigrid algorithm to eliminate CSD: For a critical model with a fundamental Hamiltonian $\mathcal{H}(\phi)$ absence of CSD can only be expected if the expansion of $\langle \mathcal{H}(\phi + \psi) \rangle$ in terms of the shift ψ contains no relevant term (mass term).

Heuristically, the physical content of this criterion can be summarized in a Leitmotiv: A piecewise constant update of a nonlocal domain should only have energy costs proportional to the surface of the domain, not energy costs proportional to the volume of the domain.

This seems to be a feature that multigrid algorithms share with cluster algorithms [9].

As a first test of the predictive power of the kinematical analysis we perform a multigrid Monte Carlo simulation of the Sine Gordon model in two dimensions. There, the criterion tells that we have to expect CSD caused by too small acceptance rates of the updates on large scales. This prediction is confirmed by the numerical experiments. In addition it is studied whether one can compensate for too small amplitudes of the updates on large blocks by accumulating many of these updates randomly.

After the introduction of the kinematical analysis of multigrid Monte Carlo algorithms in the context of spin models, where the multigrid methods have already been developed, we show that our method can also be helpful in the design of new multigrid procedures.

One of the challenges in the development of fast Monte Carlo algorithms is pure lattice gauge theory in four dimensions. In particular the nonabelian gauge groups $SU(2)$ and $SU(3)$ are important for nonperturbative calculations in the standard model of elementary particles.

For the dynamical critical behavior of the local heat bath algorithm in $SU(3)$ only very crude estimates are available up to now [21], consistent with $z \approx 2$. The present state-of-the-art algorithm for nonabelian gauge fields in four dimensions is overrelaxation [22]. For this algorithm, first estimates for z in $SU(2)$ lattice gauge theory gave $z = 1.0(1)$ in physically small volumes [23]. Effort was also spent in developing nonlocal algorithms for gauge theories. A fast cluster algorithm was found for $3 + 1$ -dimensional $SU(2)$ gauge theory on a $L^3 \times T$ lattice at finite temperature, but only in the special case $T = 1$ [24]. A cluster algorithm for $U(1)$ gauge theory in two dimensions is based on the reduction of the gauge theory to a one dimensional

XY model [25]. However, apart from these special cases, no efficient cluster algorithm for continuous gauge groups has been found up to now.

Therefore possible developments of stochastic multigrid methods for pure gauge fields are of particular interest. Multigrid algorithms for $U(1)$ gauge models were introduced and studied in two and four dimensions [18, 26]. A different but related nonlocal updating scheme for abelian lattice gauge theory is the multiscale method [27].

We propose a new multigrid algorithm for nonabelian gauge theory and analyze its kinematics.

To gain experience, we first study the case of gauge group $SU(2)$ in two dimensions. We introduce a multigrid method for nonabelian gauge theory that treats different time slices independently: the time slice blocking algorithm. The theoretical analysis predicts that CSD can be eliminated by the time slice blocking. By numerical experiments on systems with lattice sizes up to 256^2 we check whether this is indeed the case.

In a second step we generalize the time slice blocking to $SU(2)$ in four dimensions. Compared to the two dimensional case we have to face additional difficulties that are caused by the local disorder of the gauge fields. Our approximation formula turns out to be very reliable also in this case and allows for a prediction of acceptance rates for a large class of nonlocal updates. We attempt to estimate the kinematical behavior of the proposed algorithm in the weak coupling limit and study whether a reduction of CSD can be expected. In numerical simulations, the time slice blocking algorithm in $SU(2)$ in four dimensions is compared with a local heat bath algorithm.

When Parisi proposed the use of multigrid methods for Monte Carlo simulations in 1983, he stated [12]: “On the contrary [*to quadratic actions*] the application of the multigrid method to the gauge field sector seems to be particularly painful but it may be rewarding.”

We attempt to describe where we stand ten years after Parisi’s speculation.

This thesis is organized as follows: In the first part (sections 2-7) the kinematical analysis of multigrid algorithms is introduced and discussed. In the second part (sections 8-11) the method of the kinematical analysis is applied to the development of new multigrid algorithms for nonabelian gauge fields.

In section 2 we introduce multigrid Monte Carlo algorithms. Section 3 contains the derivation of our approximation formula for acceptance rates. Several coarse-to-fine-interpolation kernels are discussed in section 4. In section 5 the acceptance rates in free field theory are examined in detail. The main idea of the thesis is introduced and discussed in section 6: The kinematical analysis for the Sine Gordon, XY , ϕ^4 , $O(N)$ and CP^{N-1} models is presented. In section 7 the prediction of this analysis for the Sine Gordon model is verified by a multigrid Monte Carlo simulation.

Section 8 starts with the discussion of abelian gauge fields in two dimensions. There are two directions of increasing the difficulty of the problem: from abelian gauge group to nonabelian gauge group and from two dimensions to four dimensions. Most of the concepts that are needed for the treatment of nonabelian gauge fields are introduced in the context of $SU(2)$ lattice gauge theory in two dimensions. A new multigrid procedure, the time slice blocking, is introduced. In section 9, $SU(2)$ lattice gauge theory in two dimensions is simulated with the time slice blocking.

The new procedure is generalized from $SU(2)$ in two dimensions to $SU(2)$ in four dimensions in section 10. Section 9 contains the results of a multigrid Monte Carlo simulation of $SU(2)$

lattice gauge theory in four dimensions. A summary is given in section 12.

Parts of this thesis have been published before in refs. [28, 29, 30, 31, 32].

2 Multigrid Monte Carlo algorithms

We consider lattice models with partition functions

$$Z = \int \prod_{x \in \Lambda_0} d\phi_x \exp(-\mathcal{H}(\phi)) \quad (2.1)$$

on hypercubic d -dimensional lattices Λ_0 with periodic boundary conditions. The lattice spacing is set to one. We use dimensionless spin variables ϕ_x . An example is single-component ϕ^4 theory, defined by the Hamiltonian

$$\mathcal{H}(\phi) = \frac{1}{2}(\phi, -\Delta\phi) + \frac{m_o^2}{2} \sum_x \phi_x^2 + \frac{\lambda_o}{4!} \sum_x \phi_x^4, \quad (2.2)$$

where

$$(\phi, -\Delta\phi) = \sum_{\langle x,y \rangle} (\phi_x - \phi_y)^2. \quad (2.3)$$

The sum in eq. (2.3) is over all nearest neighbor pairs in the lattice¹.

2.1 Local Metropolis updating

A standard algorithm to perform Monte Carlo simulations in a model of the type defined above is the local Metropolis algorithm: One visits in a regular or random order the sites of the lattice and performs the following steps: At site x_o , one proposes a shift

$$\phi_{x_o} \rightarrow \phi'_{x_o} = \phi_{x_o} + s. \quad (2.4)$$

The configuration $\{\phi_x\}$ remains unchanged for $x \neq x_o$. s is a random number selected according to an a priori distribution $\rho(s)$ which is symmetric with respect to $s \rightarrow -s$. E.g., one selects s with uniform probability from an interval $[-\varepsilon, \varepsilon]$. Then one computes the change of the Hamiltonian

$$\Delta\mathcal{H} = \mathcal{H}(\phi') - \mathcal{H}(\phi). \quad (2.5)$$

Finally the proposed shift is accepted with probability $\min[1, \exp(-\Delta\mathcal{H})]$. Then one proceeds to the next site.

The local Metropolis algorithm suffers from CSD when the correlation length in the system becomes large: long wavelength fluctuations cannot efficiently be generated by a sequence of local operations. It is therefore natural to study nonlocal generalizations of the update procedure defined above.

2.2 Nonlocal multigrid updating

Consider the fundamental lattice Λ_0 as divided in hypercubic blocks of size l^d , where l denotes the coarsening factor. Typical coarsening factors are $l = 2$ or 3 . This defines a block lattice Λ_1 . By iterating this procedure one obtains a whole hierarchy of block lattices $\Lambda_0, \Lambda_1, \dots, \Lambda_K$ with increasing lattice spacing (see figure 1). This hierarchy of lattices is called multigrid.

¹The definitions for lattice gauge theory will be introduced in section 8

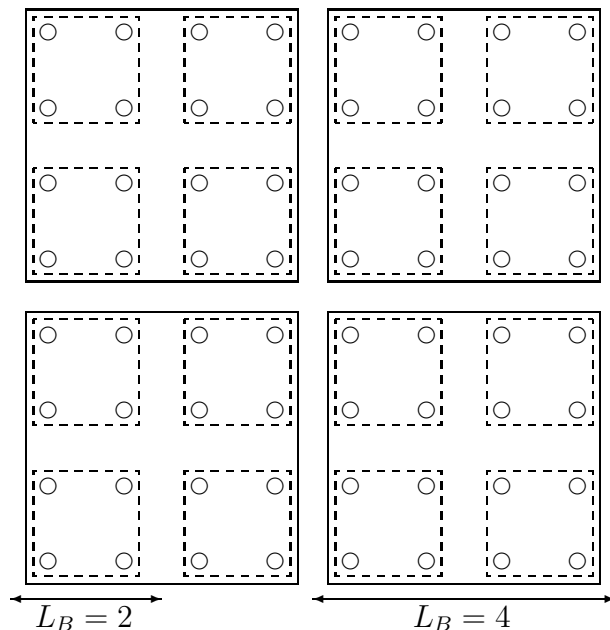


Figure 1: Division of the finest lattice in block lattices of $L_B \times L_B$ -blocks in two dimensions

Let us denote block lattice points in Λ_k by x' . Block spins $\Phi_{x'}$ are defined on block lattices Λ_k . They are averages of the fundamental field ϕ_x over blocks of side length $L_B = l^k$:

$$\Phi_{x'} = L_B^{(d-2)/2} L_B^{-d} \sum_{x \in x'} \phi_x. \quad (2.6)$$

The sum is over all points x in the block x' . The L_B -dependent factor in front of the average comes from the fact that the corresponding dimensionful block spins are measured in units of the block lattice spacing: A scalar field $\phi(x)$ in d dimensions has canonical dimension $(2-d)/2$. Thus $\phi(x) = a^{(2-d)/2} \phi_x$, where a denotes the fundamental lattice spacing. Now measure the dimensionful block spin $\Phi(x')$ in units of the block lattice spacing a' : $\Phi(x') = a'^{(2-d)/2} \Phi_{x'}$, with $a' = aL_B$. If we average in a natural way $\Phi(x') = L_B^{-d} \sum_{x \in x'} \phi(x)$ and return to dimensionless variables, we obtain eq. (2.6).

A nonlocal change of the configuration ϕ consists of a shift

$$\phi_x \rightarrow \phi_x + s \psi_x. \quad (2.7)$$

s is a real parameter, and the ‘‘coarse-to-fine interpolation kernel’’ (or shape function) ψ_x determines the shape of the nonlocal change. ψ is normalized according to

$$L_B^{-d} \sum_{x \in x'} \psi_x = L_B^{(2-d)/2} \delta_{x', x'_o}. \quad (2.8)$$

Note that by the nonlocal change (2.7), the block spin is moved as $\Phi_{x'} \rightarrow \Phi_{x'} + s$ for $x' = x'_o$, and remains unchanged on the other blocks. The simplest choice of the kernel ψ that obeys the constraint (2.8) is a piecewise constant kernel: $\psi_x = L_B^{(2-d)/2}$, if $x \in x'_o$, and 0 otherwise. Other kernels are smooth and thus avoid large energy costs from the block boundaries. A systematic study of different kernels will be given in section 4. Two one dimensional examples for ψ are given in figure 2.

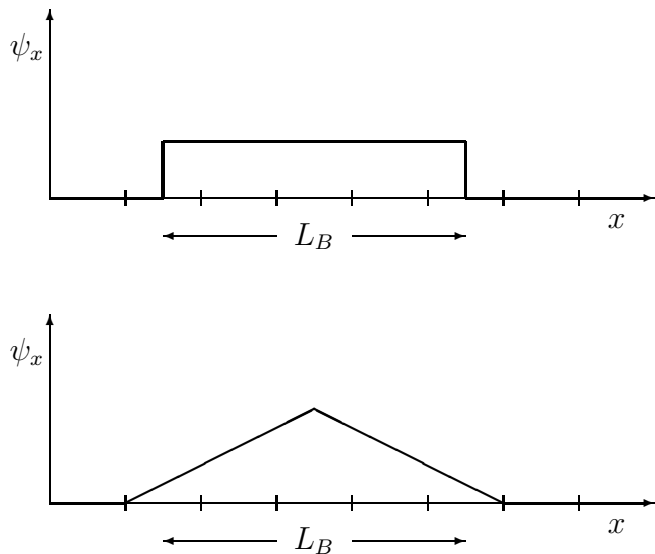


Figure 2: *Coarse-to-fine interpolation kernels ψ in one dimension: Top: piecewise constant kernel, bottom: piecewise linear kernel*

2.3 The average Metropolis acceptance rate $\Omega(s)$

The s -dependent Metropolis acceptance rate for such proposals is given by

$$\Omega(s) = \langle \min[1, \exp(-\Delta\mathcal{H})] \rangle . \quad (2.9)$$

Here, $\langle (\cdot) \rangle$ denotes the expectation value in the system defined by eq. (2.1). Furthermore,

$$\Delta\mathcal{H} = \mathcal{H}(\phi + s\psi) - \mathcal{H}(\phi) . \quad (2.10)$$

$\Omega(s)$ can be interpreted as the acceptance rate for shifting block spins by an amount of s , averaged over a sequence of configurations generated by a Monte Carlo simulation. As a static observable, $\Omega(s)$ is independent of the algorithm that we use to compute it. $\Omega(s)$ is a useful quantity when one wants to know whether updates with increasing nonlocality (i.e. increasing block size L_B) can be performed in an efficient way. Of course, different choices of the kernel ψ result in different acceptance rates.

In actual Monte Carlo simulations, s is not fixed. In the same way as in the local Metropolis algorithm, s is a random number distributed according to some a priori probability density. If we choose s to be uniformly distributed on the interval $[-\varepsilon, \varepsilon]$, the integrated acceptance rate P_{acc} (as customarily measured in Monte Carlo simulations) is obtained by averaging $\Omega(s)$ as follows:

$$P_{acc}(\varepsilon) = \frac{1}{2\varepsilon} \int_{-\varepsilon}^{\varepsilon} ds \Omega(s) . \quad (2.11)$$

It turns out to be a good rule to adjust the maximum Metropolis step size ε such that $P_{acc}(\varepsilon) \approx 0.5$.

2.4 Unigrid versus recursive multigrid

We consider every algorithm that updates stochastic variables on a hierarchy of length scales as multigrid Monte Carlo algorithm. However, there are two different classes of multigrid algorithms: multigrid algorithms in a unigrid implementation and “recursive” multigrid algorithms.

In the unigrid formulation one considers nonlocal updates of the form (2.7). Updates on the various layers of the multigrid are formulated on the level of the finest lattice Λ_0 . There is no explicit reference to block spin variables Φ defined on coarser layers Λ_k with $k > 0$. In addition, unigrid also refers to a computational scheme: Nonlocal updates are performed directly in terms of the variables on the finest grid Λ_0 in practical simulations. An example for a unigrid implementation is explained for two dimensional nonabelian gauge theory in section 9.

In contrast, the recursive multigrid formulation consists of recursively calculating conditional Hamiltonians that depend on the block spin variables Φ on coarser layers Λ_k . This formulation is possible if the conditional Hamiltonians are of the same type or similar to the Hamiltonian on the finest lattice. Then, the conditional probabilities used for the updating on the k -th layer can be computed without always going back to the finest level Λ_0 . Therefore, an recursive multigrid implementation reduces the computational work on the coarser layers (see the work estimates below). At least in free field theory, a recursive multigrid implementation with smooth interpolation is possible using 9-point prolongation kernels (a special case of piecewise linear kernels as shown in figure 2) in two dimensions and generalizations thereof in higher dimensions [33, 34]. Generally, a recursive multigrid implementation for interacting models is only feasible in special cases with piecewise constant kernels. Examples for such implementations are given for the Sine Gordon model in section 7 and in the four dimensional nonabelian gauge theory in section 11 below.

An algorithm formulated in the recursive multigrid style can always be translated to the unigrid language (that is the way we are going to use the unigrid formulation for the analysis of multigrid algorithms). The reverse is not true, since not all nonlocal changes of the field on the finest lattice can be interpreted as updates of a single block spin variable of a recursive multigrid. As an example, one can use stochastically overlapping blocks in the unigrid style by translating the fields by a randomly chosen distance [16].

If we formulate our kinematical analysis in the unigrid language we nevertheless can include all algorithms formulated in the recursive multigrid style.

2.5 Multigrid cycles

The sequence of sweeps through the different layers Λ_k of the multigrid is organized in a periodic scheme called cycle [11]. The most important cycles are illustrated in figure 3. The simplest scheme is the V-cycle: The sequence of layers visited in turn is $\Lambda_0, \Lambda_1, \dots, \Lambda_K, \Lambda_{K-1}, \dots, \Lambda_1$. More general cycles are characterized by the cycle control parameter γ . The rule is that from an intermediate layer Λ_k one proceeds γ times to the next coarser layer Λ_{k+1} before going back to the next finer layer Λ_{k-1} . A cycle control parameter $\gamma > 1$ samples coarser layers more often than finer layers. With $\gamma = 1$ we obtain the V-cycle. $\gamma = 2$ yields the W-cycle that is frequently used with piecewise constant kernels.

The computational work estimates for the different cycles are as follows [34]: The work for a recursive multigrid cycle is $\sim L^d$ if $\gamma < l^d$, where L denotes the lattice size and l is the coarsening factor. The work for a unigrid cycle is $\sim L^d \log L$ if $\gamma = 1$, and $\sim L^{d+\log_l \gamma}$ if $\gamma > 1$.

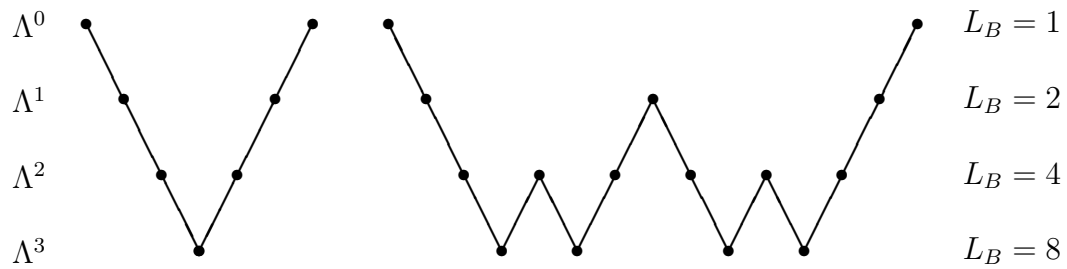


Figure 3: *V-cycle* ($\gamma = 1$) and *W-cycle* ($\gamma = 2$)

If one wants the computational work in the unigrid style not to exceed (up to a logarithm) an amount proportional to the volume L^d of the lattice, one is restricted to use a V-cycle. Simulations with $\gamma > 1$ (e.g. a W-cycle) can only be performed in the recursive multigrid style.

3 An approximation formula for $\Omega(s)$

In this section we shall derive an approximate formula for the quantity $\Omega(s)$ defined in (2.9). We can write $\Omega(s)$ as

$$\Omega(s) = \int du \min(1, e^{-u}) \int \frac{dp}{2\pi} e^{-ipu} \langle e^{ip\Delta\mathcal{H}} \rangle . \quad (3.1)$$

Let us assume that the probability distribution of $\Delta\mathcal{H}$ is approximately Gaussian. We parameterize this distribution as follows:

$$d\text{prob}(\Delta\mathcal{H}) \propto d\Delta\mathcal{H} \exp\left(-\frac{1}{4h_2}(\Delta\mathcal{H} - h_1)^2\right) , \quad (3.2)$$

with $h_1 = \langle \Delta\mathcal{H} \rangle$ and $h_2 = \frac{1}{2}(\langle \Delta\mathcal{H}^2 \rangle - \langle \Delta\mathcal{H} \rangle^2)$. Then

$$\langle \exp(ip\Delta\mathcal{H}) \rangle \approx \exp(ih_1p - h_2p^2) . \quad (3.3)$$

We now show that from the assumption that the probability distribution of $\Delta\mathcal{H}$ is Gaussian we can derive that $h_1 = h_2$. The starting point is the identity

$$1 = \frac{1}{Z} \int \prod_{x \in \Lambda_0} d\phi_x \exp(-\mathcal{H}(\phi)) . \quad (3.4)$$

If we use the translational invariance of the measure $\prod_{x \in \Lambda_0} d\phi_x = \prod_{x \in \Lambda_0} d(\phi_x + s\psi_x)$ we get

$$1 = \frac{1}{Z} \int \prod_{x \in \Lambda_0} d\phi_x \exp(-\mathcal{H}(\phi + s\psi)) = \frac{1}{Z} \int \prod_{x \in \Lambda_0} d\phi_x \exp(-\mathcal{H}(\phi + s\psi) + \mathcal{H}(\phi) - \mathcal{H}(\phi)) . \quad (3.5)$$

With the definition $\Delta\mathcal{H} = \mathcal{H}(\phi + s\psi) - \mathcal{H}(\phi)$ we obtain

$$1 = \frac{1}{Z} \int \prod_{x \in \Lambda_0} d\phi_x \exp(-\Delta\mathcal{H}) \exp(-\mathcal{H}(\phi)) = \langle \exp(-\Delta\mathcal{H}) \rangle . \quad (3.6)$$

This identity is independent of the form of the Hamiltonian. If we now set $p = i$ in eq. (3.3) and compare this with eq. (3.6), we are led to $h_1 = h_2$. Therefore eq. (3.3) reduces to

$$\langle \exp(ip\Delta\mathcal{H}) \rangle \approx \exp[(ip - p^2)h_1] , \quad (3.7)$$

and the integrations in eq. (3.1) can be performed exactly since there are only Gaussian integrals involved. The result is

$$\Omega(s) \approx \text{erfc}\left(\frac{1}{2}\sqrt{h_1}\right) . \quad (3.8)$$

with $\text{erfc}(x) = 2/\sqrt{\pi} \int_x^\infty dt \exp(-t^2)$. (For an analogous result in the context of hybrid Monte Carlo see [35].)

For free massless field theory with Hamiltonian $\mathcal{H}(\phi) = \frac{1}{2}(\phi, -\Delta\phi)$, we get $h_1 = \frac{1}{2}\alpha s^2$ with $\alpha = (\psi, -\Delta\psi)$, and our approximation formula becomes *exact*:

$$\Omega(s) = \text{erfc}\left(\sqrt{\frac{\alpha}{8}}|s|\right) . \quad (3.9)$$

Eq. (3.9) can be checked directly by using $\langle \exp(ip\Delta\mathcal{H}) \rangle = \exp[(ip - p^2)h_1]$ in eq. (3.1). This relation is exact in free field theory.

4 Coarse-to-fine interpolation

In this section we shall discuss several choices of the coarse-to-fine interpolation kernels. In order to have a “fair” comparison, all kernels ψ will be normalized according to eq. (2.8).

4.1 Optimal interpolation kernels

In free massless field theory, the quantity $\alpha = (\psi, -\Delta\psi)$ characterizes the decrease of the acceptance rate $\Omega(s)$ as given in (3.9) with increasing shift s . Therefore it is natural to minimize α in order to maximize $\Omega(s)$ for fixed s .

The optimal kernel ψ^{exact} from the point of view of acceptance rates can be defined as follows: minimize the quadratic form

$$\alpha = (\psi, -\Delta\psi) \quad (4.1)$$

under the constraints that the average of ψ over the “central block” x'_o is given by $L_B^{(2-d)/2}$, and its average over blocks $x' \neq x'_o$ vanishes:

$$L_B^{-d} \sum_{x \in x'} \psi_x = L_B^{(2-d)/2} \delta_{x', x'_o} \text{ for all } x' \in \Lambda_k \text{ .} \quad (4.2)$$

This variational problem can be solved with the help of Fourier methods. The result is

$$\psi_x^{exact} = L_B^{(2+d)/2} \mathcal{A}_{x, x'_o} \text{ ,} \quad (4.3)$$

where \mathcal{A}_{x, x'_o} denotes the Gawędzki-Kupiainen kernel (see, e.g. [15]). The use of this kernel leads to a complete decoupling of the different layers of the multigrid. This way of interpolating from a coarser block lattice Λ_k to the fine lattice Λ_0 is well known in rigorous renormalization group theory [36]. It is interesting that considerations about optimizing acceptance rates in a stochastic multigrid procedure lead to the same choice of the interpolation kernel.

Because ψ^{exact} is nonvanishing on the whole lattice, it is not convenient for numerical purposes. For an attempt to change the block spin $\Phi_{x'_o}$ on block x'_o one has to calculate contributions to the change of the Hamiltonian from all lattice points. Therefore the computational work for a single update is proportional to the volume.

4.2 Truncation of the support of the optimal kernel

4.2.1 Kernels with support on a block and its nearest neighbors

We define a “truncated kernel” ψ^{trunc} by restricting the support of ψ on the block x'_o and its nearest neighbor blocks y'_o

$$\psi_x^{trunc} = 0 \text{ if } x \notin x'_o \text{ or } x \notin y'_o \text{ , where } y'_o \text{ n.n. } x'_o \text{ .} \quad (4.4)$$

In other words, the Laplacian in eq. (4.1) is replaced by a Laplacian Δ_D with Dirichlet boundary conditions on the boundary of the support of ψ . We again minimize $\alpha = (\psi, -\Delta_D\psi)$ under the $2d + 1$ constraints that the average of ψ over the blocks x'_o and its nearest neighbor blocks is given. This minimization can be performed numerically by a relaxation procedure. In order to maintain the normalization condition, one always updates simultaneously two spins residing in the same block, keeping their sum fixed. The ψ^{trunc} -kernels were used in a multigrid simulation of the ϕ^4 model in four dimensions [37].

4.2.2 Kernels with support on a single block

From a practical point of view, it is convenient to use kernels that have support on a single block x'_o , i.e.

$$\psi_x = 0 \text{ if } x \notin x'_o. \quad (4.5)$$

We define a kernel ψ^{min} with this property by minimizing $\alpha = (\psi, -\Delta_{D,x'_o}\psi)$ under the constraint that the average of ψ over the block x'_o is given. The Laplacian with Dirichlet boundary conditions on the boundary of x'_o is defined as follows:

$$(\Delta_{D,x'_o}\phi)_x = \left[-2d\phi_x + \sum_{\substack{y \text{ n.n. } x \\ y \in x'_o}} \phi_y \right] \text{ for } x \in x'_o. \quad (4.6)$$

ψ^{min} can be calculated using an orthonormal set of eigenfunctions of Δ_{D,x'_o} .

4.3 Other kernels with support on the block

We shall now discuss other kernels with support on the block that are frequently used in the literature.

4.3.1 Piecewise constant interpolation

Piecewise constant interpolation kernels are defined by

$$\psi_x^{const} = \begin{cases} L_B^{(2-d)/2} & \text{for } x \in x'_o \\ 0 & \text{for } x \notin x'_o. \end{cases} \quad (4.7)$$

This kernel has the advantage that for many models the conditional Hamiltonians used for updating on coarse lattices are of the same type or similar to the Hamiltonian on the finest lattice. This means that the conditional probabilities used for the updating on the k -th layer can be computed without always going back to the finest level Λ_o . Therefore, an recursive multigrid implementation with cycle control parameters $\gamma > 1$, e.g. a W-cycle, can be used.

Piecewise constant kernels in a recursive multigrid implementation with a W-cycle will be used in the Sine Gordon model in section 7 and in the four dimensional nonabelian gauge theory in section 11.

4.3.2 Piecewise linear interpolation

We consider the block

$$x'_o = \{x \mid x^\mu \in \{1, 2, 3, \dots, L_B\}, \mu = 1, \dots, d\}. \quad (4.8)$$

The kernels for other blocks are simply obtained by translation. For L_B even, ψ^{linear} is given by

$$\psi_x^{linear} = \mathcal{N} \prod_{\mu=1}^d \left\{ \frac{L_B + 1}{2} - \left| x^\mu - \frac{L_B + 1}{2} \right| \right\} \text{ for } x \in x'_o. \quad (4.9)$$

\mathcal{N} is a normalization constant. Piecewise linear kernels are going to be used in the simulation of two dimensional nonabelian gauge theory in section 11. There, smooth nonlocal heat bath updates can be performed with linear interpolation.

Table 1: Results for $\alpha = (\psi, -\Delta\psi)$ in 2 dimensions, 512^2 lattice

kernel	$L_B=2$	$L_B=4$	$L_B=8$	$L_B=16$	$L_B=32$	$L_B=64$	$L_B=128$	$L_B=256$
exact	6.899	8.902	9.705	9.941	10.00	10.02	10.18	13.11
trunc	7.000	9.405	10.73	11.38	11.69	11.84	11.92	–
min	8.000	13.24	18.48	22.58	25.23	26.76	27.59	28.02
sine	8.000	13.62	19.34	23.78	26.62	28.25	29.13	29.58
linear	8.000	15.80	24.58	31.84	36.68	39.51	41.05	41.84
const	8.000	16.00	32.00	64.00	128.0	256.0	512.0	1024

4.3.3 Ground state projection

Ground state projection kernels are defined as follows: ψ^{sine} is the eigenfunction corresponding to the lowest eigenvalue of the negative Laplacian with Dirichlet boundary conditions $-\Delta_{D,x'_o}$:

$$\psi_x^{sine} = \begin{cases} \mathcal{N} \prod_{\mu=1}^d \sin\left(\frac{\pi}{L_B+1} x^\mu\right) & \text{for } x \in x'_o \\ 0 & \text{for } x \notin x'_o \end{cases} \quad (4.10)$$

Again, \mathcal{N} denotes a normalization constant. Note that this kernel is different from ψ^{min} . A generalization of this kernel was introduced for scalar fields in the background of nonabelian gauge fields in ref. [38].

4.4 Results for $\alpha = (\psi, -\Delta\psi)$ in two and four dimensions

The results for the quantities $\alpha = (\psi, -\Delta\psi)$ for different kernels in two dimensions are presented in table 1. We used a 512^2 lattice (ψ^{exact} depends on the lattice size). The different kernels are ordered according to increasing value of α .

The values of α^{exact} and α^{trunc} are close together. This shows that the truncation of the support of ψ to the block and its nearest neighbor blocks is a good approximation to ψ^{exact} (in the sense of acceptance rates). The value of α^{exact} for $L_B = 256$ is remarkably higher than on smaller blocks. This is a finite size effect because the block lattice consists only of 2^2 points. Since the nearest neighbors overlap on a 2^2 lattice, no result for α^{trunc} is quoted for $L_B = 256$. The values of α for the smooth kernels with support on the block ψ^{min} , ψ^{sine} and ψ^{linear} are of the same magnitude. We can see that ψ^{sine} is almost as good as the optimal $\psi = \psi^{min}$. In contrast to all smooth kernels, α^{const} grows linear in L_B .

The results for different kernels in four dimensions are presented in table 2. Here we used a 64^4 lattice. In principle, the α 's behave as in two dimensions. The values of α^{linear} for small blocks are higher than α^{const} . The pyramids of the piecewise linear kernels have a lot of edges in four dimensions which lead to high costs in the kinetic energy.

Table 2: Results for $\alpha = (\psi, -\Delta\psi)$ in 4 dimensions, 64^4 lattice

kernel	$L_B=2$	$L_B=4$	$L_B=8$	$L_B=16$	$L_B=32$
exact	14.48	20.38	23.48	24.71	30.62
trunc	14.67	21.61	26.54	29.26	–
min	16.00	27.72	41.56	54.18	63.33
sine	16.00	30.37	48.46	64.85	76.44
linear	16.00	39.02	70.78	101.0	122.9
const	16.00	32.00	64.00	128.0	256.0

The L_B -dependence of the α 's in d dimensions is

$$\begin{aligned} \alpha &= 2dL_B && \text{for piecewise constant kernels,} \\ \alpha &\xrightarrow{L_B \gg 1} \text{const} && \text{for smooth kernels.} \end{aligned} \quad (4.11)$$

As an example, the expression for α^{sine} in d dimensions is

$$\alpha^{sine} = L_B^{2+d} (L_B + 1)^d 2^{d+2} d \sin^{4d+2} \left[\frac{\pi}{2(L_B + 1)} \right] \sin^{-2d} \left(\frac{\pi}{L_B + 1} \right) . \quad (4.12)$$

For large block sizes we find

$$\alpha^{sine} \xrightarrow{L_B \gg 1} d \frac{\pi^{2d+2}}{2^{3d}} = \text{const} . \quad (4.13)$$

From table 1 we observe that in two dimensions α becomes almost independent of L_B for the smooth kernels if the block size is larger than 16. In four dimensions (table 2), we find $\alpha(L_B) \sim \text{const}$ only for α^{exact} . The other α 's for the smooth kernels have not become independent of L_B for the block sizes studied.

5 Acceptance rates in free field theory

In this section we discuss the scale dependence of Metropolis acceptance rates of multigrid Monte Carlo algorithms in free field theory. The kinematical behavior can be related to the dynamical critical behavior of the algorithms. This will be the starting point for the theoretical analysis of interacting models in section 6. In free field theory CSD is eliminated by a multigrid algorithm.

5.1 Massless free field theory

Recall the exact result (3.9)

$$\Omega(s) = \operatorname{erfc}\left(\sqrt{\frac{\alpha}{8}}|s|\right)$$

in massless free field theory. $\Omega(s)$ is only a function of the product αs^2 . If we increase the block size L_B , the quantity α increases as a function $\alpha(L_B)$ of the block size. In order to keep $\Omega(s)$ fixed when L_B is increased, we have to rescale the changes s like $1/\sqrt{\alpha(L_B)}$. As a consequence, to maintain a constant acceptance rate in massless free field theory, s has to be scaled down like $1/\sqrt{L_B}$ for piecewise constant kernels, whereas for smooth kernels the acceptance rates for large L_B do not depend on the block size.

Note that this behavior of the acceptance rates for large L_B is not yet reached in four dimensions for the block sizes studied (except for ψ^{exact}). See also the discussion of the Metropolis step size below.

Let us relate the scale dependence of the Metropolis amplitude s with the dynamical critical behavior. For smooth kernels we have $s \sim \text{const}$ for large L_B . This indicates that the fluctuations generated by the algorithm are of the same size on all length scales. Multigrid simulations of free massless field theory with smooth interpolation and a V-cycle yield $z = 0$ [39, 20].

For piecewise constant kernels we have to scale down the Metropolis amplitude s like $s \sim 1/\sqrt{L_B}$. In simulations with piecewise constant interpolation and a V-cycle, $z = 1$ was found [40, 20, 41]. At least for free field theory, this disadvantage of the piecewise constant kernels can be compensated for by using a W-cycle instead of a V-cycle, resulting in $z = 0$ [40, 41, 42].

Smooth kernels in a unigrid implementation can be used only in V-cycle algorithms. An exception are 9-point prolongation kernels in two dimensions and generalizations thereof in higher dimensions. They can also be used in a recursive multigrid implementation with a W-cycle, at least in free field theory (cf. section 2).

5.2 Scale dependence of the Metropolis step size

We now illustrate what this rescaling of s means for the Metropolis step size ε in an actual multigrid Monte Carlo simulation. Let us inspect the integrated acceptance probability defined in eq. (2.11). If we insert the exact result (3.9) for massless free field theory

$$P_{acc}(\varepsilon) = \frac{1}{2\varepsilon} \int_{-\varepsilon}^{\varepsilon} ds \Omega(s) = \frac{1}{2\varepsilon} \int_{-\varepsilon}^{\varepsilon} ds \operatorname{erfc}\left(\sqrt{\frac{\alpha}{8}}|s|\right), \quad (5.1)$$

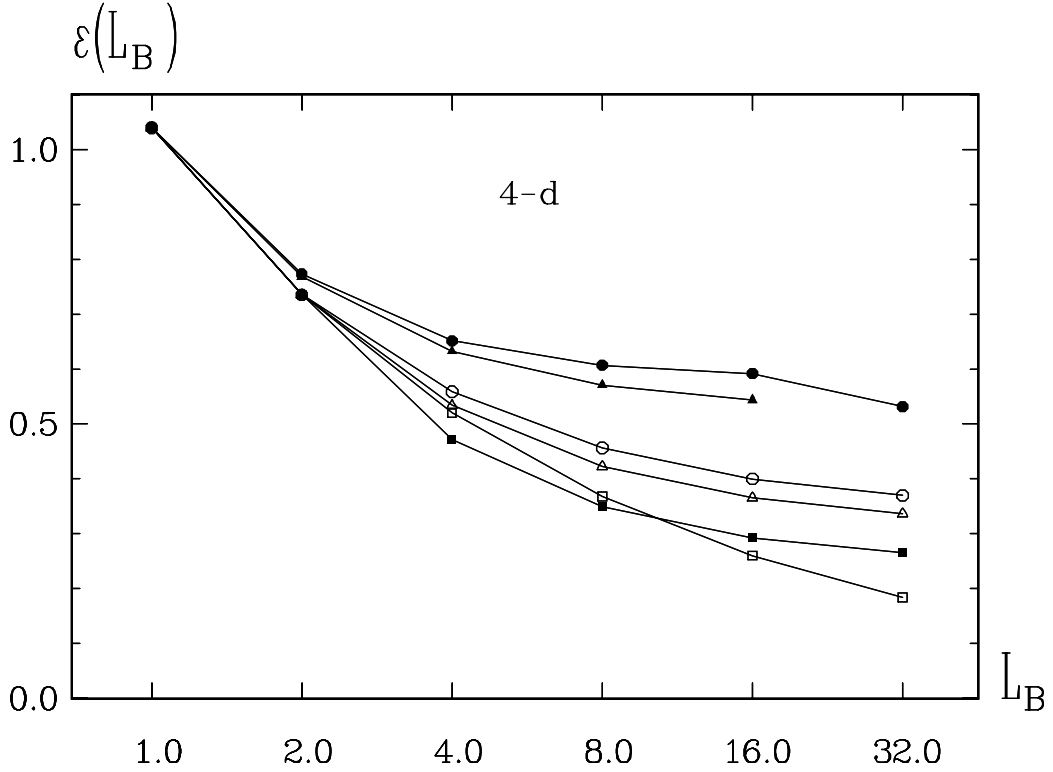
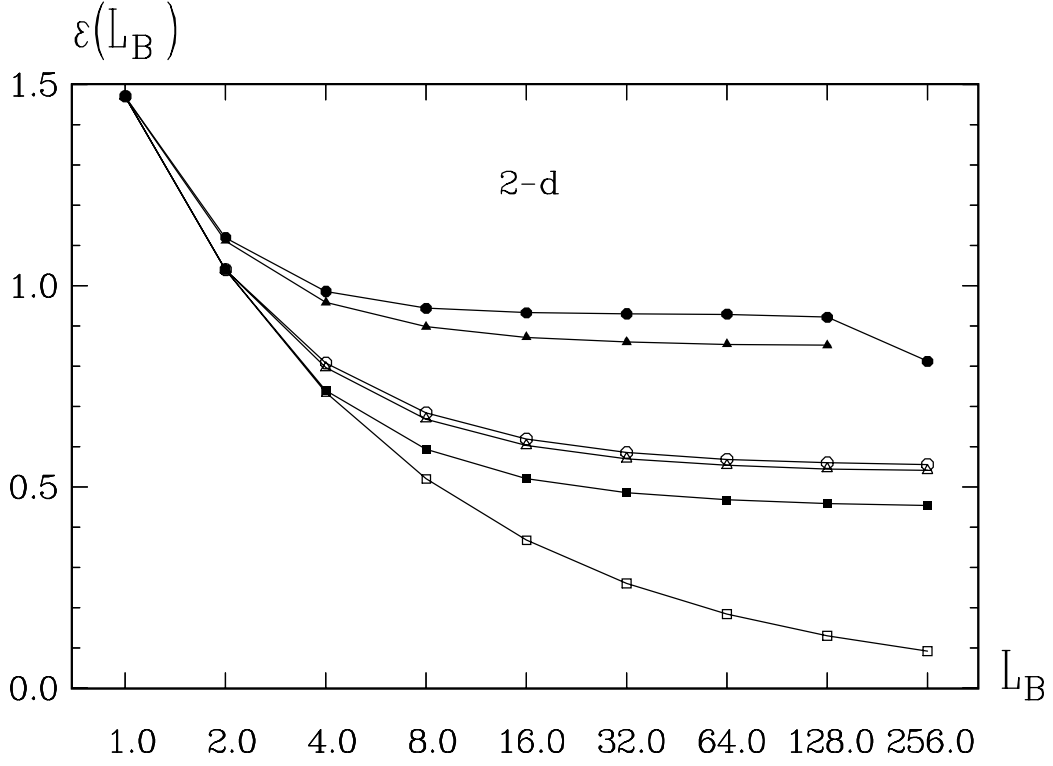


Figure 4: Top: Metropolis step sizes $\varepsilon(L_B)$ for massless free field theory in two dimensions, 512^2 -lattice. Bottom: $\varepsilon(L_B)$ for massless free field theory in four dimensions, 64^4 -lattice. $\varepsilon(L_B)$ is chosen in such a way that always $P_{acc} = 0.5$ holds. Symbols: full circles: ψ^{exact} , full triangles: ψ^{trunc} , empty circles: ψ^{min} , empty triangles: ψ^{sine} , full squares: ψ^{linear} , empty squares: ψ^{const} . Lines are only drawn to guide the eye.

we get

$$P_{acc}(\varepsilon) = \operatorname{erfc}\left(\sqrt{\frac{\alpha}{8}}\varepsilon\right) + \frac{1}{\sqrt{\frac{\pi\alpha}{8}}\varepsilon} \left[1 - e^{-\frac{\alpha}{8}\varepsilon^2}\right] . \quad (5.2)$$

P_{acc} is only a function of the product $\alpha\varepsilon^2$. In order to keep P_{acc} fixed (to, e.g. 50 percent) we have to rescale $\varepsilon(L_B)$ like $1/\sqrt{\alpha(L_B)}$, exactly in the same way as we had to rescale s to keep $\Omega(s)$ fixed. This L_B -dependence is plotted in figure 4.

5.3 Intuitive random walk picture of the W-cycle

In free field theory it is possible to overcome the disadvantage $\varepsilon(L_B) \sim 1/\sqrt{L_B}$ of the piecewise constant kernels compared to $\varepsilon(L_B) \sim \text{const}$ for smooth kernels by using a W-cycle instead of a V-cycle. This can be made plausible by a simple random walk argument.

A constant accumulated step size on all length scales can be achieved in the following way: For step sizes scaling down like $\varepsilon(L_B) \sim 1/\sqrt{L_B}$ and a coarsening by a factor of two, the Metropolis step size on a next coarser lattice is too small by a factor of $1/\sqrt{2}$. If we assume that subsequent update steps within a multigrid cycle are statistically independent and that these steps accumulate in a random-walk like way, we can expect to compensate for this decrease by increasing the number of updates on the next coarser grid by a factor of two. This can be achieved by a higher cycle with cycle control parameter $\gamma = 2$. Since higher cycles are defined recursively by going from an intermediate block lattice γ times to the next coarser lattice before going back to the next finer lattice, γ times more updates on each coarser lattice are performed.

In free field theory, the assumptions of this argument seem to be correct, and the random walk argumentation can explain that for piecewise constant kernels and a W-cycle CSD is eliminated.

5.4 Massive free field theory

We now discuss massive free field theory with Hamiltonian $\mathcal{H}(\phi) = \frac{1}{2}(\phi, [-\Delta + m^2]\phi)$. We find $h_1 = \frac{1}{2}\alpha_m s^2$, with α_m given by

$$\alpha_m = (\psi, [-\Delta + m^2]\psi) = \alpha + m^2 \sum_{x \in \Lambda_0} \psi_x^2 . \quad (5.3)$$

Therefore the exact result is $\Omega(s) = \operatorname{erfc}\left(\sqrt{\alpha_m/8}|s|\right)$. A term $\sum_x \psi_x^2$ scales $\sim L_B^2$ in arbitrary dimensions. For piecewise constant kernels

$$\sum_{x \in \Lambda_0} (\psi_x^{const})^2 = L_B^2 . \quad (5.4)$$

For ψ^{sine} -kernels we find

$$\sum_{x \in \Lambda_0} (\psi_x^{sine})^2 = 2^d L_B^{2+d} (L_B + 1)^d \sin^{4d} \left[\frac{\pi}{2(L_B + 1)} \right] \sin^{-2d} \left(\frac{\pi}{L_B + 1} \right) , \quad (5.5)$$

and for large block sizes

$$\sum_{x \in \Lambda_0} (\psi_x^{sine})^2 \xrightarrow{L_B \gg 1} \frac{\pi^{2d}}{2^{3d}} L_B^2 . \quad (5.6)$$

If the block size L_B is smaller than the correlation length $\xi = 1/m$, h_1 is still dominated by the kinetic term $s^2(\psi, -\Delta\psi)$, and the discussion is the same as in the massless case.

As soon as the block size L_B becomes larger than ξ , h_1 is dominated by the “mass” term $s^2 m^2 \sum_x \psi_x^2 \sim s^2 L_B^2$, and s has to be rescaled like $s \sim 1/L_B$ in order to maintain constant acceptance rates. Of course this is a dramatic decrease for large block sizes compared to $s \sim \text{const}$ in the massless case (using smooth kernels). Block spins on large blocks are essentially “frozen”. However this is not a problem for the performance of the algorithm in massive free field theory: The effective probability distribution for the block spins Φ is given by $\exp(-\mathcal{H}_{\text{eff}}(\Phi))$, where $\mathcal{H}_{\text{eff}}(\Phi)$ denotes the effective Hamiltonian in the sense of the block spin renormalization group [43]. The physical fluctuations of the block spins are dictated by an effective mass term

$$m_{\text{eff}}^2 \sum_{x' \in \Lambda_k} \Phi_{x'}^2 \quad \text{with} \quad m_{\text{eff}}^2 \sim m^2 L_B^2. \quad (5.7)$$

Thus, the algorithmic fluctuations (described by the mass term $m^2 \sum_x \psi_x^2 \sim m^2 L_B^2$) and the physical fluctuations (described by the effective mass $\sim m^2 L_B^2$) behave similarly, and the multi-grid algorithm is able to create fluctuations just of the size that is needed by the physics of the model. Moreover there is no need to do updates at length scales larger than ξ in order to beat CSD.

In this sense, the discussed algorithmic mass term $m^2 \sum_x \psi_x^2$ is well behaved for free field theory, since it decreases with the physical mass in the vicinity of the critical point. Stated differently, in massive free field theory the algorithmic mass term scales with the physical mass. As we shall see in section 6, for interacting models close to criticality, a different scenario is possible. There, it can happen that an algorithmic mass term $\sim \sum_x \psi_x^2$ persists, whereas the physical mass vanishes. If this happens, the multigrid algorithm is not able to produce the large critical fluctuations required by the physics, and we can *not* expect that CSD will be eliminated.

5.5 Behavior of a term $\sum_x \psi_x^4$

The L_B -dependence of a term $\sum_x \psi_x^4$ will also be needed in the study of the ϕ^4 theory in section 6 below. In d dimensions such a term scales $\sim L_B^{4-d}$: For piecewise constant kernels

$$\sum_{x \in \Lambda_0} (\psi_x^{\text{const}})^4 = L_B^{4-d}, \quad (5.8)$$

whereas using ψ^{sine} -kernels we find

$$\sum_{x \in \Lambda_0} (\psi_x^{\text{const}})^4 = 6^d L_B^{4+2d} (L_B + 1)^d \sin^{8d} \left[\frac{\pi}{2(L_B + 1)} \right] \sin^{-4d} \left(\frac{\pi}{L_B + 1} \right). \quad (5.9)$$

In the limit of large block sizes this term behaves like

$$\sum_{x \in \Lambda_0} (\psi_x^{\text{sine}})^4 \xrightarrow{L_B \gg 1} \left(\frac{3\pi^4}{128} \right)^d L_B^{4-d}. \quad (5.10)$$

5.6 Degree of relevance

In order to summarize the different large- L_B -behavior of local operators in the kernel ψ , let us introduce the *degree of relevance* in the sense of the perturbative renormalization group: The (superficial) degree r of relevance of a local operator in ψ which is a polynomial of m scalar fields with n derivatives is defined by $r = d + m(2 - d)/2 - n$. This definition is valid for smooth kernels. For large L_B , an operator with degree of relevance r behaves like L_B^r . An operator is called relevant if $r > 0$. As we have seen in the examples above, a mass term has $r = 2$, and a ψ^4 -term has $r = 4 - d$. A kinetic term $\alpha = (\psi, -\Delta\psi)$ has $r = 0$ for smooth kernels.

The only difference for piecewise constant kernels is that a kinetic term behaves like $\alpha = (\psi, -\Delta\psi) \propto L_B$.

6 Acceptance rates for interacting models

In this section, we shall apply formula (3.8) in the discussion of multigrid procedures for various spin models in two dimensions: the Sine Gordon model, the XY model, the single-component ϕ^4 theory, the $O(N)$ nonlinear σ -model and the CP^{N-1} model. The scale dependence of acceptance rates for interacting models will be compared with the kinematical behavior in free field theory, where CSD is known to be eliminated by a multigrid algorithm. A necessary criterion for the successful acceleration of a simulation by a multigrid algorithm is formulated.

6.1 The two dimensional Sine Gordon model

The two dimensional Sine Gordon model is defined by the Hamiltonian

$$\mathcal{H}(\phi) = \frac{1}{2\beta}(\phi, -\Delta\phi) - \zeta \sum_x \cos 2\pi\phi_x. \quad (6.1)$$

From the point of view of statistical mechanics, this system can be considered as a two dimensional surface in a periodic potential. The model exhibits a Kosterlitz-Thouless phase transition at $\beta_c(\zeta)$. In the limit of vanishing fugacity ζ , β_c takes the value $2/\pi = 0.6366\dots$. For $\beta > \beta_c$ the model is in the massless (rough) phase. The fluctuations of the surface are given by the surface thickness

$$\sigma^2 = \langle (\phi_x - \bar{\phi})^2 \rangle, \quad (6.2)$$

where $\bar{\phi}$ denotes the average of the field over the lattice. In the massless (rough) phase, the surface thickness σ^2 scales with $\log L$ [44]. In this phase, the cosine-term of the Hamiltonian is irrelevant, and the flow of the effective Hamiltonian (in the sense of the block spin renormalization group) converges to that of a massless free field theory: the long distance behavior of the theory is that of a Gaussian model. Since multigrid algorithms have proven to be efficient in generating long wavelength Gaussian modes, one might naively conclude that multigrid should be the right method to fight CSD in the simulation of the Sine Gordon model in the massless phase. But this is not so:

The energy change of a nonlocal update $\phi_x \rightarrow \phi_x + s\psi_x$ is

$$\begin{aligned} \Delta\mathcal{H} &= \mathcal{H}(\phi + s\psi) - \mathcal{H}(\phi) = \frac{s^2}{2\beta}(\psi, -\Delta\psi) + \frac{s}{\beta}(\psi, -\Delta\phi) \\ &- \zeta \sum_x \{ \cos(2\pi\phi_x) [\cos(2\pi s\psi_x) - 1] - \sin(2\pi\phi_x) \sin(2\pi s\psi_x) \}. \end{aligned} \quad (6.3)$$

The Hamiltonian is globally invariant under $\phi_x \rightarrow -\phi_x$. Therefore, $\langle \phi_x \rangle = 0$ and $\langle \sin 2\pi\phi_x \rangle = 0$ on finite lattices. Using this, we find for the average energy change $h_1 = \langle \Delta\mathcal{H} \rangle$ the expression

$$h_1 = \frac{\alpha}{2\beta} s^2 + \zeta C \sum_x [1 - \cos(2\pi s\psi_x)], \quad (6.4)$$

with $C = \langle \cos(2\pi\phi_x) \rangle$. Recall that h_1 is the quantity that determines the acceptance rates $\Omega(s)$ by eq. (3.8):

$$\Omega(s) \approx \operatorname{erfc}(\tfrac{1}{2}\sqrt{h_1}).$$

The essential point is that the second term in (6.4) is proportional to the block volume L_B^2 for piecewise constant *and* for smooth kernels (cf. the discussion in section 5). This can be

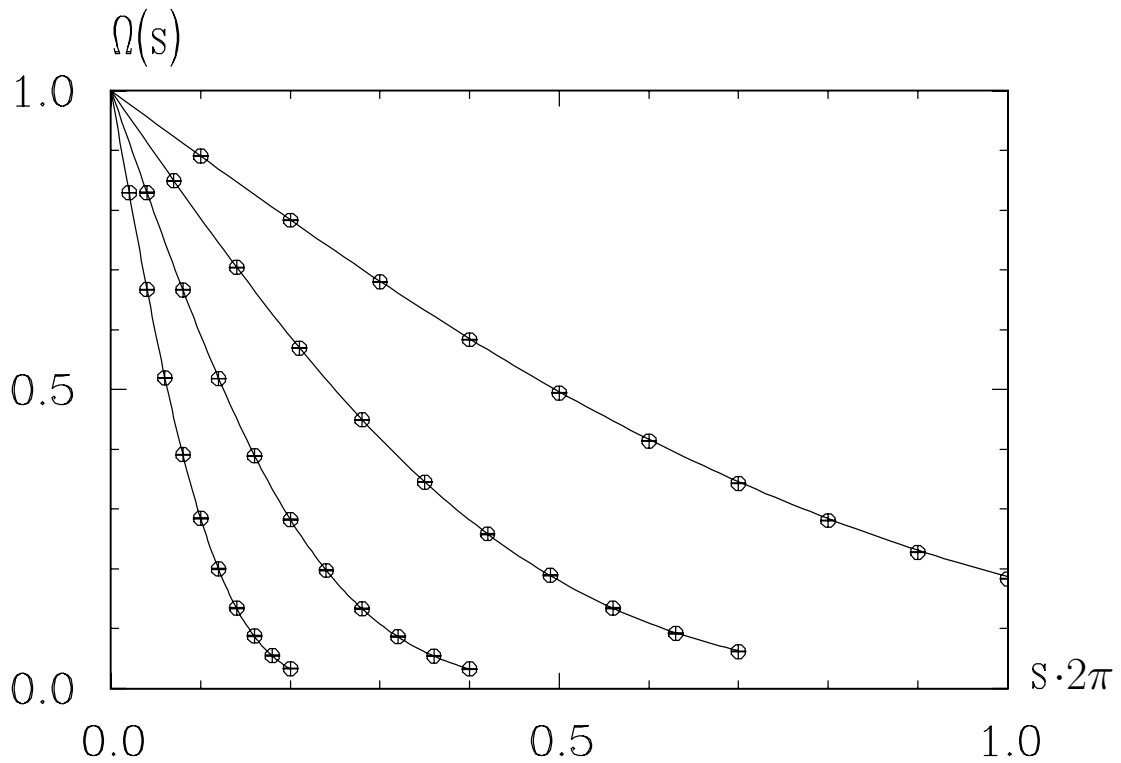


Figure 5: $\Omega(s)$ for piecewise constant kernels in the two dimensional Sine Gordon model, $\beta = 1.0$, $\zeta = 1.0$. From top to bottom: $L_B = 4, 8, 16, 32$ on a $16^2, 32^2, 64^2, 128^2$ lattice, respectively. Points with error bars: Monte Carlo results, lines: analytical results

checked for small s by expanding the cosine term in s . One therefore has to face a dramatic decrease of acceptance when the blocks become large, even for small fugacity ζ . A constant acceptance rate is achieved only when the proposed update steps are scaled down like $1/L_B$. It is therefore unlikely that any multigrid algorithm - based on nonlocal updates of the type discussed here - will be successful for this model. This prediction will be verified by a multigrid Monte Carlo simulation of the two dimensional Sine Gordon model in section 7.

We demonstrate the validity of formula (3.8) (using a Monte Carlo estimate for C) by comparing with Monte Carlo results at $\beta = 1.0$, $\zeta = 1.0$. This point is in the massless phase. There, the physical scale of the system is set by the linear size L of the lattice. In figure 5 we show both the numerical and analytical results for $\Omega(s)$ for $L_B = 4, 8, 16, 32$ on lattices of size $16^2, 32^2, 64^2$ and 128^2 , respectively.

We tested the precision of our approximation formula for piecewise constant kernels only. However, we have no doubts that the quality of the approximation is also very good for other interpolation kernels ψ .

6.2 The two dimensional XY model

We now discuss the two dimensional XY model, defined by the partition function

$$Z = \int \prod_x d\theta_x \exp(\beta \sum_{\langle x,y \rangle} \cos(\theta_x - \theta_y)). \quad (6.5)$$

The sum in the exponent is over all unordered pairs of nearest neighbors in the lattice. As the Sine Gordon model, the XY model has a massless (spin wave) phase for $\beta > \beta_c$, and a massive (vortex) phase for $\beta < \beta_c$. The best available estimate for the critical coupling is $\beta_c = 1.1197(5)$ [45].

Nonlocal updates are defined by

$$\theta_x \rightarrow \theta_x + s\psi_x, \quad (6.6)$$

with ψ obeying again the normalization condition (2.8). To define a (linear) block spin, we rewrite the partition function (6.5) in terms of 2-component unit vector spin variables s_x :

$$Z = \int \prod_x (d^2 s_x \delta(s_x^2 - 1)) \exp(\beta \sum_{\langle x,y \rangle} s_x \cdot s_y) \quad (6.7)$$

The block spins $S_{x'}$ are then defined as block averages of the unit vectors s_x .

Note that the proposal (6.6) changes the block spin by an amount $\approx s$ only when the spins inside the block are sufficiently aligned. This will be the case in the spin wave phase for large enough β . For smaller β , the correct (or “fair”) normalization of the kernels ψ is a subtle point. We believe, however, that our argument is not affected by this in a qualitative way.

Let us inspect the energy change of the nonlocal update (6.6):

$$\begin{aligned} \Delta\mathcal{H} &= -\beta \sum_{\langle x,y \rangle} \{ \cos(\theta_x - \theta_y + s(\psi_x - \psi_y)) - \cos(\theta_x - \theta_y) \} \\ &= -\beta \sum_{\langle x,y \rangle} \{ \cos(\theta_x - \theta_y) [\cos(s(\psi_x - \psi_y)) - 1] - \sin(\theta_x - \theta_y) \sin(s(\psi_x - \psi_y)) \} . \end{aligned} \quad (6.8)$$

Since the Hamiltonian is globally invariant under $\theta_x \rightarrow -\theta_x$, the expectation value $\langle \sin(\theta_x - \theta_y) \rangle$ vanishes on finite lattices. Therefore, the relevant quantity h_1 is

$$h_1 = \beta E \sum_{\langle x,y \rangle} [1 - \cos(s(\psi_x - \psi_y))], \quad (6.9)$$

with $E = \langle \cos(\theta_x - \theta_y) \rangle$, x and y nearest neighbors. For piecewise constant kernels, h_1 is proportional to L_B . For smooth kernels h_1 will become independent of L_B for large enough blocks. For small s ,

$$h_1 \approx \frac{1}{2} s^2 \beta E \sum_{\langle x,y \rangle} (\psi_x - \psi_y)^2 = \frac{1}{2} s^2 \beta E \alpha. \quad (6.10)$$

As above, $\alpha = \langle \psi, -\Delta \psi \rangle$. This quantity becomes nearly independent of L_B already for L_B larger than 16 (cf. section 4).

From the point of view of acceptance rates the XY model therefore behaves like massless free field theory. A dynamical critical exponent z consistent with zero was observed in the massless phase [46]. In this phase, the physically dominant excitations are spin waves. From this comparison we conclude that the analysis of the kinematics of multigrid algorithms can tell us whether spin wave excitations can be accelerated by the algorithm.

In the massive phase the physically important excitations are vortices, which are topologically nontrivial objects. In this phase multigrid Monte Carlo simulations with piecewise constant kernels yielded $z \approx 1.4$ [46]. This is an example for the fact that good acceptance rates are not sufficient to overcome CSD. The kinematical analysis is not sensitive to topological problems.

We again checked the accuracy of formula (3.8) by comparing with Monte Carlo results at $\beta = 1.2$ (which is in the massless phase). The results are displayed in figure 6. The only numerical input for the analytical formula was the link expectation value E .

6.3 The ϕ^4 theory in d dimensions

Let us now turn to single-component d -dimensional ϕ^4 theory ($d = 2, 3, 4$), defined by the Hamiltonian

$$\mathcal{H}(\phi) = \frac{1}{2} \langle \phi, -\Delta \phi \rangle + \frac{m_o^2}{2} \sum_x \phi_x^2 + \frac{\lambda_o}{4!} \sum_x \phi_x^4. \quad (6.11)$$

A nonlocal update $\phi_x \rightarrow \phi_x + s\psi_x$ leads to the energy change

$$\begin{aligned} \Delta \mathcal{H} &= \mathcal{H}(\phi + s\psi) - \mathcal{H}(\phi) = s^2 \frac{1}{2} \langle \psi, -\Delta \psi \rangle + s \langle \psi, -\Delta \phi \rangle \\ &+ \frac{m_o^2}{2} \sum_x [s^2 \psi_x^2 + 2s\psi_x \phi_x] + \frac{\lambda_o}{4!} \sum_x [s^4 \psi_x^4 + 4s^3 \psi_x^3 \phi_x + 6s^2 \psi_x^2 \phi_x^2 + 4s\psi_x \phi_x^3]. \end{aligned} \quad (6.12)$$

Since $\mathcal{H}(-\phi) = \mathcal{H}(\phi)$, the expectation values $\langle \phi_x^3 \rangle$ and $\langle \phi_x \rangle$ vanish on finite lattices. Therefore we find for $h_1 = \langle \Delta \mathcal{H} \rangle$

$$h_1 = s^2 \left\{ \frac{1}{2} \alpha + \left[\frac{m_o^2}{2} + \frac{\lambda_o}{4} P \right] \sum_x \psi_x^2 \right\} + s^4 \frac{\lambda_o}{4!} \sum_x \psi_x^4, \quad (6.13)$$

where $P = \langle \phi_x^2 \rangle$. Recall that $\sum_x \psi_x^2$ increases with L_B^2 , independent of d , whereas $\sum_x \psi_x^4$ scales like L_B^{4-d} , for smooth and for piecewise constant kernels (cf. the discussion of the different

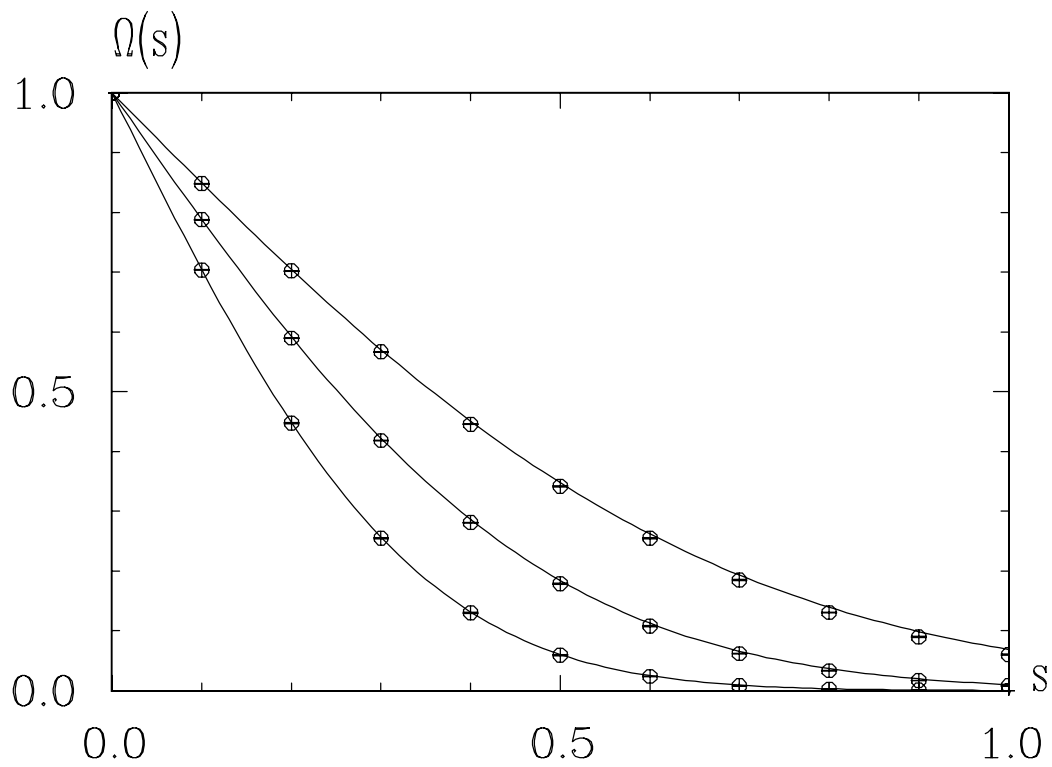


Figure 6: $\Omega(s)$ for piecewise constant kernels in the two dimensional XY model, $\beta = 1.2$. From top to bottom: $L_B = 4, 8, 16$ on a $16^2, 32^2, 64^2$ lattice, respectively. Points with error bars: Monte Carlo results, lines: analytical results

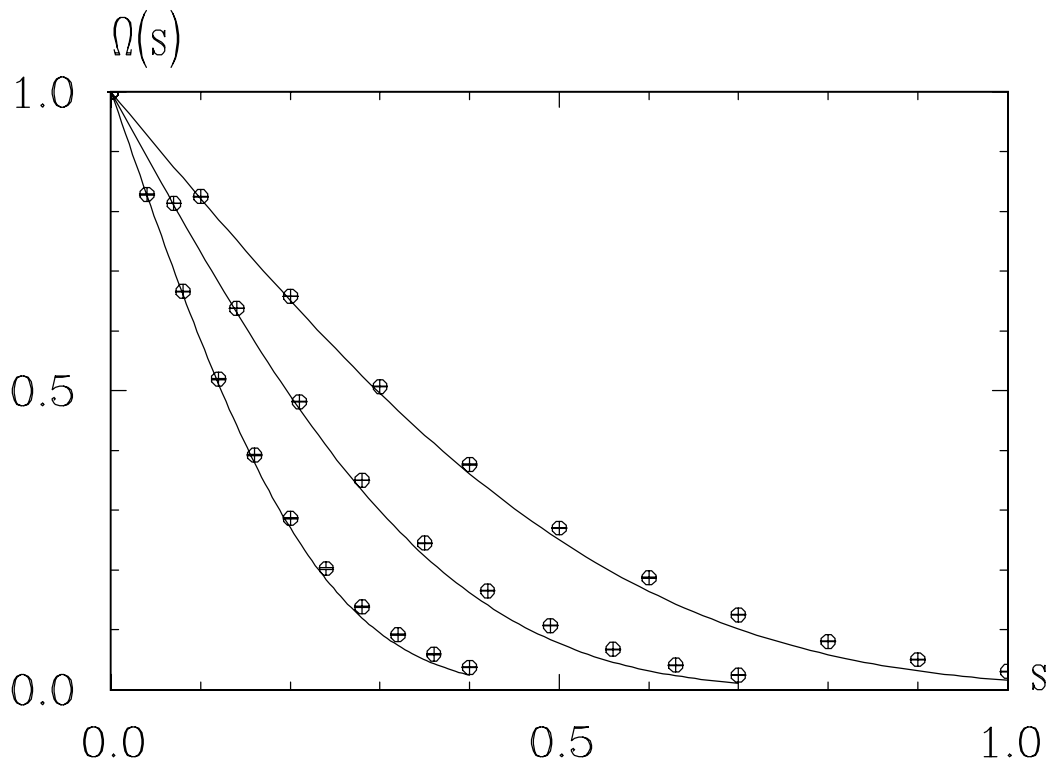


Figure 7: $\Omega(s)$ for piecewise constant kernels in the two dimensional ϕ^4 theory, $m_o^2 = -0.56$, $\lambda_o = 2.4$. From top to bottom: $L_B = 4, 8, 16$ on a $16^2, 32^2, 64^2$ lattice, respectively. Points with error bars: Monte Carlo results, lines: analytical results

kernels in section 5). We conclude that also in this model we have to face rapidly decreasing acceptance rates when the blocks become large. As in the case of the Sine Gordon model, s has to be rescaled like $1/L_B$ in order to maintain constant acceptance rates.

Therefore there is little hope that multigrid algorithms of the type considered here can overcome CSD in the single-component ϕ^4 model. In numerical simulations of two dimensional ϕ^4 theory, a dynamical critical behavior is found that is consistent with $z \approx 2$ for piecewise constant and for smooth kernels [14, 34, 20]. In four dimensions, there is no definite estimate for z [37].

Figure 7 shows a comparison of Monte Carlo results for two dimensional ϕ^4 theory with the theoretical prediction based on the numerical evaluation of P . The simulations were performed in the symmetric phase at $m_o^2 = -0.56$ and $\lambda_o = 2.4$. The correlation length at this point is $\xi \approx 15$ [20].

The quantitative comparison of the approximation formula (3.8) with numerical results for acceptance rates justified our approximations in three different models. For the remainder of this section we assume that the approximation formula is valid. We now discuss the kinematical behavior of two other spin models that are asymptotically free in two dimensions.

6.4 The two dimensional $O(N)$ nonlinear σ -model

The two dimensional $O(N)$ nonlinear σ -model is defined by the partition function

$$Z = \int \prod_x \left(d^N s_x \delta(s_x^2 - 1) \right) \exp\left(\beta \sum_{\langle x,y \rangle} s_x \cdot s_y\right), \quad (6.14)$$

where the s_x are N -component real unit vector spin variables. The case $N = 2$ corresponds to the XY model. For $N > 2$ the $O(N)$ nonlinear σ -model is in a disordered phase for all values of β . In the limit $\beta \rightarrow \infty$, the correlation length diverges exponentially in β . The critical behavior of the model is described the perturbative renormalization group which implies asymptotic freedom.

Nonlocal Metropolis updates can be defined in close analogy to the XY model by updating in $U(1)$ subgroups of $O(N)$. Let us consider the special case where the updates act on the first two components of the s_x variables by

$$s_x \rightarrow s'_x = R_x s_x, \quad (6.15)$$

with

$$s_x = \begin{pmatrix} s_x^{(1)} \\ s_x^{(2)} \\ s_x^{(3)} \\ \vdots \\ s_x^{(N)} \end{pmatrix}, \quad R_x = \begin{pmatrix} \cos(s\psi_x) & -\sin(s\psi_x) & 0 & \cdots & 0 \\ \sin(s\psi_x) & \cos(s\psi_x) & 0 & \cdots & 0 \\ 0 & 0 & 1 & & \\ \vdots & \vdots & & \ddots & \\ 0 & 0 & & & 1 \end{pmatrix}. \quad (6.16)$$

Again ψ obeys the normalization condition (2.8). Other directions of the $U(1)$ subgroup in $O(N)$ can be obtained by applying a randomly chosen global $O(N)$ rotation to the configuration before updating according to eq. (6.15).

The nonlocal updating proposal (6.15) changes the Hamiltonian by

$$\begin{aligned}\Delta\mathcal{H} &= -\beta \sum_{\langle x,y \rangle} \{(R_x s_x) \cdot (R_y s_y) - s_x \cdot s_y\} \\ &= -\beta \sum_{\langle x,y \rangle} \left\{ s_x^{(1)} s_y^{(1)} [\cos(s(\psi_x - \psi_y)) - 1] + s_x^{(1)} s_y^{(2)} \sin(s(\psi_x - \psi_y)) \right. \\ &\quad \left. - s_x^{(2)} s_y^{(1)} \sin(s(\psi_x - \psi_y)) + s_x^{(2)} s_y^{(2)} [\cos(s(\psi_x - \psi_y)) - 1] \right\}. \quad (6.17)\end{aligned}$$

The Hamiltonian of the $O(N)$ model is invariant under a global reflection of a fixed component $s_x^{(i)} \rightarrow -s_x^{(i)}$. Therefore all expectation values which change sign under such a transformation vanish. Using this, we obtain for $h_1 = \langle \Delta\mathcal{H} \rangle$

$$h_1 = \beta E_2 \sum_{\langle x,y \rangle} [1 - \cos(s(\psi_x - \psi_y))], \quad (6.18)$$

with

$$E_2 = \langle s_x^{(1)} s_y^{(1)} + s_x^{(2)} s_y^{(2)} \rangle = \frac{2}{N} \langle s_x \cdot s_y \rangle, \quad (6.19)$$

where x and y are nearest neighbors. For piecewise constant kernels, h_1 is proportional to L_B . For smooth kernels h_1 will become independent of L_B for large enough blocks. For small s ,

$$h_1 \approx \frac{1}{2} s^2 \beta E_2 \sum_{\langle x,y \rangle} (\psi_x - \psi_y)^2 = \frac{1}{2} s^2 \beta E_2 \alpha, \quad (6.20)$$

with $\alpha = \langle (\psi, -\Delta\psi) \rangle$. This quantity becomes independent of L_B for large block sizes.

As in the XY model, the scale dependence of acceptance rates in the $O(N)$ nonlinear σ -model with $N > 2$ is like in massless free field theory. This behavior of the acceptance rates was already observed numerically in multigrid Monte Carlo simulations of the $O(3)$ nonlinear σ -model in two dimensions with smooth and piecewise constant kernels [17]. Using a V-cycle and smooth interpolation in a unigrid implementation, a dynamical critical exponent $z \approx 0.2$ was observed. With a V-cycle and piecewise constant interpolation the result was $z \approx 1.3$. These values for z are very similar to the results for z in massless free field theory (cf. section 5).

In the $O(4)$ model, $z \approx 0.6$ was found [19], using piecewise constant interpolation and a W-cycle in a recursive multigrid scheme.

One can do an analogous discussion for nonlinear σ -models with global $SU(N) \times SU(N)$ invariance, leading to a similar prediction for the scale dependence of the acceptance rates. In numerical experiments with a multigrid algorithm for the $SU(3) \times SU(3)$ nonlinear σ -model $z \approx 0.2$ was found [16].

6.5 The two dimensional CP^{N-1} model

A different class of nonlinear σ -models in two dimensions are the CP^{N-1} models. The complex projective space CP^{N-1} is a complex manifold with the topological structure of a $2N - 1$ dimensional sphere, where points related by a $U(1)$ transformation are identified. A simple realization of a lattice action with a local $U(1)$ invariance is

$$\mathcal{H}(z) = 2\beta \sum_{\langle x,y \rangle} [1 - |\bar{z}_x \cdot z_y|^2] \quad (6.21)$$

where the z_x are N -component complex unit vectors. The CP^1 model is equivalent to the $O(3)$ nonlinear σ -model. For all N , the CP^{N-1} models are in a disordered phase at all values of β . As for all nonlinear σ -models in two dimensions, the critical behavior of the model is described by the perturbative renormalization group which implies asymptotic freedom for $\beta \rightarrow \infty$. In this limit the correlation length diverges exponentially in β .

Nonlocal Metropolis updates are formulated by updating in an embedded two dimensional XY model. Consider the special case where the updates act on the real and imaginary part of the first component of the z_x variables by

$$z_x \rightarrow z'_x = R_x z_x , \quad (6.22)$$

with

$$z_x = \begin{pmatrix} z_x^{(1)} \\ z_x^{(2)} \\ \vdots \\ z_x^{(N)} \end{pmatrix}, \quad R_x = \begin{pmatrix} \exp(is\psi_x) & 0 & \cdots & 0 \\ 0 & 1 & & 0 \\ \vdots & & \ddots & \\ 0 & 0 & & 1 \end{pmatrix}. \quad (6.23)$$

As above, ψ is normalized according to eq. (2.8). Other orientations of the embedded $U(1)$ subgroup can be obtained by acting on other components of the z_x -variables, where the component is selected randomly.

The energy change of such an update is

$$\begin{aligned} \Delta\mathcal{H} &= -2\beta \sum_{\langle x,y \rangle} \left[|\overline{R_x z_x} \cdot R_y z_y|^2 - |\overline{z_x} \cdot z_y|^2 \right] \\ &= -4\beta \sum_{\langle x,y \rangle} \text{Re} \left\{ \overline{z_x^{(1)}} z_y^{(1)} \sum_{i=2}^N z_x^{(i)} \overline{z_y^{(i)}} \left[e^{-is(\psi_x - \psi_y)} - 1 \right] \right\}. \end{aligned} \quad (6.24)$$

The Hamiltonian of the CP^{N-1} model is invariant under a global complex conjugation $z_x \rightarrow \overline{z_x}$. Therefore the expectation value

$$Q = \left\langle \overline{z_x^{(1)}} z_y^{(1)} \sum_{i=2}^N z_x^{(i)} \overline{z_y^{(i)}} \right\rangle, \quad (6.25)$$

where x and y are nearest neighbors, is real. Using this property, we find for the average energy change of the update (6.22)

$$h_1 = 4\beta Q \sum_{\langle x,y \rangle} [1 - \cos(s(\psi_x - \psi_y))] . \quad (6.26)$$

For piecewise constant kernels, h_1 is proportional to L_B . For smooth kernels h_1 will become independent of L_B for large enough blocks. For small s ,

$$h_1 \approx 2s^2\beta Q \sum_{\langle x,y \rangle} (\psi_x - \psi_y)^2 = 2s^2\beta Q \alpha . \quad (6.27)$$

As above, $\alpha = \langle (\psi, -\Delta\psi) \rangle$. α becomes independent of L_B for large block sizes.

As in the XY model and in the $O(N)$ nonlinear σ -model, the scale dependence of acceptance rates in the CP^{N-1} model is like in massless free field theory.

In multigrid Monte Carlo simulations of the CP^3 model with smooth interpolation and a V -cycle in a unigrid implementation, a dynamical critical exponent $z \approx 0.2$ was found [16].

6.6 Summary

A detailed quantitative analysis of the scale dependence of Metropolis updates was performed. Our approximation formula has proven to be quite precise in three different models. The results for all models are consistent with the following rule:

Sufficiently high acceptance rates for a complete elimination of CSD can only be expected if $h_1 = \langle \mathcal{H}(\phi + s\psi) - \mathcal{H}(\phi) \rangle$ contains no relevant operator in ψ .

As we have seen above, the typical candidate for a relevant operator in ψ is always an algorithmic mass term of the type $\sim s^2 \sum_x \psi_x^2$ with degree of relevance $r = 2$.

This rule is formulated for smooth kernels. For piecewise constant kernels, it has to be modified. There, the kinetic term $\alpha \propto L_B$ is relevant as well. At least in free field theory this disadvantage can be compensated for by using a W-cycle. Apart from this modification the rule carries over to the case of piecewise constant kernels.

With the help of this rule it is possible to predict whether a given method will have a chance to eliminate CSD.

Let us reformulate the rule in heuristic way. Recall the normalization condition (2.8) for the interpolation kernels ψ

$$L_B^{(d-2)/2} L_B^{-d} \sum_{x \in x'} \psi_x = \delta_{x', x'_o} .$$

The factor $L_B^{(d-2)/2}$ in front of the average $L_B^{-d} \sum_{x \in x'} (\dots)$ was chosen such that the behavior of different terms in ψ was analogous to the perturbative renormalization group. We observed that

$$\sum_x \psi_x^2 \sim L_B^2 \tag{6.28}$$

for piecewise constant and for smooth interpolation. The quantity α behaved like

$$\alpha = (\psi, -\Delta\psi) \sim \text{const} \tag{6.29}$$

for smooth interpolation and

$$\alpha = (\psi, -\Delta\psi) \sim L_B \tag{6.30}$$

for piecewise constant interpolation, independent of the dimension d . See also the definition of the degree of relevance at the end of section 5.

Let us switch to dimensionless kernels

$$\hat{\psi}_x = L_B^{(d-2)/2} \psi_x , \tag{6.31}$$

which are now normalized according to

$$L_B^{-d} \sum_{x \in x'} \hat{\psi}_x = \delta_{x', x'_o} . \tag{6.32}$$

E.g. a d -dimensional piecewise constant interpolation kernel in this normalization is just

$$\hat{\psi}_x^{\text{const}} = \begin{cases} 1 & \text{for } x \in x'_o \\ 0 & \text{for } x \notin x'_o \end{cases} . \tag{6.33}$$

Then we find

$$\sum_x \hat{\psi}_x^2 \sim L_B^d, \quad (6.34)$$

for piecewise constant and for smooth interpolation. A kinetic term in the kernels $\hat{\psi}$ now behaves as

$$\hat{\alpha} = (\hat{\psi}, -\Delta\hat{\psi}) \sim L_B^{d-2} \quad (6.35)$$

for smooth interpolation and

$$\hat{\alpha} = (\hat{\psi}, -\Delta\hat{\psi}) \sim L_B^{d-1} \quad (6.36)$$

for piecewise constant interpolation.

Assume that we use piecewise constant interpolation kernels $\hat{\psi}$. Then the terms that appear in the average energy change $h_1 = \langle \mathcal{H}(\phi + s\hat{\psi}) - \mathcal{H}(\phi) \rangle$ of a nonlocal update can be interpreted as follows:

- a kinetic term $(\hat{\psi}, -\Delta\hat{\psi})$ is a *surface term*, i. e. the energy costs of a nonlocal update are proportional to the surface of the block
- a mass term $\sim \sum_x \hat{\psi}^2$ is a *volume term*, i. e. the energy costs of a nonlocal update are proportional to the volume of the block

There are two different ways how multigrid algorithms can deal with a surface term: First, one can put more emphasis on the updating of coarse levels by using a W-cycle. Second, one can switch from piecewise constant interpolation to smooth interpolation. Then the energy change at the surface of a block is spread uniformly over the entire block, leading to $(\hat{\psi}, -\Delta\hat{\psi}) \sim L_B^{(d-2)}$.

However, up to now there is no way how to overcome the effect of a volume term that causes CSD in multigrid Monte Carlo simulations of critical models.

The different role of surface and volume terms seems to be a general feature of nonlocal update methods that multigrid algorithms share with cluster algorithms. In cluster algorithms nonlocal moves are performed by stochastically growing a cluster of spins and then flipping all spins in the cluster simultaneously. In ref. [9] it is argued that if the energy cost of this global flip is a “bulk term” that is proportional to the volume of the cluster, a cluster algorithm is expected to work badly.

The natural way to construct nonlocal piecewise constant updates that only have surface energy costs is to look for a global symmetry of the Hamiltonian of the model under consideration. Then the idea is to apply the corresponding symmetry transformation locally on blocks. E. g. in the massless free field theory, the global symmetry is the shift symmetry $\phi_x \rightarrow \phi_x + \text{const}$, which is then applied locally on blocks. In the XY-model, the global $O(2)$ -symmetry of the model is applied locally by performing piecewise constant $O(2)$ -rotations on blocks.

To summarize this discussion we give an intuitive Leitmotiv for the development of new multigrid methods:

A piecewise constant update of a nonlocal domain should have energy costs proportional to the surface of the domain, but not energy costs proportional to the volume of the domain.

We will use this heuristic criterion in the development of multigrid algorithms for nonabelian gauge theories. The intuitive Leitmotiv can then be made precise by performing a quantitative acceptance analysis.

7 Multigrid Simulation of the Sine Gordon model

7.1 Motivation

In this section we report on a multigrid Monte Carlo study of the Sine Gordon model in two dimensions. We have two questions in mind:

First, we want to check the theoretical prediction that a W-cycle (cycle control parameter $\gamma = 2$) with piecewise constant interpolation will not eliminate CSD in the rough (massless) phase of the Sine Gordon model. Recall the analysis of this model in the previous section: The Sine Gordon model was an example for a critical model where the expansion of $\langle \mathcal{H}(\phi + \psi) \rangle$ contained a relevant (mass) term. If such a term is present, Metropolis step sizes $\varepsilon(L_B)$ on block lattices with increasing block size L_B have to be scaled down like $\varepsilon(L_B) \sim 1/L_B$ in order to obtain block size independent acceptance rates. This strong decrease of step sizes on large blocks will lead to CSD.

Second, we want to ask the question whether one can circumvent this slowing down caused by too small steps on large blocks by accumulating many of these steps randomly.

We applied an intuitive random walk argument for free field theory in section 5. There this reasoning explained why one can compensate for the disadvantage of $\varepsilon(L_B) \sim 1/\sqrt{L_B}$ with piecewise constant interpolation by using a W-cycle with $\gamma = 2$. We can use the same argument when the Metropolis step sizes decrease even stronger:

A constant accumulated step size on all length scales could in principle be achieved in the following way: For step sizes scaling down like $\varepsilon(L_B) \sim 1/L_B$ and a coarsening by a factor of two, the Metropolis step size on a next coarser grid is too small by a factor of two. If we assume that subsequent update steps within a multigrid cycle are statistically independent and that these steps accumulate in a random-walk like way, we can expect to compensate for this decrease by increasing the number of updates on the next coarser grid by a factor of four. This can be achieved by a higher cycle with cycle control parameter $\gamma = 4$. By applying a higher

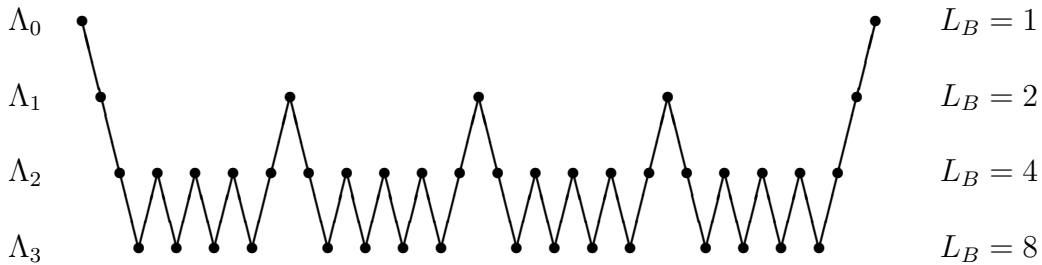


Figure 8: *Higher cycle with $\gamma = 4$*

cycle with $\gamma > 1$, γ times more updates on each coarser lattice are performed. An example for a higher cycle with $\gamma = 4$ is given in figure 8.

For a recursive multigrid algorithm, the computational effort is $\sim L^d$ for $\gamma < 2^d$ and $\sim L^d \log L$ for $\gamma = 2^d$ in d dimensions [34]. Therefore a higher cycle with $\gamma = 4$ is practical for

$d > 2$ and borderline practical for $d = 2$.

In summary, if the random-walk picture is correct, we can expect to overcome the problem of strongly decreasing step sizes on large scales by doing more work on coarser lattices.

7.2 The multigrid algorithm

The Hamiltonian of the two dimensional Sine Gordon model is

$$\mathcal{H}(\phi) = \frac{1}{2\beta}(\phi, -\Delta\phi) - \zeta \sum_x \cos 2\pi\phi_x \quad (7.1)$$

on an $L \times L$ lattice Λ_0 . Our simulations are organized as follows: In order to allow for high cycle control parameters γ , we use a recursive multigrid algorithm, piecewise constant interpolation and a coarsening with a factor of two, as illustrated in figure 1. Let us describe the details of the recursive multigrid algorithm. An update to the current fine grid field ϕ_x is given by

$$\phi_x \rightarrow \phi'_x = \phi_x + \Phi_{x'} \quad \text{if } x \in x' . \quad (7.2)$$

The point x on the fine grid is contained in the 2×2 block x' on the coarse grid, and $\Phi_{x'}$ denotes the displacement field² corresponding to the block x' .

The conditional coarse grid Hamiltonian is calculated by substituting eq. (7.2) into eq. (7.1). Its general form on the block lattice Λ_k is

$$\mathcal{H}_k(\Phi) = \frac{\alpha}{2} \sum_{\langle x', y' \rangle \in \Lambda_k} (\Phi_{x'} - \Phi_{y'})^2 - \sum_{x' \in \Lambda_k} f_{x'} \Phi_{x'} - \zeta \sum_{x' \in \Lambda_k} (a_{x'} \cos 2\pi\Phi_{x'} + b_{x'} \sin 2\pi\Phi_{x'}) . \quad (7.3)$$

Note that the fundamental Hamiltonian \mathcal{H} on the fine grid Λ_0 is a special case of this general coarse grid Hamiltonian \mathcal{H}_k on Λ_k with

$$\alpha = 1/\beta , \quad (7.4)$$

$$f_x = 0 \quad \text{for all } x \in \Lambda_0 , \quad (7.5)$$

$$a_x = 1 \quad \text{for all } x \in \Lambda_0 , \quad (7.6)$$

$$b_x = 0 \quad \text{for all } x \in \Lambda_0 . \quad (7.7)$$

The set of coefficients $\{\alpha', f', a', b'\}$ of \mathcal{H}_{k+1} on the next coarser grid Λ_{k+1} can be calculated from the set of coefficients $\{\alpha, f, a, b\}$ on Λ_k by recursion:

$$\alpha' = 2\alpha , \quad (7.8)$$

$$f'_{x'} = \sum_{x \in x'} \left[f_x - 2\alpha \sum_{yn.n.x} (\phi_x - \phi_y) \right] , \quad (7.9)$$

$$a'_{x'} = \sum_{x \in x'} (a_x \cos 2\pi\phi_x + b_x \sin 2\pi\phi_x) , \quad (7.10)$$

$$b'_{x'} = \sum_{x \in x'} (-a_x \sin 2\pi\phi_x + b_x \cos 2\pi\phi_x) . \quad (7.11)$$

Here ϕ_x denotes the configuration on Λ_k when we switch to the next coarser grid.

²Although we use the same letter Φ , the displacement field as used here and the block spin field as introduced in section 2 differ by a constant

For the updating of the variables on Λ_k within the multigrid cycle, we choose a sweep of single hit Metropolis updates before the coarsening and after the interpolation, respectively. The maximum Metropolis step size $\varepsilon(L_B)$ is scaled down like $1/L_B$. Then, acceptance rates of approximately 50% are observed on all block lattices, in accordance with the theoretical analysis of section 6. We tested the implementation of the algorithm by comparison with exact results in the Gaussian model ($\zeta = 0$) and against Monte Carlo data obtained on small lattices by a cluster algorithm for the Sine Gordon model [47].

7.3 Simulation and results

We study the dynamical critical behavior of the different versions of the algorithm in the rough phase, where the correlation length is infinite and the physical length scale is set by the linear size of the lattice L . Thus, we expect the autocorrelation time τ to diverge with the dynamical critical exponent z like $\tau \sim L^z$.

As observables we take the energy

$$E = \frac{1}{L^2} \sum_{\langle x,y \rangle} (\phi_x - \phi_y)^2 \quad (7.12)$$

and the surface thickness σ^2 as defined in eq. (6.2).

The simulations were performed at $\beta = 1.0$, $\zeta = 0.5$. This is deep in the rough phase. Note that in the limit $\zeta \rightarrow \infty$ which corresponds to the discrete Gaussian model the critical coupling is $\beta_c = 0.7524(8)$ [45]. Starting from an ordered configuration, measurements were taken after equilibration at each visit of the finest lattice. The run parameters and results are summarized in table 3 for the W-cycle and in table 4 for the higher cycle with $\gamma = 4$.

From the autocorrelation function for the observable A

$$\rho_A(t) = \frac{\langle A_s A_{s+t} \rangle - \langle A \rangle^2}{\langle A^2 \rangle - \langle A \rangle^2}, \quad (7.13)$$

we compute the integrated autocorrelation time

$$\tau_{int,A} = \frac{1}{2} + \sum_{t=1}^{\infty} \rho_A(t). \quad (7.14)$$

The asymptotic decay of the autocorrelation function $\rho_A(t)$ is described by the exponential autocorrelation time $\tau_{exp,A}$:

$$\rho_A(t) \sim \exp(-t/\tau_{exp,A}) \text{ for } t \rightarrow \infty. \quad (7.15)$$

If $\rho_A(t)$ is a single exponential, $\tau_{int,A} \approx \tau_{exp,A}$.

The errors on $\tau_{int,A}$ were calculated by a window method [48]. For the self consistent truncation window we took $4\tau_{int}$, which is sufficiently large if the autocorrelation function shows an exponential decay. This is indeed the case, see figure 9.

The numerical results for the autocorrelation times τ_{int} are listed in table 3 for $\gamma = 2$ and in table 4 for $\gamma = 4$. The values for τ_{int} are measured in the number of visits on the finest lattice. Note that our runs are longer than 10 000 τ_{int} (longer than 4 000 τ_{int} on the 128^2 lattice). Figure 10 shows the dependence of τ_{int,σ^2} on L for $\gamma = 2$ and $\gamma = 4$. For comparison, we plotted lines which correspond to $z = 2$.

Table 3: Numerical results for the W-cycle ($\gamma = 2$) in the 2-d Sine Gordon model on $L \times L$ lattices in the rough phase, $\beta = 1.0$, $\zeta = 0.5$

L	statistics	discarded	E	$\tau_{int,E}$	σ^2	τ_{int,σ^2}
4	25 000	2 000	0.934(4)	0.90(3)	0.268(1)	0.96(3)
8	50 000	2 000	0.986(1)	0.97(2)	0.3809(9)	1.35(3)
16	100 000	2 000	0.9956(5)	1.04(2)	0.4896(7)	2.70(8)
32	300 000	2 000	0.9987(2)	1.03(1)	0.5996(7)	8.54(19)
64	500 000	2 000	0.99945(5)	1.04(1)	0.7105(10)	30.5(1.0)
128	500 000	4 000	0.99966(3)	1.04(1)	0.8218(19)	113.7(6.9)

Table 4: Numerical results for the higher cycle with $\gamma = 4$ in the 2-d Sine Gordon model on $L \times L$ lattices in the rough phase, $\beta = 1.0$, $\zeta = 0.5$

L	statistics	discarded	E	$\tau_{int,E}$	σ^2	τ_{int,σ^2}
4	25 000	2 000	0.940(4)	0.89(3)	0.268(1)	0.91(3)
8	25 000	2 000	0.986(2)	0.94(3)	0.380(1)	1.14(4)
16	25 000	2 000	0.9965(10)	0.94(3)	0.488(1)	1.67(6)
32	100 000	2 000	0.9985(3)	0.95(1)	0.5997(9)	4.15(11)
64	300 000	2 000	0.99945(7)	0.96(1)	0.7113(9)	14.2(4)
128	300 000	2 000	0.99962(4)	0.95(1)	0.8213(18)	58.2(3.3)

If we fit our data for the autocorrelation time of the surface thickness in the range $32 \leq L \leq 128$ with the Ansatz $\tau_{int,\sigma^2} = cL^z$, we obtain $z = 1.86(4)$ with $\chi^2/\text{dof} = 0.22$ for the W-cycle ($\gamma = 2$), and $z = 1.86(4)$ with $\chi^2/\text{dof} = 4.6$ for the higher cycle ($\gamma = 4$). The uncertainty in z is dominated by the relative error of τ_{int} on the largest lattice, which is about 6% in both cases. We therefore estimate

$$\begin{aligned} z &= 1.9(1) && \text{for the W-cycle } (\gamma = 2) , \\ z &= 1.9(1) && \text{for the higher cycle } (\gamma = 4) . \end{aligned}$$

7.4 Summary

In this section we reported on a simulation of the two dimensional Sine Gordon model with a multigrid Monte Carlo algorithm. Using a recursive multigrid implementation with piecewise constant interpolation we studied the dynamical critical behavior of the two variants of the algorithm ($\gamma = 2$ and $\gamma = 4$) in the rough phase. From this study we confirm that, as already predicted in section 6, CSD is not reduced by a W-cycle with piecewise constant interpolation. According to the acceptance analysis, we would expect the same result with smooth interpolation. Moreover, the results clearly show that the attempt to compensate for decreasing acceptance rates on large blocks by choosing a higher cycle with $\gamma = 4$ does not improve the dynamical critical behavior of the algorithm. We conclude that a random-walk argument as stated above is not correct in the case of the Sine Gordon model.

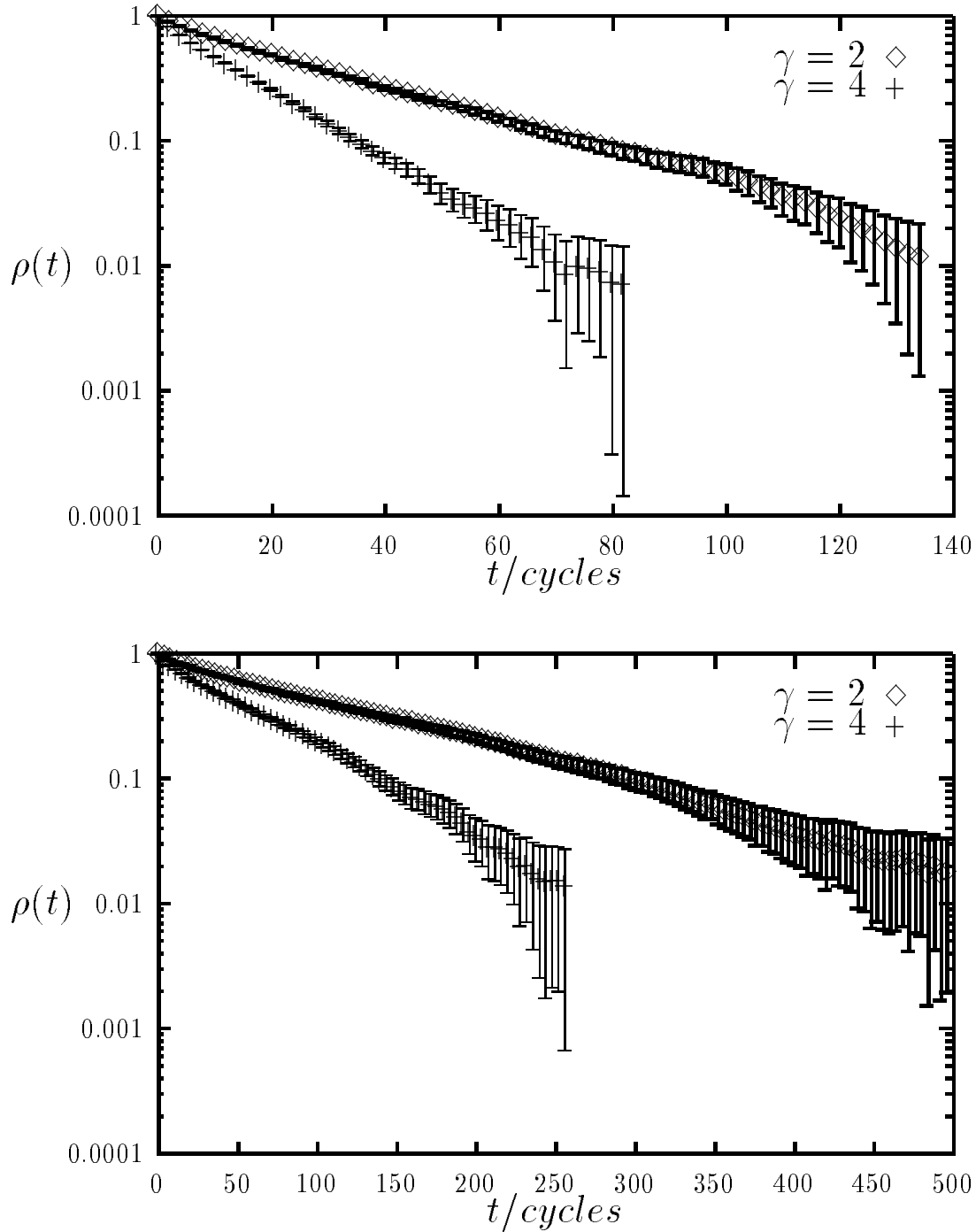


Figure 9: Autocorrelation functions $\rho(t)$ for the surface thickness σ^2 in the rough phase of the two dimensional Sine Gordon model, $\beta = 1.0$, $\zeta = 0.5$. Top: 64^2 lattice, bottom: 128^2 lattice. $\rho(t)$ is shown for the W-cycle ($\gamma = 2$) and the higher cycle ($\gamma = 4$) respectively.

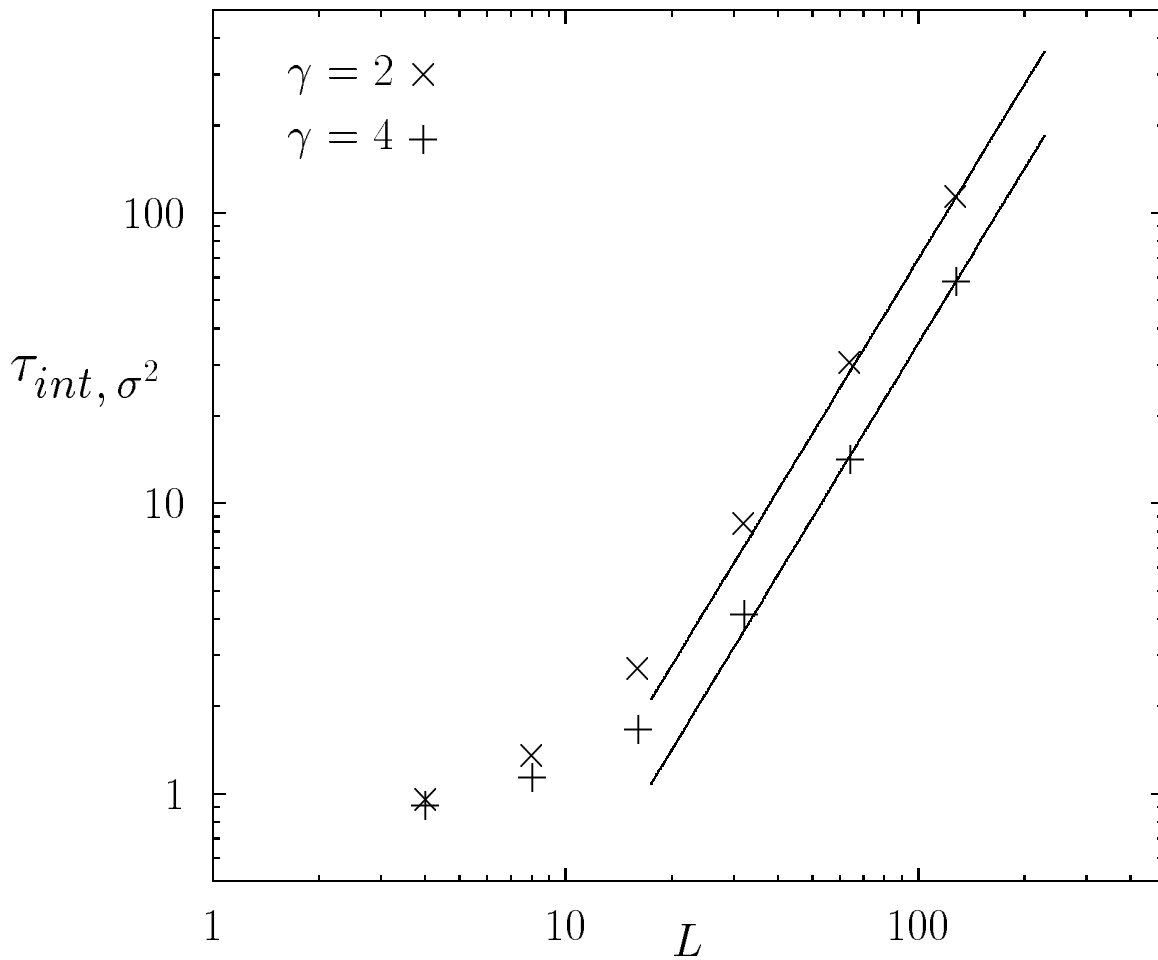


Figure 10: *Dependence of the integrated autocorrelation time for the surface thickness σ^2 on the lattice size L in the rough phase of the 2-d Sine Gordon model, $\beta = 1.0$, $\zeta = 0.5$. Errors are smaller than the symbols used. The lines correspond to $z = 2$.*

8 Multigrid algorithms for lattice gauge fields in two dimensions

In this section, we start the discussion of multigrid algorithms for lattice gauge theory. We begin with a review of the method by Laursen, Smit and Vink for abelian gauge fields in two dimensions. An new difficulty is to change from an abelian to a nonabelian gauge group. The concepts that are needed for nonlocal updates of nonabelian gauge fields in in two dimensional $SU(2)$ lattice gauge theory are discussed. We introduce a new updating procedure, the time slice blocking, and analyze its kinematics.

Let us introduce the notations for lattice gauge theory in d dimensions. We consider partition functions

$$Z = \int \prod_{x,\mu} dU_{x,\mu} \exp(-\mathcal{H}(U)). \quad (8.1)$$

The link variables $U_{x,\mu}$ take values in the gauge group $U(1)$ or $SU(N)$, and dU denotes the corresponding invariant Haar measure. The standard Wilson action $\mathcal{H}(U)$ is given by

$$\mathcal{H}(U) = \beta \sum_{\mathcal{P}} [1 - \frac{1}{N} \text{Re Tr } U_{\mathcal{P}}]. \quad (8.2)$$

The sum in (8.2) is over all plaquettes in the lattice. The $U_{\mathcal{P}}$ are path ordered products around plaquettes \mathcal{P} ,

$$U_{\mathcal{P}} = U_{x,\mu} U_{x+\hat{\mu},\nu} U_{x+\hat{\nu},\mu}^* U_{x,\nu}^* . \quad (8.3)$$

U^* denotes the hermitean conjugate (= inverse) of U .

8.1 Abelian gauge fields: $U(1)$ in two dimensions

8.1.1 The algorithm of Laursen, Smit and Vink

A first multigrid Monte Carlo algorithm for abelian gauge fields was implemented and tested by Laursen, Smit and Vink for $U(1)$ lattice gauge theory in two dimensions [18]. It was inspired by a deterministic multigrid procedure for the minimization of a Hamiltonian of the form arising in lattice gauge theory [34]. As an example and a starting point for the following discussion of nonabelian gauge fields we review their algorithm in the unigrid language.

In the case of gauge group $U(1)$ the link variables are parameterized with an angle $-\pi \leq \theta_{x,\mu} < \pi$ through

$$U_{x,\mu} = \exp(i\theta_{x,\mu}) . \quad (8.4)$$

Nonlocal updates are defined as illustrated in figure 11: One chooses a square block x'_o of size L_B^2 and a direction τ with $\tau = 1$ or 2 . During the update, τ will be kept fixed. All the link variables $U_{x,\tau}$ attached to sites x inside the block x'_o are proposed to be “rotated” simultaneously:

$$U_{x,\tau} \rightarrow \exp(is\psi_x) U_{x,\tau} , \quad (8.5)$$

or in terms of the link angles

$$\theta_{x,\tau} \rightarrow \theta_{x,\tau} + s\psi_x . \quad (8.6)$$

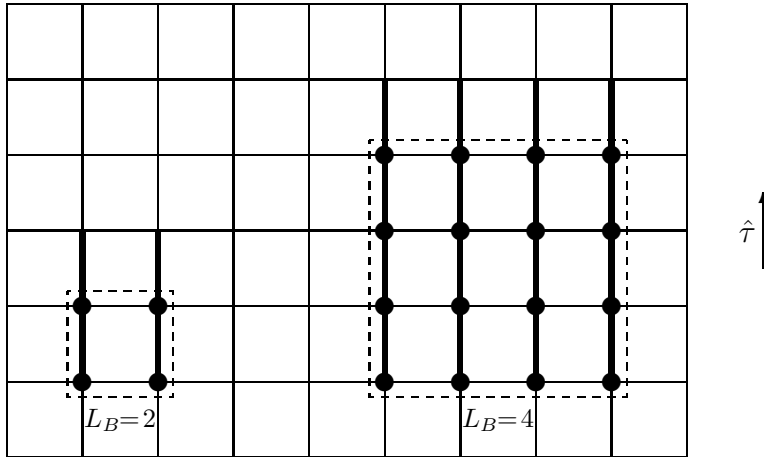


Figure 11: *Blocking of link variables for two dimensional $U(1)$ gauge fields*

ψ denotes an interpolation kernel as introduced in section 4. In the reported work a two dimensional piecewise constant kernel

$$\psi_x^{const} = \begin{cases} 1 & \text{for } x \in x'_o \\ 0 & \text{for } x \notin x'_o \end{cases} \quad (8.7)$$

was taken. For this choice of interpolation, a recursive multigrid implementation with a W -cycle is feasible [18]. Another interesting feature of this implementation is (in contrast to the time slice blocking below) that both directions of link variables pointing from the block x'_o in the $\tau = 1$ and in the $\tau = 2$ direction can be updated on a coarse layer without going back to the finest lattice.

The reported result for the dynamical critical exponent z for the simulation with a W -cycle is $z \approx 0.2$ with respect to the autocorrelation times of Polyakov loop observables. However, it was also observed that the multigrid algorithm is not able to move efficiently between different topological sectors. This leads to autocorrelation times $\tau \sim \exp(c\beta)$ with $c \approx 1.9$ for the topological charge. If the physical size of the lattice is fixed, this will lead to $\tau \sim \exp(c'L)$, i.e. super-CSD increasing exponentially in L . The exponent quoted above should therefore be interpreted with some care.

Let us analyze the kinematical behavior of this algorithm with the help of eq. (3.8)

$$\Omega(s) \approx \text{erfc} \left(\frac{1}{2} \sqrt{h_1} \right) .$$

For $h_1 = \langle \Delta \mathcal{H} \rangle$ we find in the case of piecewise constant interpolation

$$h_1 = 2\beta P L_B [1 - \cos(s)] = \beta P L_B s^2 + O(s^4) \quad (8.8)$$

with $P = \langle \text{Tr} U_{\mathcal{P}} \rangle$. The derivation of this expression is described in appendix A. In order to obtain acceptance rates independent of the block size, we have to rescale the amplitudes for the nonlocal updates like $s \sim 1/\sqrt{L_B}$, as in massless free field theory with piecewise constant interpolation. With respect to this, the behavior of this multigrid algorithm in the $U(1)$ lattice gauge theory in two dimensions is similar to a multigrid algorithm in massless free field theory. Therefore the reported acceleration for Polyakov loop observables can be understood by our analysis.

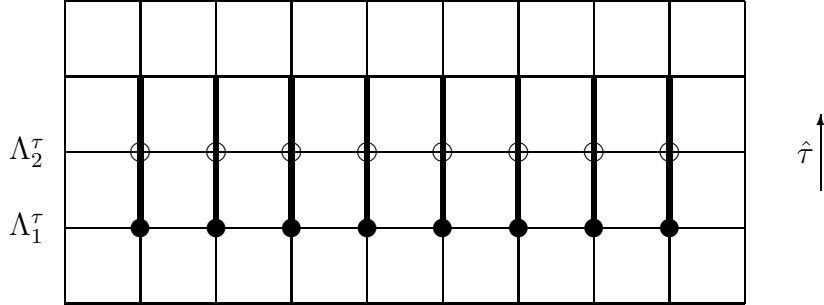


Figure 12: *Decoupling of time slices Λ_1^τ and Λ_2^τ .*

On the other hand the problems with topological quantities are again an example (cf. the discussion of the two dimensional XY -model in the vortex phase in section 6) for the fact that good acceptance rates alone are not sufficient to overcome CSD.

8.1.2 Comments and possible modifications

Let us denote the time slice of lattice sites with τ -component t as $\Lambda_t^\tau = \{x \in \Lambda_0 \mid x_\tau = t\}$. Here the name “time” direction has no physical meaning. We use this word to label the fixed direction of link variables that are updated simultaneously. Of course, the time direction in an update algorithm will be changed periodically from $\tau = 1$ to $\tau = 2$. In the following, we will denote the time direction with τ and the spatial direction(s) different from τ with μ .

In the unigrid picture a general feature of nonlocal updating schemes in lattice gauge theory is transparent: As long as we restrict the possible nonlocal changes in the configuration to link variables $U_{x,\tau}$ of a fixed time direction τ and keep all other variables $U_{x,\mu}$ with $\mu \neq \tau$ unchanged, adjacent time slices decouple. This is illustrated in figure 12.

Here, link variables $U_{x,\tau}$ pointing from sites in two different adjacent time slices Λ_1^τ and Λ_2^τ are shown. The point is that there are only plaquette terms in the Hamiltonian that contain link variables $U_{x,\tau}$ pointing from sites x in the same time slice Λ_t^τ , i.e. either in Λ_1^τ or Λ_2^τ . This means that the link variables pointing from sites in Λ_1^τ and from sites in Λ_2^τ are independent as long as all other $U_{x,\mu}$ with $\mu \neq \tau$ are fixed.

A possible modification of the algorithm is the use of smooth interpolation kernels ψ . If we repeat the acceptance analysis with the help of formula (3.8) for a general kernel ψ we obtain for $h_1 = \langle \Delta \mathcal{H} \rangle$ (cf. appendix A)

$$h_1 = \beta P \sum_{\substack{x \in \Lambda_0 \\ \mu \neq \tau}} [1 - \cos(s(\psi_{x+\hat{\mu}} - \psi_x))] \quad . \quad (8.9)$$

The sum does not include contributions from links which point in the time-direction τ . Therefore h_1 is a sum of independent contributions from time slices Λ_t^τ orthogonal to the τ -direction. This is a consequence of the independence of time slices. In particular, no smoothness of kernels is needed in the τ -direction. From now on we choose ψ_x to be constant in that direction and assume that the support of ψ in τ -direction is restricted to the L_B time slices Λ_t^τ that contain

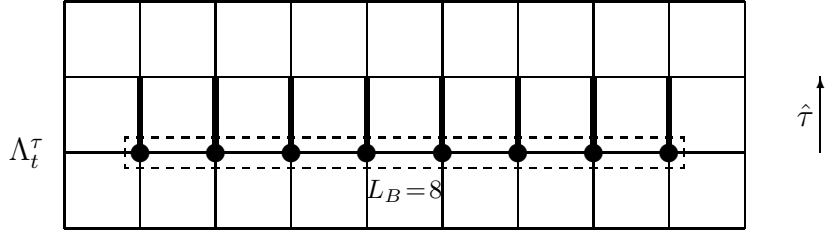


Figure 13: Geometry of the time slice blocking: The marked link variables are updated simultaneously. The bottom of the block is indicated by a dashed line.

the square block x'_o . Then we find

$$h_1 = \beta P L_B \sum_{\substack{x \in \Lambda_t^\tau \\ \mu \neq \tau}} [1 - \cos(s(\psi_{x+\hat{\mu}} - \psi_x))] \quad . \quad (8.10)$$

For small s , this can be approximated by

$$h_1 \approx \frac{1}{2} s^2 \beta P L_B \sum_{\substack{x \in \Lambda_t^\tau \\ \mu \neq \tau}} (\psi_{x+\hat{\mu}} - \psi_x)^2 = \frac{1}{2} s^2 \beta P \alpha_1 \quad . \quad (8.11)$$

with $\alpha_1 = (\psi', -\Delta\psi')$. Here, ψ' denotes the kernel ψ restricted to the one dimensional time slice Λ_t^τ . A factor of $L_B^{1/2}$ is absorbed in ψ' such that ψ' is properly normalized as a one dimensional kernel.

This means that for smooth interpolation we can obtain acceptance rates independent of the block size by choosing the amplitudes for the nonlocal updates like $s \sim \text{const}$. The kinematical behavior of this version of the multigrid algorithm is similar to a multigrid algorithm with smooth interpolation in massless free field theory. Therefore we expect a successful acceleration for Polyakov loop observables also for this version.

In summary, the independence property of time slices has several consequences: First, interpolation kernels ψ do not need to be smooth in the time direction. Second, since updates of link variables in different time slices are statistically independent, two different nonlocal update schemes are possible: the time slice blocking and the square blocking. In the time slice blocking method updates of one dimensional blocks of size L_B are performed on separate time slices Λ_t^τ in sequence. In the square blocking scheme as used by Laursen, Smit and Vink one builds $L_B \times L_B$ blocks out of “staples” of L_B one dimensional blocks of size L_B and performs the updates on this square block simultaneously. The analysis of the kinematics is the same for both schemes. For simplicity we are going to adopt the time slice blocking in the following.

An important point is that the decoupling of time slices is independent of the gauge group and carries over to higher dimensions. We are going to use this fact as a basic ingredient of nonlocal updating schemes for nonabelian gauge fields.

8.2 Nonabelian gauge fields: $SU(2)$ in two dimensions

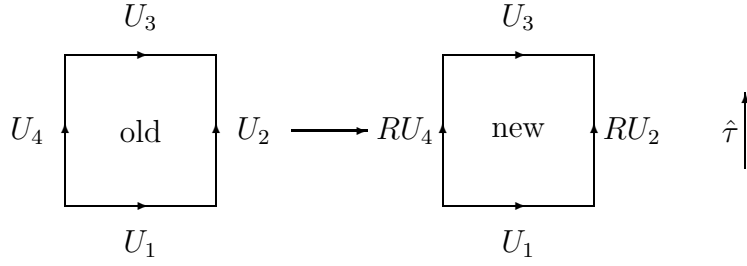


Figure 14: *Change of plaquette during naive nonlocal updating*

8.2.1 The nonabelian character of the gauge field

Our method for a nonlocal updating procedure for nonabelian $SU(2)$ gauge fields in two dimensions is based on the time slice blocking. It is illustrated in figure 13. We start the discussion with a naive generalization of the updates in the abelian case: Choose a one dimensional block x'_o of size L_B within a time slice Λ_t^τ and update all link variables $U_{x,\tau}$ pointing from this block in the τ -direction

$$U_{x,\tau} \rightarrow U'_{x,\tau} = R_x U_{x,\tau} \quad \text{for all } x \in x'_o, \quad (8.12)$$

where the “rotation” matrices R_x are in $SU(2)$. We parametrize them as

$$R_x(\vec{n}, s) = \cos(s\psi_x/2) + i \sin(s\psi_x/2) \vec{n} \cdot \vec{\sigma}, \quad (8.13)$$

where \vec{n} denotes a three dimensional real unit vector, and the σ_i are Pauli matrices. \vec{n} will be taken randomly from the three dimensional unit sphere, and ψ will have support on the one dimensional block x'_o .

The simplest version is a piecewise constant “rotation” where R_x is a rotation matrix R independent of x . Let us examine how a plaquette in the interior of the block (as illustrated in figure 14) changes under this update:

$$P_{old} = \frac{1}{2} \text{Tr}(U_1 U_2 U_3^* U_4^*) \rightarrow P_{new} = \frac{1}{2} \text{Tr}(U_1 R U_2 U_3^* (R U_4)^*) = \frac{1}{2} \text{Tr}(R^* U_1 R U_2 U_3^* U_4^*) \quad (8.14)$$

with the notations as in figure 14. Let denote the links

$$(x, x + \mu) \quad \text{for all } x, x + \mu \in x'_o \quad (8.15)$$

as the links in the bottom of the block, as marked in figure 13. In the abelian case the rotation matrix R and the link variable in the bottom of the block U_1 would commute, and we would have $P_{old} = P_{new}$, i.e. the plaquettes in the interior of the block would remain unchanged.

But since our gauge group is nonabelian the resulting change of the plaquette by this naive generalization would lead to energy costs proportional to the volume of the block.

Recall the intuitive Leitmotiv for the development of new multigrid methods from section 6: *A piecewise constant update of a nonlocal domain should have energy costs proportional to the surface of the domain, but not energy costs proportional to the volume of the domain.*

Energy costs proportional to the volume of the block lead to an algorithmic mass term that suppresses the amplitudes of the nonlocal moves on large scales. Therefore the naive generalization will suffer from CSD.

This does not come as a surprise. Due to the gauge invariance of the model, the link variables do not have a gauge invariant meaning. Therefore the rotation R that is constant over the block for a given gauge can be arbitrarily rough and disordered after a gauge transformation. It is therefore natural to assume that the rotation matrices have to be chosen in a gauge covariant way.

8.2.2 Gauge covariant time slice blocking algorithm

We use the additional gauge degrees of freedom and generalize (8.12) to

$$U_{x,\tau} \rightarrow U'_{x,\tau} = R_x(g)U_{x,\tau} \quad \text{for all } x \in x'_o, \quad (8.16)$$

with $R_x(g) = g_x^* R_x g_x$ and g -matrices $g_x \in SU(2)$. In the abelian case we obtain nothing new, because g_x and R_x commute. In the nonabelian case a plaquette in the interior of the block changes under a piecewise constant rotation R according to

$$P_{old} = \frac{1}{2} \text{Tr}(U_1 U_2 U_3^* U_4^*) \rightarrow P_{new} = \frac{1}{2} \text{Tr}(R^* U_1^g R U_2^g U_3^{g*} U_4^{g*}). \quad (8.17)$$

The gauge transformed link variables are given by $U_{x,\mu}^g = g_x U_{x,\mu} g_{x+\mu}^*$. If we choose the g -matrices in such a way that the link variable U_1^g in the bottom of the block is equal to unity, it will commute with an arbitrary rotation matrix R . Then the plaquettes in the interior of the block stay unchanged as in the abelian case.

From this discussion we are led to the following gauge condition: Choose the g -matrices in the bottom of the one dimensional block x'_o such that

$$U_{x,\mu}^g = g_x U_{x,\mu} g_{x+\hat{\mu}}^* = 1 \quad \text{for all } (x, x + \hat{\mu}) \in x'_o. \quad (8.18)$$

(The bottom of the block is indicated in figure 13.) In other words: All gauge transformed link variables in the one dimensional bottom of the block should be equal to unity. We denote this gauge condition as block axial gauge. Note that we still have the freedom of a constant gauge transformation within each block x' ,

$$g_x \rightarrow h_{x'} g_x \quad \text{for all } x \in x'. \quad (8.19)$$

Although we use the term ‘‘gauge condition’’ here, we do not intend to perform the gauge transformation g . We use the concept of gauging only to define covariant rotations $R_x(g) = g_x^* R_x g_x$.

The gauge transformation properties of these updates are as follows: If we apply an arbitrary gauge transformation h to the gauge field U

$$U_{x,\mu} \rightarrow U_{x,\mu}^h = h_x U_{x,\mu} h_{x+\hat{\mu}}^* \quad (8.20)$$

the g -matrices transform like

$$g_x \rightarrow g_x^h = g_x h_x^* \quad (8.21)$$

and the covariant rotation matrix $R_x(g) = g_x^* R_x g_x$ transforms according to the adjoint representation:

$$R_x(g) \rightarrow (R_x(g))^h = h_x R_x(g) h_x^*. \quad (8.22)$$

As a consequence, if we apply the updates to the gauge transformed configuration U^h

$$U_{x,\tau}^h \rightarrow (U_{x,\tau}^h)' = (R_x(g))^h U_{x,\tau}^h = h_x R_x(g) h_x^* h_x U_{x,\tau} h_{x+\hat{\tau}}^*$$

$$= h_x R_x(g) U_{x,\tau} h_{x+\hat{\tau}}^* = h_x U'_{x,\tau} h_{x+\hat{\tau}}^* = (U'_{x,\tau})^h, \quad (8.23)$$

the updating commutes with a gauge transformation h and is therefore gauge covariant.

Let us summarize the steps of the time slice blocking scheme for $SU(2)$ in the unigrid language:

1. Choose a block x'_o of size L_B that is contained in the slice Λ_t^τ . All link variables $U_{x,\tau}$ pointing from sites x inside the block in τ -direction will be moved simultaneously.
2. Find the gauge transformation g defined by the block axial gauge condition (8.18) such that $U_{x,\mu}^g = 1$ for all link variables in the bottom of the block.
3. Propose new link variables $U'_{x,\tau}$ by

$$U_{x,\tau} \rightarrow U'_{x,\tau} = R_x(g) U_{x,\tau}, \quad (8.24)$$

with $R_x(g) = g_x^* R_x g_x$ and

$$R_x(\vec{n}, s) = \cos(s\psi_x/2) + i \sin(s\psi_x/2) \vec{n} \cdot \vec{\sigma}. \quad (8.25)$$

s is a uniformly distributed random number from the interval $[-\varepsilon, \varepsilon]$, \vec{n} is a vector selected randomly from the three dimensional unit sphere, and ψ is a one dimensional kernel.

4. Calculate the associated change of the Hamiltonian $\Delta\mathcal{H}$ and accept the proposed link variables with probability $\min[1, \exp(-\Delta\mathcal{H})]$.

The detailed balance condition is fulfilled by this updating scheme: For the naive version with $g = 1$ it is straightforward to show that the detailed balance condition holds, since the rotation matrices R_x are chosen according to a probability distribution which is symmetric around unity.

If we now take g according to some gauge condition, we have to be careful that we get the same g before and after the move $U_{x,\tau} \rightarrow U'_{x,\tau}$ is performed. Otherwise this move would not be reversible. In other words: The gauge condition yielding g must not depend on $U_{x,\tau}$. This is indeed the case, since only link variables $U_{x,\mu}$ with $\mu \neq \tau$ enter in the block axial gauge condition.

The details of an implementation and simulation of the covariant time slice blocking algorithm for $SU(2)$ gauge fields will be described in section 9.

8.2.3 Acceptance analysis of the proposal

The energy change associated with the update proposal (8.16) is

$$\Delta\mathcal{H} = -\frac{\beta}{2} \sum_{\mathcal{P}} \text{Tr}(U'_{\mathcal{P}} - U_{\mathcal{P}}) = -\frac{\beta}{2} \sum_{\substack{x \in \Lambda_t^\tau \\ \mu \neq \tau}} \text{Tr}\{(R_x(g)^* U_{x,\mu} R(g)_{x+\hat{\mu}} - U_{x,\mu}) H_{x,\mu}^*\}, \quad (8.26)$$

where $H_{x,\mu}^* = U_{x+\hat{\mu},\tau} U_{x+\hat{\tau},\mu}^* U_{x,\tau}^*$, and ψ stands for a one dimensional interpolation kernel. The relevant quantity for the acceptance rates is $h_1 = \langle \Delta\mathcal{H} \rangle$. If we assume that the g -matrices are chosen according to the block axial gauge condition and that ψ vanishes outside the block x'_o we find

$$h_1 = \beta P \sum_{\substack{x \in \Lambda_t^\tau \\ \mu \neq \tau}} [1 - \cos(s(\psi_x - \psi_{x+\hat{\mu}})/2)]$$

$$= \frac{s^2}{8} \beta P \sum_{\substack{x \in \Lambda_t^T \\ \mu \neq \tau}} (\psi_x - \psi_{x+\hat{\mu}})^2 + O(s^4) = \frac{s^2}{8} \beta P \alpha_1 + O(s^4) \quad (8.27)$$

with $P = \langle \frac{1}{2} \text{Tr} U_{\mathcal{P}} \rangle$ and $\alpha_1 = (\psi, -\Delta\psi)$. The derivation of eq. (8.27) is described in appendix A. Remember that for the time slice blocking in two dimensions ψ is a one dimensional kernel.

Thus the kinematical behavior of this method is the same as that of the massless Gaussian model in one dimension. In contrast to $U(1)$ lattice gauge theory in two dimensions we do not expect any additional topological problems to occur for $SU(2)$. Therefore we expect a successful acceleration of the simulation by the proposed time slice blocking algorithm. This prediction will be verified in in section 9.

8.3 Summary

In this section we discussed multigrid algorithms for lattice gauge theory in two dimensions. The successful acceleration of Polyakov loop observables in the simulation of abelian gauge fields in two dimensions by Laursen, Smit and Vink can be understood by the kinematical analysis.

An important observation is the statistical decoupling of adjacent time slices as long as only link variables in the time direction are updated. The time slice blocking algorithm is based on this property. The statistical independence of adjacent time slices is independent of the gauge group and of the dimensionality.

The nonabelian character of the gauge field was discussed. We proposed the gauge covariant time slice blocking for $SU(2)$ in two dimensions that is particularly adapted to the nonabelian character. From the kinematical analysis we expect a strong reduction of CSD in a simulation of the proposed algorithm.

9 Multigrid Monte Carlo simulation of $SU(2)$ lattice gauge fields in two dimensions

In this section we simulate $SU(2)$ lattice gauge theory in two dimensions by a multigrid algorithm. The acceptance analysis of the previous section predicted that CSD can be eliminated by the time slice blocking. To verify this statement, we perform numerical experiments on systems with lattice sizes up to 256^2 . The details of the implementation of the time slice blocking are discussed. Then the run parameters and numerical results are reported.

9.1 Implementation of the time slice blocking

For a concrete implementation of the time slice blocking method as introduced in section 8 we choose a unigrid algorithm with piecewise linear interpolation and a V-cycle.

9.1.1 Smooth nonlocal heat bath updates in $U(1)$ subgroups

Although the analysis of nonlocal updates in section 8 was performed in terms of a Metropolis version, we are going to use a heat bath version of the nonlocal moves in our simulation. We think that the change of the update method from Metropolis to heat bath will not affect the dynamical critical behavior in a substantial way. The advantage of the heat bath updating is that there are no tuneable parameters such as the Metropolis step size $\varepsilon(L_B)$.

A heat bath implementation of nonlocal time slice blocking updates is possible if we use one dimensional piecewise linear interpolation and update in $U(1)$ subgroups of $SU(2)$. This will be described in the following.

Compared to section 8, we formulate the piecewise linear interpolation in a different language: Assume that the g -matrices defined according to the block axial gauge condition (8.18) have been applied as a gauge transformation in the bottom of the block x'_o . Then the gauged link variables in the bottom of the block are equal to unity. Now a piecewise linear block update is formulated by multiplying the L_B gauged link variables $U_{x,\tau}^g$ pointing in τ -direction from left to right by the $SU(2)$ -matrices $R, R^2, R^3, \dots, R^{L_B/2}, R^{L_B/2}, R^{L_B/2-1}, \dots, R$. R is given by

$$R(\vec{n}, \theta) = \cos(\theta) + i \sin(\theta) \vec{n} \cdot \vec{\sigma}, \quad (9.1)$$

where the randomly chosen three-dimensional vector \vec{n} specifies the direction of a $U(1)$ subgroup in $SU(2)$. All changes of plaquettes that are generated by this update can be written in the form

$$\text{Tr}(U'_p) = \text{Tr}(RV) = \text{Tr}(V) \cos(\theta) + \text{Tr}(i\vec{n} \cdot \vec{\sigma} V) \sin(\theta), \quad (9.2)$$

with the $SU(2)$ matrix $V = U_p^g$ or $V = U_p^{g*}$. By summing over all changed plaquettes (9.2) we obtain an overall change in the Hamiltonian of the form

$$\mathcal{H}(U') = a \cos(\theta) + b \sin(\theta) + \text{const}, \quad (9.3)$$

with real constants a and b . To generate $U(1)$ random numbers distributed according to the distribution

$$d\text{prob}(\theta) \propto e^{a \cos(\theta) + b \sin(\theta)} d\theta \quad (9.4)$$

we use the fast vectorizable method of Hattori and Nakajima [49].

9.1.2 Sequence of updates

The sequence of updates is organized as follows: We start with a V-cycle of time slice blocking updates on the links $U_{x,\tau}$ pointing in the $\tau = 1$ direction. The largest block size is $L/2$ on a $L \times L$ lattice. This means that the sequence of updated block sizes is $L_B = 2, 4, \dots, L/2, L/2, L/4, \dots, 2$. When all time slices have been updated by a V-cycle, we perform a sweep of local $SU(2)$ heat bath updates through all links on the lattice. Here we use the “incomplete” Kennedy-Pendleton [50] heat bath algorithm with one trial per link. This means that in a sweep through the lattice not all links but only a very high percentage of them are updated. The advantage is that scalar operations on a vector computer are avoided [51]. Then we do a V-cycle on all links pointing in the $\tau = 2$ direction and again a local heat bath sweep. This sequence is repeated periodically.

Measurements are performed after each local heat bath sweep. To avoid effects from fixed block boundaries, we use stochastically overlapping blocks [16] by applying a random translation before each V-cycle.

9.1.3 Axial gauge

In order to save computer time we use a slight modification of the gauge condition. Recall the block axial gauge (8.18): Take the g -matrices in the bottom of a block x'_o such that

$$U_{x,\mu}^g = g_x U_{x,\mu} g_{x+\hat{\mu}}^* = 1 \quad \text{for all } (x, x + \hat{\mu}) \in x'_o . \quad (9.5)$$

We modify it to the axial gauge: Take the g -matrices in the bottom of a time slice Λ_t^τ such that

$$U_{x,\mu}^g = g_x U_{x,\mu} g_{x+\hat{\mu}}^* = 1 \quad \text{for } (x, x + \hat{\mu}) \in \Lambda_t^\tau, \quad x_\mu = 1, \dots, L - 1 . \quad (9.6)$$

In other words: all spatial links but the last link are gauged to one within the bottom of a time slice.

The computational advantage of this slight change in the gauge condition is that for the block axial gauge the g -matrices have to be calculated for each block lattice individually. For the axial gauge the g -matrices are the same for all block lattices and they do not change during the updating on different block lattices with different L_B . Therefore we have to calculate them only once before performing the entire V-cycle. The gauge covariance properties of the update is not affected by this modification.

9.2 Simulation and results

9.2.1 Observables

The observables measured are square Wilson loops

$$W(I, I) = \langle \frac{1}{2} \text{Tr}(U(C_{I,I})) \rangle , \quad (9.7)$$

where $U(C_{I,I})$ is the parallel transporter around a rectangular Wilson loop $C_{I,I}$ of size $I \times I$. On an $L \times L$ -lattice we measure $W(1, 1), W(2, 2), W(4, 4), W(8, 8), \dots, W(L/2, L/2)$. Another important class of quantities is built up from timelike Polyakov loops. A Polyakov loop at the one dimensional spatial point r is defined by

$$P_r = \frac{1}{2} \text{Tr} \prod_{t=1}^L U_{(r,t),2} . \quad (9.8)$$

We measure the lattice averaged Polyakov loop

$$\bar{P} = \left\langle \frac{1}{L} \sum_{r=1}^L P_r \right\rangle, \quad (9.9)$$

and the lattice averaged Polyakov loop squared

$$\bar{P}^2 = \left\langle \left(\frac{1}{L} \sum_{r=1}^L P_r \right)^2 \right\rangle. \quad (9.10)$$

9.2.2 Run parameters and results

In order to investigate the dynamical critical behavior of the multigrid algorithm, we simulate a sequence of lattices with fixed physical size $L \approx 10\xi$, where the correlation length ξ is related to the string tension by κ by $\xi = 1/\sqrt{\kappa}$. Then we have to use lattice sizes and β values such that L^2/β is constant. If we choose this large ratio of L/ξ , finite size effects are negligible. The detailed run parameters are given in table 5. The quoted correlation length is calculated by the exact solution [52] in the infinite volume limit. The main results of this solution are summarized in appendix B. We started our runs from ordered configurations with all link variables set equal to unity. After equilibration, measurements were taken after each local heat bath sweep through the lattice.

Table 5: Run parameters for the multigrid Monte Carlo simulation of two dimensional $SU(2)$ lattice gauge theory.

β	4	16	64	256	1024
L	16	32	64	128	256
ξ	1.55	3.22	6.51	13.05	26.12

The static results of the simulation are given in table 6. All our results for the Wilson loops are consistent with the exact solution (B.4) in the infinite volume limit. Here only results for $W(\frac{L}{16}, \frac{L}{16})$ and $W(\frac{L}{8}, \frac{L}{8})$ are quoted, which are the loops of about the size of a correlation length squared. We observed that these loop sizes have the largest autocorrelation times among the Wilson loops.

In general we found a very fast decorrelation of subsequent configurations in the Markov chain. Typically the autocorrelation function $\rho(t)$ dropped to zero within errors after 3 – 5 measurements (see figure 15). Therefore it was impossible to look for an exponential regime in the decay of $\rho(t)$. We tried to estimate integrated autocorrelation times τ_{int} with a self consistent truncation window of $4\tau_{int}$ according to the method of ref. [48]. The results for the integrated autocorrelation times are given in table 7. Estimates for τ_{int} are only quoted if we observed that $\rho(t)$ was positive in the entire interval from $t = 0$ to $t = 4\tau_{int}$. Note that τ_{int} is defined such that $\tau_{int} = 0.5$ in the case of complete decorrelation. All our runs are longer than $30\,000\tau_{int}$.

In summary, all τ 's are smaller or consistent with one in the range of parameters studied, with a very weak tendency to increase with increasing lattice size. Due to the ambiguities of the estimation of τ in the situation of almost complete decorrelation, we do not want to give

an estimate for z here. We only state that the results indicate that CSD is almost completely eliminated by the time slice blocking algorithm.

Table 6: Static observables in the two dimensional $SU(2)$ lattice gauge theory on $L \times L$ lattices, $L/\xi \approx 10$.

L	statistics	discarded	$W(\frac{L}{16}, \frac{L}{16})$	$W(\frac{L}{8}, \frac{L}{8})$	\bar{P}	\bar{P}^2
16	100 000	10 000	0.65816(10)	0.18751(14)	0.0002(4)	0.01564(7)
32	100 000	10 000	0.67917(4)	0.21287(12)	0.0002(3)	0.00855(4)
64	50 000	10 000	0.68525(6)	0.2204(2)	-0.0003(5)	0.00610(5)
128	40 000	5 000	0.68688(6)	0.2222(3)	0.0008(9)	0.00545(8)
256	40 000	5 000	0.68720(7)	0.2232(2)	0.0001(6)	0.00519(4)

Table 7: Integrated autocorrelation times τ_{int} for the two dimensional $SU(2)$ lattice gauge theory on $L \times L$ lattices, $L/\xi \approx 10$. If no value is given, we found almost complete decorrelation.

L	statistics	discarded	$\tau_{int, W(\frac{L}{16}, \frac{L}{16})}$	$\tau_{int, W(\frac{L}{8}, \frac{L}{8})}$	$\tau_{int, \bar{P}}$	τ_{int, \bar{P}^2}
16	100 000	10 000	0.54(1)	-	-	-
32	100 000	10 000	-	0.60(1)	-	-
64	50 000	10 000	0.67(1)	0.70(1)	0.71(1)	0.59(1)
128	40 000	5 000	0.76(2)	0.74(2)	0.92(2)	-
256	40 000	5 000	0.88(3)	0.83(2)	1.01(3)	-

9.3 Summary

In this section we reported on a multigrid Monte Carlo simulation of $SU(2)$ lattice gauge theory in two dimensions. The time slice blocking algorithm with piecewise linear interpolation was implemented in the unigrid style with a V-cycle. We used a heat bath version in randomly chosen $U(1)$ subgroups. The simulations were performed on physically large lattices of the size $10\xi \times 10\xi$.

All observed integrated autocorrelation times are found to be smaller or consistent with one on lattice sizes up to 256^2 , with a very weak tendency to increase with increasing lattice size. Therefore we conclude that the time slice blocking algorithm eliminates CSD almost completely.

It is fair to say that we used a special feature of two dimensional lattice gauge theory: In the infinite volume limit or for open boundary conditions one can decouple two dimensional lattice gauge theory to a set of independent one dimensional spin models by choosing the axial gauge. Although we use periodic boundary conditions here, our method is very much in the spirit of updating on independent time slices.

It will be discussed in the next section whether this concept is still successful if we generalize it to four dimensions.

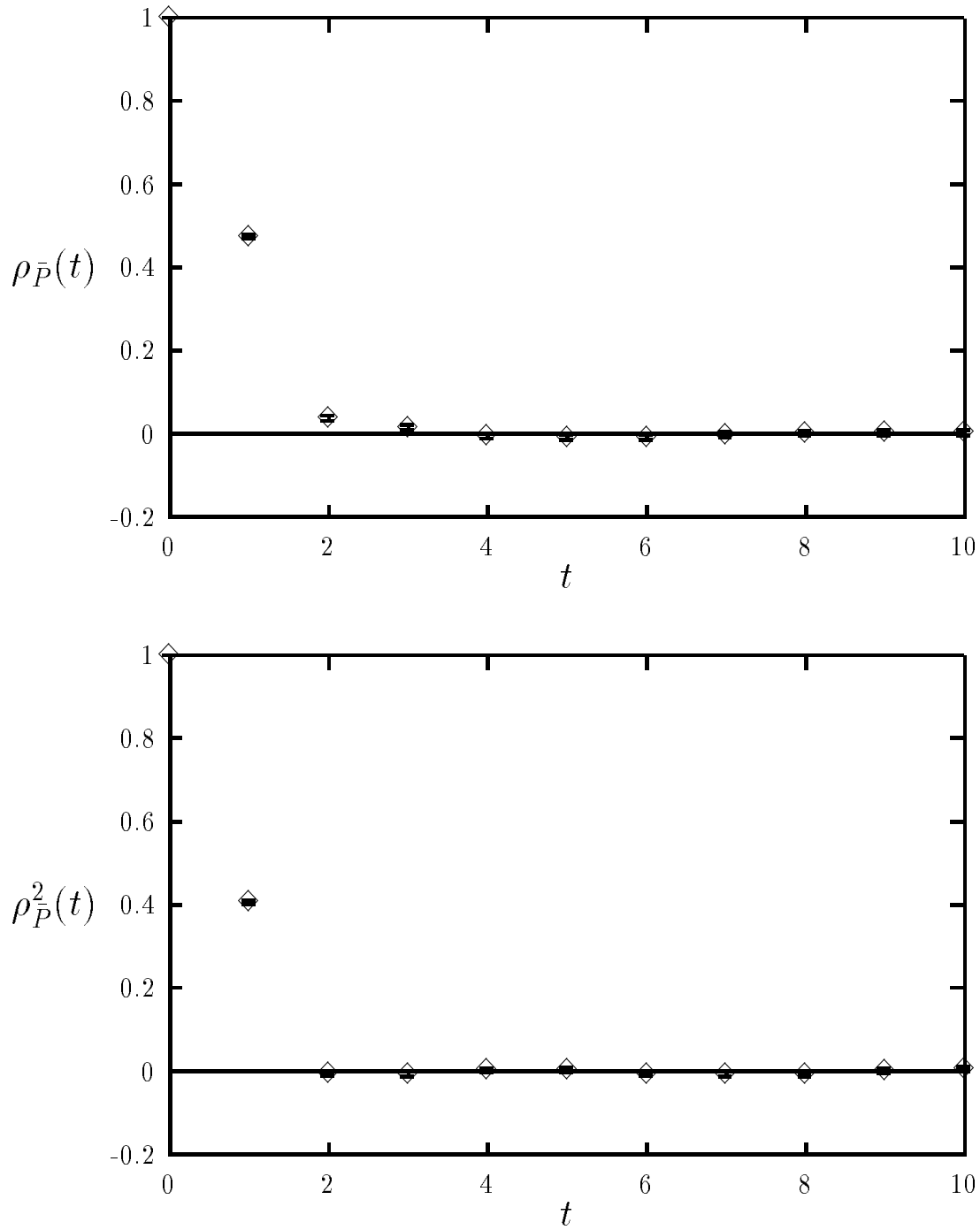


Figure 15: Autocorrelation functions $\rho(t)$ in the two dimensional $SU(2)$ pure lattice gauge theory, $\beta = 1024$ on a 256^2 lattice. Top: $\rho(t)$ for \bar{P} , bottom: $\rho(t)$ for \bar{P}^2 .

10 Multigrid methods for lattice gauge fields in four dimensions

In this section we generalize the multigrid procedure for pure lattice gauge theory from two dimensions to four dimensions. We start with a discussion of the abelian case.

For nonabelian gauge fields in four dimensions additional difficulties arise because of the more complicated geometrical structure of nonlocal updates in four dimensions compared to two dimensions. We study the behavior of acceptance rates with increasing block size L_B and analyze the special features of the algorithm in the four dimensional case in detail.

10.1 The abelian case

The generalization of the multigrid algorithm for $U(1)$ gauge fields of Laursen, Smit and Vink (as discussed in section 8) from two dimensions to higher dimensions is straightforward:

Nonlocal updates are formulated as follows: One chooses a hypercubic block x'_o of size L_B^d and a direction τ with $1 \leq \tau \leq d$. All the link variables $U_{x,\tau}$ attached to sites x inside the block x'_o are proposed to be changed simultaneously:

$$U_{x,\tau} \rightarrow \exp(is\psi_x)U_{x,\tau}, \quad (10.1)$$

or in terms of the link angles

$$\theta_{x,\tau} \rightarrow \theta_{x,\tau} + s\psi_x. \quad (10.2)$$

The kernel ψ obeys the normalization condition (2.8). The canonical dimension of the kernel ψ and of the angle θ is that of a vector potential, i.e. $(2-d)/2$ in d dimensions. The simplest choice for ψ is again a piecewise constant kernel,

$$\psi_x^{const} = \begin{cases} L_B^{(2-d)/2} & \text{for } x \in x'_o \\ 0 & \text{for } x \notin x'_o. \end{cases} \quad (10.3)$$

Let us now study the acceptance rates for these update proposals with the help of formula (3.8). We consider general kernels ψ . For $h_1 = \langle \Delta \mathcal{H} \rangle$ we find (cf. appendix A)

$$h_1 = \beta P \sum_{x \in \Lambda_0} \sum_{\mu \neq \tau} [1 - \cos(s(\psi_{x+\hat{\mu}} - \psi_x))] \quad , \quad (10.4)$$

with $P = \langle \text{Tr} U_P \rangle$.

Because of the statistical independence of adjacent time slices we choose ψ_x to be constant in the τ -direction, with the support of ψ in τ -direction restricted to the block x'_o . Then we obtain

$$h_1 = \beta P L_B \sum_{x \in \Lambda_t^\tau} \sum_{\mu \neq \tau} [1 - \cos(s(\psi_{x+\hat{\mu}} - \psi_x))] \quad . \quad (10.5)$$

For small s , this can be approximated by

$$h_1 \approx \frac{1}{2} s^2 \beta P L_B \sum_{x \in \Lambda_t^\tau} \sum_{\mu \neq \tau} (\psi_{x+\hat{\mu}} - \psi_x)^2 = \frac{1}{2} s^2 \beta P \alpha_{d-1} \quad , \quad (10.6)$$

with $\alpha_{d-1} = \langle \psi', -\Delta \psi' \rangle$. As in two dimensions ψ' denotes the kernel ψ , restricted to the $d-1$ dimensional time slice Λ_t^τ . We absorbed a factor $L_B^{1/2}$ in ψ' (now normalized as a $d-1$ dimensional kernel).

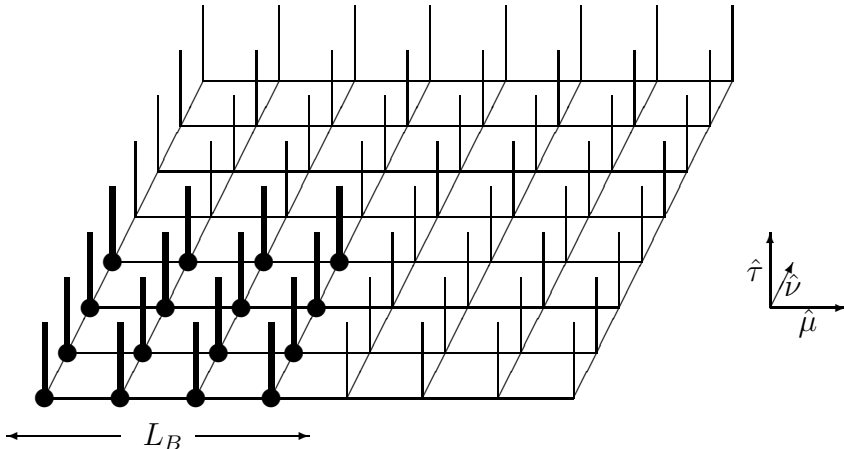


Figure 16: *Illustration of the geometry of time slice blocking in three dimensional lattice gauge theory.*

In the special case of piecewise constant kernels we find for h_1

$$h_1 = 2(d-1)\beta PL_B^{d-1}[1 - \cos(sL_B^{(2-d)/2})]. \quad (10.7)$$

From the kinematical point of view, the behavior of acceptance rates in the $U(1)$ lattice gauge theory in d dimensions is the same as in massless free field theory.

This multigrid algorithm with constant interpolation and a W-cycle was studied for the simulation of four dimensional $U(1)$ theory by Laursen and Vink [26]. In this model there is a deconfinement phase transition between a confinement phase and a Coulomb phase. The transition is believed to be of weakly first order [53]. The authors report on an acceleration of the Monte Carlo dynamics in both phases close to the transition point. This can be understood by our kinematical analysis. However the very low frequency of changes from one phase to the other on larger lattices in the simulation with a local algorithm could not be accelerated by the nonlocal updating. Like the topological problems in the XY -model and in the two dimensional $U(1)$ model, the problem of metastability can not be resolved from a purely kinematical point of view.

10.2 The nonabelian case: gauge group $SU(2)$

10.2.1 Covariant time slice blocking for $SU(2)$ in four dimensions

We now discuss a generalization of the covariant time slice blocking algorithm of section 8 from two dimensions to four dimensions. Many steps of the two dimensional method can be translated directly to the four dimensional case. Other features such as the nontrivial background field in the bottom of higher dimensional blocks will require a refined treatment.

Nonlocal updates can be defined as shown in figure 16 (for simplicity illustrated in three dimensions). Let us consider a fixed time direction τ with $1 \leq \tau \leq 4$ and a three dimensional time slice $\Lambda_t^\tau = \{x \in \Lambda_0 \mid x_\tau = t\}$. One chooses a cubic block x'_o of size L_B^3 that is contained in Λ_t^τ . All the link variables $U_{x,\tau}$ attached to sites x inside the block x'_o are proposed to be changed simultaneously:

$$U_{x,\tau} \rightarrow U'_{x,\tau} = R_x(g) U_{x,\tau}, \quad (10.8)$$

where $R_x(g) = g_x^* R_x g_x$ and $g_x \in SU(2)$. The rotation matrices $R_x \in SU(2)$ are again parametrized as

$$R_x(\vec{n}, s) = \cos(s\psi_x/2) + i \sin(s\psi_x/2) \vec{n} \cdot \vec{\sigma}, \quad (10.9)$$

where \vec{n} denotes a three-dimensional real unit vector, and the σ_i are Pauli matrices. ψ will have support on the three dimensional block x'_o .

Up to now the g -matrices are arbitrary. In the two dimensional case we have chosen them according to the block axial gauge (8.18): Choose the g -matrices in the one dimensional bottom of the block x'_o such that

$$U_{x,\mu}^g = g_x U_{x,\mu} g_{x+\hat{\mu}}^* = 1 \quad \text{for all } (x, x + \hat{\mu}) \in x'_o. \quad (10.10)$$

The gauge transformed link variables $U_{x,\mu}^g$ in the bottom of the block were equal to unity and for the case of piecewise constant interpolation the plaquettes in the interior of the block stayed unchanged (recall the discussion following figure 14). Therefore only the two plaquettes at the boundary of a block contributed to the energy change of a piecewise constant update. The energy cost was proportional to the surface of the block, not proportional to the volume of the block.

By choosing the block axial gauge in two dimensions we used the fact that we always can gauge link variables along a one dimensional open line to unity. Any nontrivial content of the gauge field in the one dimensional bottom of the block could be shifted outside of the block by applying the block axial gauge.

However in more than two dimensions, the bottom of a block will contain closed loops (see figure 16). Since a parallel transporter along a closed loop is gauge invariant, we can not get rid of the nontrivial curvature that is contained in the loop by any gauge transformation. Therefore for nontrivial gauge fields we can not find a gauge transformation g such that $U^g = 1$ for all link variables in the bottom of the block x'_o . This means that for nontrivial gauge fields all timelike plaquettes that share a link with the bottom of the block will contribute to the average energy change of the update.

The intuitive Leitmotiv for the development of new multigrid methods from section 6 was: *A piecewise constant update of a nonlocal domain should have energy costs proportional to the surface of the domain, but not energy costs proportional to the volume of the domain.*

Unfortunately, according to the discussion above, the nontrivial background field in the bottom of the block will lead to energy costs proportional to the volume of the block. Let us nevertheless attempt to have as little energy costs as possible:

Consider the extreme case of $\beta \rightarrow \infty$. Then the allowed configurations are pure gauges, i.e. configurations that are gauge equivalent to $U_{x,\mu} = 1$ for all x, μ . If we choose g as the transformation that brings all links to unity, it is obvious that the plaquettes in the interior of the block will not be changed by a piecewise constant update. In particular, to have this property, it is sufficient to gauge all links inside the bottom of the block to unity. This consideration leads to the following gauge condition: Choose g as the gauge transformation that maximizes the functional

$$G_{C,x'_o}(U, g) = \sum_{(x, x+\hat{\mu}) \in x'_o} \text{Tr}(g_x U_{x,\mu} g_{x+\hat{\mu}}^*). \quad (10.11)$$

We call this gauge “block Coulomb gauge”.³ For finite β this gauge will not bring all the links in the bottom of the block to unity, but still as close to unity as possible. Therefore the gauge

³ Gauge conditions on the lattice and their relation to transversality conditions for the gauge potential A are discussed in appendix C

field in the bottom of the block is as smooth as possible. This leads to a kind of minimization of the energy costs from the interior of the block. Note that in two dimensions the block Coulomb gauge condition reduces to the block axial gauge (8.18).

The main difference compared to the two dimensional case is that we have to expect that the energy change of the update will be proportional to the volume of the block x'_o . This property is caused by the fact that in four dimensions the gauge field in the bottom of the block is smooth but nonzero. This will lead to an algorithmic mass term that grows quadratic with the block dimension L_B . We are going to investigate the behavior of this algorithmic mass in detail below.

Let us summarize the steps of the nonlocal updating scheme for $SU(2)$ in four dimensions:

1. Choose a block x'_o of size L_B^3 that is contained in the time slice Λ_t^τ . All link variables $U_{x,\tau}$ pointing from sites x inside the block in τ -direction will be moved simultaneously.
2. Find the g -matrices defined by the block Coulomb gauge condition

$$G_{C,x'_o}(U, g) = \sum_{(x,x+\hat{\mu}) \in x'_o} \text{Tr}(g_x U_{x,\mu} g_{x+\hat{\mu}}^*) \stackrel{!}{=} \text{maximal}. \quad (10.12)$$

3. Propose new link variables $U'_{x,\tau}$ by

$$U_{x,\tau} \rightarrow U'_{x,\tau} = R_x(g) U_{x,\tau}, \quad (10.13)$$

with $R_x(g) = g_x^* R_x g_x$ and

$$R_x(\vec{n}, s) = \cos(s\psi_x/2) + i \sin(s\psi_x/2) \vec{n} \cdot \vec{\sigma}. \quad (10.14)$$

s is a uniformly distributed random number from the interval $[-\varepsilon, \varepsilon]$, and \vec{n} is a vector selected randomly from the three dimensional unit sphere.

4. Calculate the associated change of the Hamiltonian $\Delta\mathcal{H}$ and accept the proposed link variables with probability $\min[1, \exp(-\Delta\mathcal{H})]$.

The argument that the detailed balance condition is fulfilled by this updating scheme is analogous to two dimensions (cf. section 8). The only additional point is that although we only have an iterative gauge fixing algorithm in four dimensions, we do not have to fix the gauge perfectly. If we always use the same procedure in finding g (e.g. a given number of relaxation sweeps starting from $g = 1$), we will always get the same g and the nonlocal update is reversible.

The detailed implementation and simulation of nonlocal block updates will be described in section 11.

10.2.2 Acceptance analysis for nonlocal $SU(2)$ -updates

First numerical studies revealed that there is no substantial difference in the acceptance rates when instead of using the block Coulomb gauge condition one uses the Coulomb gauge condition for the whole slice Λ_t^τ :

$$G_C(U, g) = \sum_{(x,x+\hat{\mu}) \in \Lambda_t^\tau} \text{Tr}(g_x U_{x,\mu} g_{x+\hat{\mu}}^*) \stackrel{!}{=} \text{maximal}. \quad (10.15)$$

For a detailed discussion of Landau and Coulomb gauges on the lattice see appendix C. From a practical point of view the Coulomb gauge condition is very convenient: The g -matrices can be calculated once and then be used for all block sizes L_B . In the block Coulomb gauge they would have to be recalculated for every individual block lattice. In addition, the relaxation algorithm to determine the g -matrices according to the Coulomb gauge condition can be vectorized in a straightforward way.

The energy change associated with the update proposal (10.8) is

$$\Delta\mathcal{H} = -\frac{\beta}{2} \sum_{\mathcal{P}} \text{Tr}(U'_{\mathcal{P}} - U_{\mathcal{P}}) = -\frac{\beta}{2} \sum_{x \in \Lambda_{\vec{t}}} \sum_{\mu \neq \tau} \text{Tr}\{(R_x^* U_{x,\mu}^g R_{x+\hat{\mu}} - U_{x,\mu}^g) H_{x,\mu}^{g*}\}, \quad (10.16)$$

with $H_{x,\mu}^* = U_{x+\hat{\mu},\tau} U_{x+\hat{\tau},\mu}^* U_{x,\tau}^*$ and $U_{x,\mu}^g = g_x U_{x,\mu} g_{x+\hat{\mu}}^*$. H^g is defined analogously. The relevant quantity for the acceptance rates is $h_1 = \langle \Delta\mathcal{H} \rangle$. For piecewise constant kernels and the gauge condition (10.15) we get (cf. appendix A)

$$h_1 = 3\beta A (L_B - 1) L_B^2 \sin^2(sL_B^{-1/2}/2) + 6\beta P L_B^2 [1 - \cos(sL_B^{-1/2}/2)], \quad (10.17)$$

with

$$A = \langle \frac{1}{2} \text{Tr}((U_{x,\mu}^g - \vec{n} \cdot \vec{\sigma} U_{x,\mu}^g \vec{n} \cdot \vec{\sigma}) H_{x,\mu}^{g*}) \rangle, \quad (10.18)$$

$$P = \langle \frac{1}{2} \text{Tr} U_{\mathcal{P}} \rangle. \quad (10.19)$$

To the first term in eq. (10.17) all links contribute that are entirely inside the block, whereas the second term contains the contributions of all links that have one site in common with the surface of the block. For small s , the first term behaves like $s^2 L_B^2$. This is exactly the behavior of a mass term that, as we have learned in the previous sections, can be toxic for the multigrid algorithm. Note that the Coulomb gauge attempts to minimize this mass term by minimizing the quantity A . We identify the square root of βA with a “disorder mass” m_D ,

$$m_D = \sqrt{\beta A}. \quad (10.20)$$

To have a physical interpretation of m_D let us discuss the “disorder scale” l_D that is given by the inverse of the disorder mass:

$$l_D = \frac{1}{m_D} = \frac{1}{\sqrt{\beta A}}. \quad (10.21)$$

If the block size L_B gets of the order of the disorder scale l_D , the mass term in eq. (10.17) becomes of order one, and the amplitudes of the nonlocal moves become suppressed. Now the crucial question is: How does the scale l_D behave for large β in comparison with the physical correlation length ξ ? (ξ is given by the inverse glueball mass or the inverse square root of the string tension.) If l_D scaled with ξ the algorithm could efficiently create fluctuations up to the scale of ξ , as required by the physics of the model. Everything would be all right if for large ξ

$$\frac{l_D}{\xi} \xrightarrow{\beta \rightarrow \infty} \text{const}. \quad (10.22)$$

In 4-dimensional $SU(2)$ lattice gauge theory the correlation length is known to increase exponentially fast with β . Therefore, for eq. (10.22) to hold, we would need that the disorder mass m_D decreased exponentially fast with increasing β . Formulated differently, the crucial question is whether or not m_D scales like a physical mass.

10.2.3 Monte Carlo study of m_D

We computed m_D by Monte Carlo simulations for several values of β . To maximize G_C we used a standard Gauss-Seidel relaxation algorithm vectorized over a checkerboard structure. The relaxation procedure consists in going through the lattice and minimizing the gauge functional (10.15) locally. For production runs it would be advantageous to use an accelerated gauge fixing algorithm such as overrelaxation or multigrid [54, 55]. In the Monte Carlo studies reported in this section, we always used 50 Gauß-Seidel sweeps to determine g . Note that by this procedure G_C is not entirely maximized, especially on very large lattices where the relaxation algorithm suffers from CSD. However, for the detailed balance to be fulfilled, we only need that one uses always the same number of relaxation sweeps. Several tests revealed that increasing the number of relaxation sweeps beyond 50 did not affect the acceptance rates in a substantial way. In our implementation, 50 Gauß-Seidel sweeps over all slices of a given direction τ required the same CPU time (on a CRAY Y-MP) as four Creutz heat bath $SU(2)$ update sweeps.

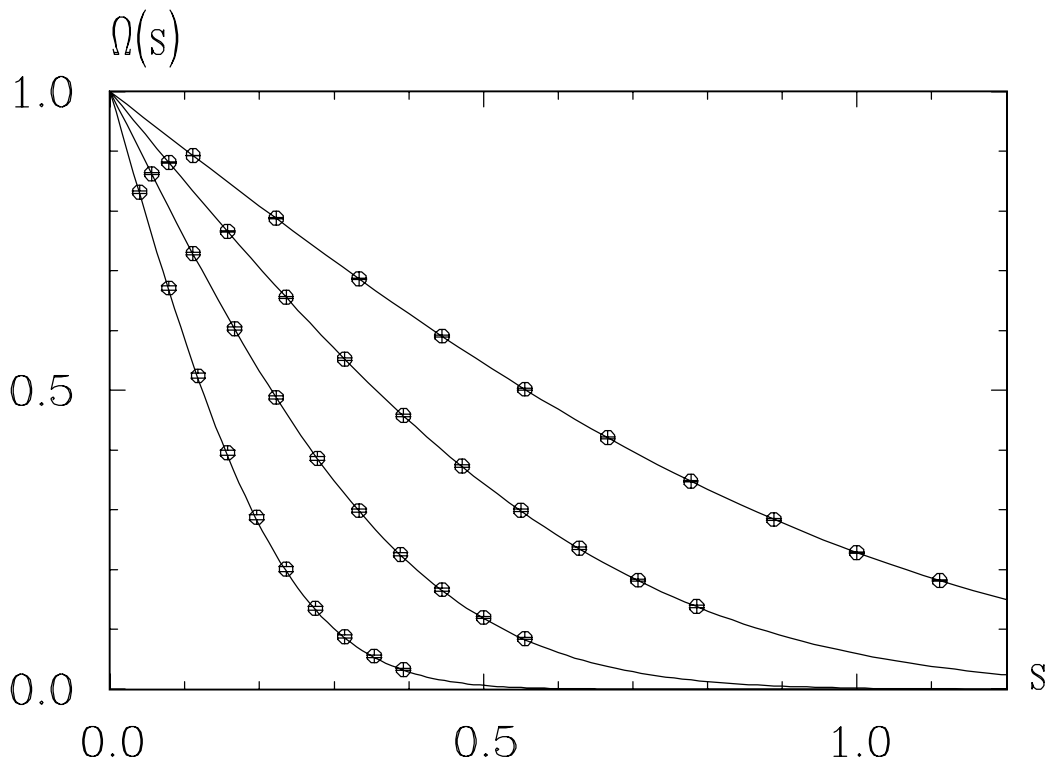


Figure 17: $\Omega(s)$ in 4-dimensional $SU(2)$ lattice gauge theory using piecewise constant kernels, $\beta = 2.6$ on a 20^4 -lattice. From top to bottom: $L_B = 2, 4, 8, 16$. Points with error bars: Monte Carlo results, lines: analytical results using m_D and P from Monte Carlo (errors smaller than line width).

We checked the validity of the acceptance formula (3.8) using Monte Carlo estimates for m_D and P . Figure 17 shows results for $\beta = 2.6$ on a 20^4 lattice. The results perfectly justify the usage of the approximation formula. It is therefore sufficient to study the behavior of the quantities m_D and P . Our Monte Carlo results are presented in table 8. The last column gives the statistics in sweeps (equilibration sweeps are not counted here). We used a mixture of four microcanonical overrelaxation sweeps followed by a single Creutz heat bath sweep. Measurements (including the determination of g) were performed every 25 sweeps.

Table 8: Monte Carlo results for m_D and P

lattice size	β	m_D	P	statistics
8^4	2.4	0.507(2)	0.6305(3)	10 000
12^4	2.4	0.4957(4)	0.6300(2)	10 000
16^4	2.4	0.4955(2)	0.62996(5)	10 000
8^4	2.6	0.497(4)	0.6703(1)	30 000
12^4	2.6	0.465(2)	0.6702(1)	20 000
16^4	2.6	0.4644(3)	0.67004(5)	10 000
20^4	2.6	0.4650(2)	0.67008(5)	5 000

Table 9: Comparison of m_D with physical masses

lattice size	β	m_D	$\sqrt{\kappa}$	m_{0+}	$m_D/\sqrt{\kappa}$	m_D/m_{0+}
16^4	2.4	0.4955(2)	0.258(2)	0.94(3)	1.92	0.53
20^4	2.6	0.4650(2)	0.125(4)	0.52(3)	3.72	0.89

In table 9 we display the ratios of the disorder mass m_D with two physical masses, the square root of the string tension κ and the lowest glue ball mass m_{0+} . The estimates for the physical masses are taken from ref. [56]. The results show that the disorder mass is nearly independent of β in the range studied, whereas the physical masses decrease by roughly a factor of two. Thus, m_D is not scaling like a physical mass for the couplings studied here. We conclude from this that for large blocks the term quadratic in L_B will strongly suppress the acceptance rates even when the ratio of correlation length and block size L_B is kept constant.

From this kinematical analysis it is clear that we can not expect that CSD will be eliminated by such nonlocal updates.

Let us give a plausibility argument for the large β behavior of $m_D = \sqrt{\beta A}$: From the definition (10.18) of A it is clear that A vanishes for large β because $U_{x,\mu}^g$ goes to unity in this limit. Since A is a quantity that is defined on the scale of the plaquette, it is dominated by the local disorder. A has nothing to do with collective excitations of the gauge field that are responsible for the formation of glueballs with a mass that decreases exponentially in β . The leading weak coupling behavior of the plaquette is [57]

$$P = 1 - \frac{3}{4\beta} + O\left(\frac{1}{\beta^2}\right). \quad (10.23)$$

Therefore it is natural to expect a weak coupling behavior for A like

$$A = \frac{c}{\beta} + O\left(\frac{1}{\beta^2}\right), \quad (10.24)$$

with a constant c . If this conjecture was true we would get

$$m_D = \sqrt{\beta A} \xrightarrow{\beta \rightarrow \infty} const. \quad (10.25)$$

In four dimensions the range of β values and lattice sizes studied here is too small to check the large β behavior of m_D in detail. Let us study the analogous situation in two dimensions.

10.2.4 Digression: Monte Carlo study of m_D in two dimensions

We want to study the kinematical effect of a remaining nontrivial background field $U_{x,\mu}$ for $\mu \neq \tau$ in the bottom of a block in two dimensions. This is of course an artificial complication of the situation in two dimensions. We always can choose the block coulomb gauge there, as we did in the previous sections. Nevertheless we can use the two dimensional case as a simple example where the region of large β is easily accessible, in contrast to four dimensions. In analogy to the four dimensional case we are going to take the g -matrices within a time slice according to the Coulomb gauge condition

$$G_C(U, g) = \sum_{(x, x+\hat{\mu}) \in \Lambda_t^\tau} \text{Tr}(g_x U_{x,\mu} g_{x+\hat{\mu}}^*) \stackrel{!}{=} \text{maximal} . \quad (10.26)$$

In two dimensions this maximization has a simple solution: Take the g -matrices such that

$$U_{x,\mu}^g = g_x U_{x,\mu} g_{x+\hat{\mu}}^* = P_t^{1/L} \text{ for all } x \in \Lambda_t^\tau . \quad (10.27)$$

P_t is the Polyakov loop in space direction,

$$P_t = \prod_{\substack{x_\mu=1 \\ x_\tau=t}}^L U_{x,\mu} \quad (10.28)$$

on a $L \times L$ lattice, and $P_t^{1/L}$ is the closest root to unity.

By taking the Coulomb gauge condition in two dimensions we now have a smooth but nontrivial background field in the bottom of the block. Let us study the effect on the kinematics. For piecewise constant interpolation we have (cf. appendix A)

$$h_1 = 2\beta P \left[1 - \cos \left(sL_B^{1/2} \right) \right] + \beta A (L_B - 1) \sin^2 \left(sL_B^{1/2} \right) , \quad (10.29)$$

with

$$A = \left\langle \frac{1}{2} \text{Tr} \left((U_{x,\mu}^g - \vec{n} \cdot \vec{\sigma} U_{x,\mu}^g \vec{n} \cdot \vec{\sigma}) H_{x,\mu}^{g*} \right) \right\rangle , \quad (10.30)$$

where g is taken according to eq. (10.26).

We computed A and $m_D = \sqrt{\beta A}$ by Monte Carlo simulations in the region of large β close to the continuum. Our Monte Carlo results are presented in table 10. The statistics are counted in sweeps (we started from equilibrated configurations). We used a mixture of four microcanonical overrelaxation sweeps followed by a single heat bath sweep. Measurements were performed every 5 sweeps.

The large β behavior of A is shown in figure 18. It is consistent with $A \sim 1/\beta$. In table 11 we display the ratios of the disorder mass m_D with the physical mass, the square root of the string tension κ . The values for the string tension are taken from the exact solution in the infinite volume limit (appendix B). The results show that the disorder mass in two dimension goes to a constant for large β , whereas the physical mass decreases like $1/\sqrt{\beta}$. Therefore, m_D is definitely not scaling like a physical mass in the continuum limit in two dimensions.

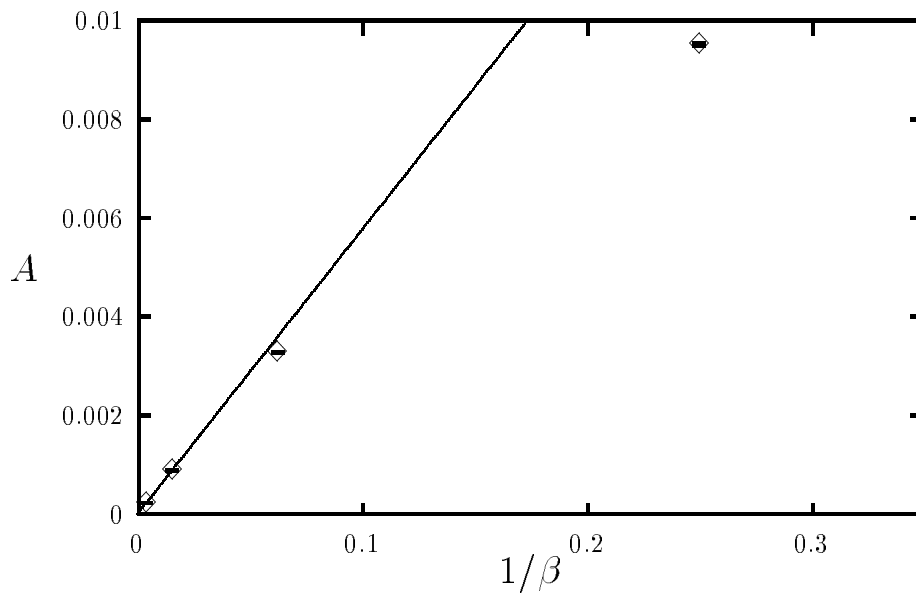


Figure 18: Dependence of the quantity A on $1/\beta$ in two dimensional $SU(2)$ lattice gauge theory. Diamonds: Monte Carlo results. The line corresponds to $A \sim 1/\beta$.

Table 10: Monte Carlo results for P , A and m_D in two dimensions

lattice size	β	P	A	m_D	statistics
8^2	1	0.2400(4)	0.01357(15)	0.1165(7)	20 000
16^2	4	0.65791(14)	0.00951(3)	0.1950(4)	20 000
32^2	16	0.90783(2)	0.003284(6)	0.2292(2)	20 000
64^2	64	0.976655(3)	0.000887(1)	0.2383(2)	20 000
128^2	256	0.9941462(3)	0.000225(2)	0.2400(1)	20 000

Table 11: Comparison of m_D with physical masses in two dimensions

lattice size	β	ξ	m_D	$\sqrt{\kappa}$	$m_D/\sqrt{\kappa}$
8^2	1	0.8373	0.1165(7)	1.1942	0.0976
16^2	4	1.5458	0.1950(4)	0.6469	0.301
32^2	16	3.2155	0.2292(2)	0.3110	0.737
64^2	64	6.5065	0.2383(2)	0.1536	1.55
128^2	256	13.0511	0.2400(1)	0.0766	3.13

We conclude from this that for large blocks the term quadratic in L_B will strongly suppress the acceptance rates also in two dimensions. Therefore the smooth but nontrivial background field in the coulomb gauge that is still left in the one dimensional bottom of the time slice will cause CSD in this variant of the algorithm.

In analogy to this result in two dimensions we expect the same behavior of m_D in the large β limit in four dimensions.

10.2.5 Comparison of volume and surface effects in four dimensions

By the kinematical analysis in four dimensions we found that CSD has to be expected because of a mass m_D generated by the local disorder in the bottom of the blocks. However, one could hope that the value of the unwanted mass term is so small that it is only harmful at very large values of β on huge lattices. Let us examine the effect of this term in more detail.

Recall that h_1 is built up from two contributions. The first contribution is that related to the gauge field disorder inside the block and is quantitatively represented by the mass m_D . The second contribution is associated with the block surface. The latter can of course be made smaller by using smooth kernels ψ instead of the piecewise constant kernels discussed so far. However, the disorder term cannot be expected to become smaller for smooth kernels (see below). In figure 19 we plotted separately the two contributions to h_1

$$\begin{aligned}
 h_{1,A} &= 3\beta A (L_B - 1) L_B^2 \sin^2(sL_B^{-1/2}/2), \\
 h_{1,P} &= 6\beta P L_B^2 (1 - \cos(sL_B^{-1/2}/2)),
 \end{aligned}
 \tag{10.31}$$

for $\beta = 2.6$ and block size $L_B = 8$ on a 20^4 lattice. The plot shows that already for this block

size the disorder contribution is by no means small – it is comparable to the surface effect. It is therefore not clear that one could achieve any significant improvement by using smooth kernels. To investigate this in more detail, we derive an expression for h_1 (cf. appendix A), valid for smooth kernels as well:

$$h_1 = \frac{3\beta}{4}s^2A \sum_{x \in \Lambda_t^\tau} \psi_x^2 + \frac{\beta}{8}s^2(P - A)\alpha_3 + O(s^4). \quad (10.32)$$

Since $\sum \psi_x^2 \sim L_B^2$, we get essentially the same behavior for the disorder contribution as in the case of piecewise constant kernels.

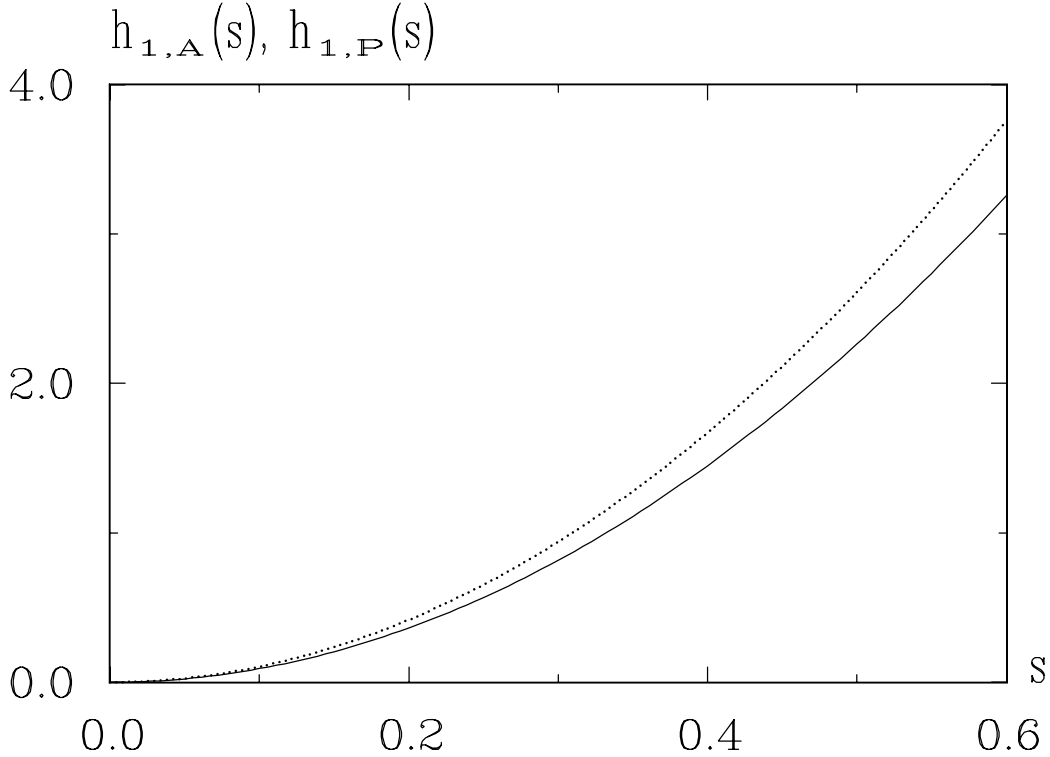


Figure 19: Comparison of disorder and surface effects for four dimensional $SU(2)$ lattice gauge theory using piecewise constant kernels on an 8^3 -block, $\beta = 2.6$ on a 20^4 -lattice. Solid line: $h_{1,A}(s)$ (disorder effects), dashed line: $h_{1,P}(s)$ (surface effects).

We checked this quadratic approximation against the exact expression (10.17) in the case of piecewise constant kernels. For $L_B = 8$ the deviations are already negligible in the range of s -values displayed in figure 19. For smooth ψ^{sine} kernels we show separately in figure 20 the two contributions to h_1

$$h_{1,A} = \frac{3\beta}{4}s^2A \sum_{x \in \Lambda_t^\tau} \psi_x^2, \quad h_{1,P-A} = \frac{\beta}{8}s^2(P - A)\alpha_3, \quad (10.33)$$

for $\beta = 2.6$ and block size $L_B = 8$ on a 20^4 lattice. We observe that the surface effects are lowered by the smooth kernels, but the disorder contribution is even higher than for piecewise constant kernels.

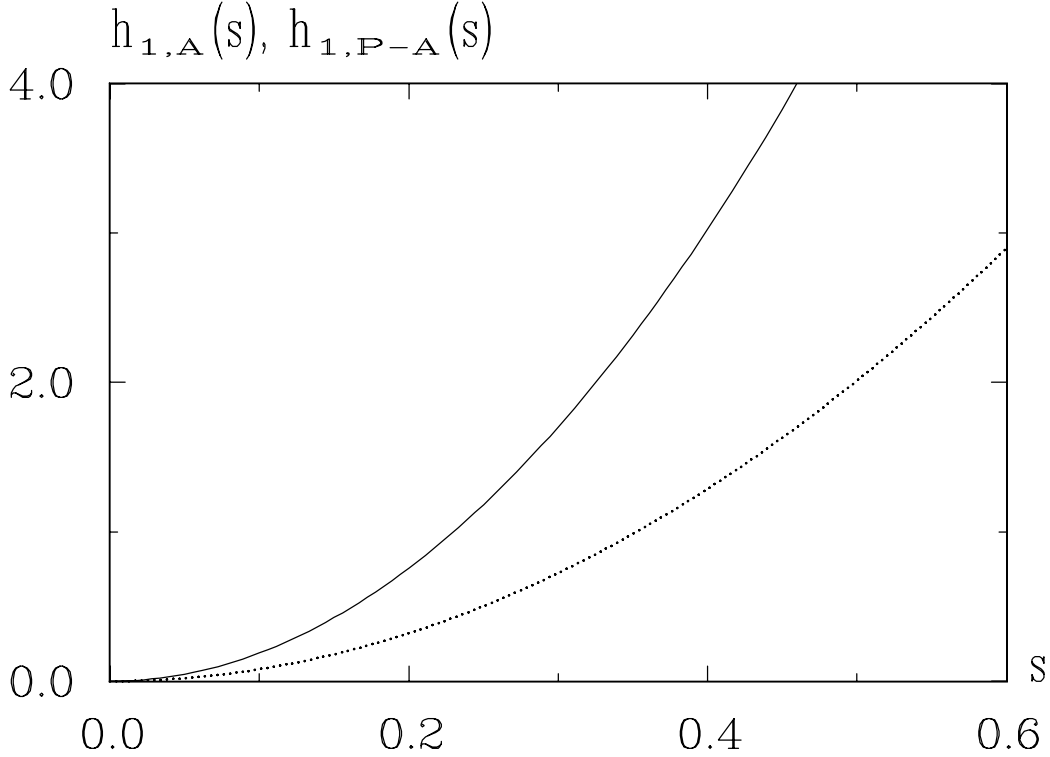


Figure 20: Comparison of disorder and surface effects for the four dimensional $SU(2)$ lattice gauge theory using smooth ψ^{sine} kernels on a 8^3 -block, $\beta = 2.6$ on a 20^4 -lattice, quadratic approximation used. Solid line: $h_{1,A}(s)$ (disorder effects), dashed line: $h_{1,P-A}(s)$ (surface effects).

Piecewise constant kernels have the practical feature that once the change of the Hamiltonian has been calculated, one can perform multihit Metropolis updating or microcanonical overrelaxation. In a special case, even a recursive multigrid implementation with a W-cycle is possible (see section 11 below). For smooth kernels the change in the Hamiltonian would have to be calculated again and again. Also the advantages of smooth kernels are not that clear on small three or four dimensional blocks. For the concrete simulation we will use piecewise constant kernels.

10.2.6 Maximally abelian gauge

Our proposal for the choice for g was motivated by the desire to minimize the quantity A . We now ask whether there is a better choice for g than the g determined by the Coulomb gauge condition. For the sake of simplicity let us take $\vec{n} = (0, 0, 1)$, i.e. $\vec{n} \cdot \vec{\sigma} = \sigma_3$. Then A is given by

$$A = \langle \frac{1}{2} \text{Tr}((U_{x,\mu}^g - \sigma_3 U_{x,\mu}^g \sigma_3) H_{x,\mu}^{g*}) \rangle. \quad (10.34)$$

The choice of the Coulomb gauge condition aimed at bringing $U_{x,\mu}^g$ as close to unity as possible. Alternatively, one might require that $U_{x,\mu}^g$ should be as close as possible to a $SU(2)$ -matrix of the form $a_0 + ia_3 \sigma_3$. This will also lead to a small A . The corresponding gauge transformation g can be found by maximizing the functional

$$G_A(U, g) = \sum_{(x, x+\hat{\mu}) \in \Lambda_t^{\tau}} \text{Tr}(\sigma_3 U_{x,\mu}^g \sigma_3 U_{x,\mu}^{g*}), \quad (10.35)$$

leading to the maximally abelian gauge [58], here implemented only on a slice. We computed m_D also using the g 's resulting from this gauge condition and compared the results with the ones obtained by using the Coulomb gauge condition. We did not find a substantial difference. We prefer the Coulomb gauge condition because it does not depend on the direction \vec{n} and thus saves computer time.

10.3 Summary

In this section we discussed the generalization of multigrid Monte Carlo methods for the simulation of pure gauge fields from two dimensions to four dimensions.

In the abelian case the generalization is straightforward. We have seen that the kinematical behavior of the resulting method is similar to massless free field theory. Therefore a considerable acceleration can be expected and was indeed observed in four dimensional $U(1)$ lattice gauge theory [26]. However, metastability causes additional problems close to the phase transition which can not be understood in terms of our method.

In the second part of this section we have generalized the time slice blocking algorithm that lead to successful acceleration of the simulation of $SU(2)$ gauge fields in two dimensions to four dimensions. In four dimensions, new difficulties occur that are due to the nontrivial background field in the bottom of the blocks. We investigated the scale dependence of acceptance rates in detail. Here we found that an algorithmic mass term generated by the disorder in the background field suppresses the acceptance rates on large blocks. From our kinematical analysis we can not expect that the proposed algorithm will have a chance to reduce the dynamical critical exponent below $z \approx 2$. However, compared to local Monte Carlo algorithms there could still be an acceleration of the dynamics by a constant factor, depending on the details of the implementation. This question will be investigated in the following section.

11 Multigrid Monte Carlo simulation of $SU(2)$ lattice gauge fields in four dimensions

In this section we study whether our nonlocal Monte Carlo updating can accelerate the Monte Carlo dynamics of a local heat bath algorithm by a constant factor. We do not aim at estimating the dynamical critical exponent z .

We begin with a description of the implementation of the time slice blocking scheme for $SU(2)$ in four dimensions as a recursive multigrid algorithm with piecewise constant interpolation and a W-cycle. Then we give a detailed report on a comparison of the time slice blocking algorithm with the local heat bath algorithm.

11.1 Implementation of the time slice blocking

For a concrete implementation of the multigrid Monte Carlo algorithm in four dimensions we choose the time slice blocking method: In a basic time slice blocking step, all links pointing from a given three dimensional time slice Λ_t^τ in the τ -direction are going to be updated. First we are going to describe the implementation of such a basic step for a given time slice Λ_t^τ . In particular we explain a recursive multigrid procedure that can be constructed by updating in a global $U(1)$ subgroup of $SU(2)$. How time slice blocking steps are applied to different time slices Λ_t^τ and to different orientations τ in sequence will be explained in a second paragraph.

11.1.1 Organization of a basic time slice blocking step

We now describe the time slice blocking method for a fixed three dimensional time slice $\Lambda_t^\tau = \{x \in \Lambda_0 \mid x_\tau = t\}$.

The basic updating step is based on a local, site dependent “rotation” of all link variables pointing from sites $x \in \Lambda_t^\tau$ in the τ -direction by

$$U_{x,\tau} \rightarrow U'_{x,\tau} = R_x(g) U_{x,\tau}, \quad (11.1)$$

with $R_x(g) = g_x^* R_x g_x$ and

$$R_x(\vec{n}_x, \theta_x) = \cos(\theta_x) + i \sin(\theta_x) \vec{n}_x \cdot \vec{\sigma}. \quad (11.2)$$

The gauge transformation g is obtained by imposing the Coulomb gauge condition (10.15) on slices Λ_t^τ as defined in section 10.

We are interested in a recursive multigrid implementation. Therefore we use piecewise constant kernels and update a fixed $U(1)$ subgroup of $SU(2)$ globally. In this special case an explicit multigrid scheme can be constructed. This feature was explained in ref. [26] in a related context.

The restriction to a global $U(1)$ subgroup is defined by taking the directions \vec{n}_x of the embedded $U(1)$ -subgroups to be independent of the site x within the time slice, i.e. $\vec{n}_x = \vec{n}$ for all $x \in \Lambda_t^\tau$. The global \vec{n} direction is taken as a random vector from the three dimensional unit sphere. Then a conditional Hamiltonian on the finest lattice can be calculated by substituting the “rotated” gauge field U' in the fundamental Hamiltonian. The resulting conditional Hamiltonian $\mathcal{H}_0(S)$ is of the type of a generalized three dimensional XY-model:

$$-\mathcal{H}_0(S) = \sum_{x \in \Lambda_t^\tau} \sum_{\mu \neq \tau} S_x^T B_{x,\mu} S_{x+\hat{\mu}} + const, \quad (11.3)$$

where S_x denotes the XY -spin variable

$$S_x = \begin{pmatrix} \cos(\theta_x) \\ \sin(\theta_x) \end{pmatrix}, \quad (11.4)$$

and S_x^T its transpose. $B_{x,\mu}$ is a link dependent real 2×2 matrix

$$B_{x,\mu} = \begin{pmatrix} B_{x,\mu}^{11} & B_{x,\mu}^{12} \\ B_{x,\mu}^{21} & B_{x,\mu}^{22} \end{pmatrix} \quad (11.5)$$

with the matrix elements

$$\begin{aligned} B_{x,\mu}^{11} &= \frac{\beta}{2} \text{Tr} \left(U_{x,\mu}^g H_{x,\mu}^{g*} \right), \\ B_{x,\mu}^{12} &= \frac{\beta}{2} \text{Tr} \left(U_{x,\mu}^g i\vec{n} \cdot \vec{\sigma} H_{x,\mu}^{g*} \right), \\ B_{x,\mu}^{21} &= -\frac{\beta}{2} \text{Tr} \left(i\vec{n} \cdot \vec{\sigma} U_{x,\mu}^g H_{x,\mu}^{g*} \right), \\ B_{x,\mu}^{22} &= -\frac{\beta}{2} \text{Tr} \left(i\vec{n} \cdot \vec{\sigma} U_{x,\mu}^g i\vec{n} \cdot \vec{\sigma} H_{x,\mu}^{g*} \right). \end{aligned} \quad (11.6)$$

Now we set up a recursive multigrid procedure to update the three dimensional generalized XY -model on a time slice Λ_t^r . The first blocking step is performed by dividing the fine lattice Λ_t^r in cubic blocks x' of size 2^3 . This defines a three dimensional block lattice Λ_1 . Then a nonlocal block update consists of a constant rotation of all XY -spins S_x within a three dimensional block $x' \in \Lambda_1$ by the block angle $\theta_{x'}$:

$$S_x = \begin{pmatrix} \cos(\theta_x) \\ \sin(\theta_x) \end{pmatrix} \rightarrow S'_x = \begin{pmatrix} \cos(\theta_x + \theta_{x'}) \\ \sin(\theta_x + \theta_{x'}) \end{pmatrix} \text{ for } x \in x'. \quad (11.7)$$

An equivalent parametrization of this update is

$$S_x \rightarrow S'_x = A_x S_{x'}, \quad (11.8)$$

where the $SO(2)$ -matrix A_x and the block- XY -spin $S_{x'}$ are given by

$$A_x = \begin{pmatrix} \cos(\theta_x) & -\sin(\theta_x) \\ \sin(\theta_x) & \cos(\theta_x) \end{pmatrix}, \quad S_{x'} = \begin{pmatrix} \cos(\theta_{x'}) \\ \sin(\theta_{x'}) \end{pmatrix}. \quad (11.9)$$

By iterating this procedure one gets conditional Hamiltonians $\mathcal{H}_k(S)$ on three dimensional coarser layers Λ_k . An important point is that in the special case considered here $\mathcal{H}_k(S)$ always stays of the form

$$-\mathcal{H}_k(S) = \sum_{x \in \Lambda_k} \sum_{\mu \neq \tau} S_x^T B_{x,\mu} S_{x+\mu} + \sum_{x \in \Lambda_k} S_x^T M_x S_x + \text{const} \quad (11.10)$$

with 2×2 coupling matrices $B_{x,\mu}$ and M_x that depend on the links (x, μ) and on the sites x in Λ_k respectively. The coupling matrices $B_{x',\mu}$ and $M_{x'}$ that depend on the block links (x', μ) or blocks x' on the next coarser lattice Λ_{k+1} can be calculated recursively:

$$\begin{aligned} B_{x',\mu} &= \sum_{\substack{x \in x' \\ x+\hat{\mu} \in x'+\hat{\mu}}} A_x^T B_{x,\mu} A_{x+\hat{\mu}} \\ M_{x'} &= \sum_{\substack{x \in x' \\ x+\hat{\mu} \in x'}} A_x^T B_{x,\mu} A_{x+\hat{\mu}} + \sum_{x \in x'} A_x^T M_x A_x. \end{aligned} \quad (11.11)$$

Here $x' + \hat{\mu}$ denotes the next neighbor block of the block x' in the coarse layer Λ_{k+1} . Note that by the recursion the conditional Hamiltonian $\mathcal{H}_k(S)$ on a coarser layer Λ_k contains not only next neighbor couplings of the XY-variables (as the conditional Hamiltonian $\mathcal{H}_0(S)$ in eq. (11.3) on the finest lattice) but also site-site couplings of the type of a mass term with site dependent mass matrix M_x . The algorithmic mass term discussed in section 10 that leads to a decrease of acceptance rates on large blocks originates exactly from this site-site term in the conditional Hamiltonian.

This recursive blocking procedure is repeated until we end up with the coarsest layer that consists of a single point. (I. e. in our simulation on a 8^4 -lattice we are going to update on block lattices of the size 4^3 , 2^3 and 1^3 .)

After a blocking step to a coarser layer Λ_{k+1} the initial configuration on this coarse layer is

$$\theta_{x'} = 0 \Leftrightarrow S_{x'} = \begin{pmatrix} 1 \\ 0 \end{pmatrix} \text{ for all } x' \in \Lambda_{k+1} . \quad (11.12)$$

On each layer we perform one sweep of 10 Hit Metropolis updates in terms of the θ_x variables:

$$\theta_x \rightarrow \theta'_x = \theta_x + \Delta\theta , \quad (11.13)$$

where $\Delta\theta$ is taken to be equally distributed from the interval $[-\varepsilon, \varepsilon]$. We tuned the Metropolis step size ε in order to obtain acceptance rates of $\approx 50\%$ on each layer. If we return from a coarse layer Λ_{k+1} to the next finer layer Λ_k , the configuration $\{S\}$ on the finer layer is updated according to eq. (11.7).

In this implementation, the sequence of visiting the different three dimensional layers of a time slice is organized according to a W-cycle. From the point of view of numerical work this is possible because of the recursive definition of the algorithm. In principle the described implementation is not only feasible in the time slice blocking formulation but also with hypercubic four dimensional blocks.

11.1.2 Sequence of basic time slice blocking steps

The sequence of the updating on different time slices is as follows: On an L^4 -lattice we visit the L time slices Λ_t^1 , $t = 1, \dots, L$. In this way, all link variables $U_{x,1}$ on the lattice that point in the 1-direction are updated in a nonlocal way on block lattices with $L_B = 2, 4, \dots$. Then we perform a local Creutz heat bath sweep through all links on the lattice. Now we change the time direction τ from $\tau = 1$ to $\tau = 2$: We visit the L time slices Λ_t^2 , $t = 1, \dots, L$, again followed by a sweep of local heat bath updates. The same scheme (a visit of all time slices and a local heat bath sweep) is repeated also for the $\tau = 3$ and $\tau = 4$ direction, such that all the link variables $U_{x,\tau}$ have been updated in a nonlocal manner for all $\tau = 1, \dots, 4$. This sequence is repeated periodically.

Observables are measured after each local heat bath sweep. In addition, we perform a random translation of the lattice after each local heat bath sweep in order to avoid effects from fixed block boundaries [16].

To reduce the computer time needed for gauge fixing we use a slight modification: If all the link variables $U_{x,\mu}$ with $\mu \neq \tau$ lying in the bottom of the time slice Λ_t^τ have been gauged according to the Coulomb gauge condition, we update not only the link variables $U_{x,\tau}$ pointing from this time slice in the positive τ -direction, but we update also the links pointing from this time slice to the negative τ -direction. Thus, only every second time slice Λ_t^τ has to be gauged. This leads to a decrease of the numerical work required for gauge fixing by a factor of two.

11.2 Simulation and Results

11.2.1 Observables

The observables measured are square Wilson loops

$$W(I, I) = \langle \frac{1}{2} \text{Tr}(U(C_{I,I})) \rangle, \quad (11.14)$$

where $U(C_{I,I})$ is the parallel transporter around a rectangular Wilson loop $C_{I,I}$ of size $I \times I$. On the 8^4 -lattice we measure $W(1, 1)$, $W(2, 2)$, and $W(4, 4)$. Another important class of quantities is built up from timelike Polyakov loops. A Polyakov loop at the three dimensional spatial point \vec{x} is defined by

$$P_{\vec{x}} = \frac{1}{2} \text{Tr} \prod_{t=1}^L U_{(\vec{x}, t), 4}. \quad (11.15)$$

We measure the lattice averaged Polyakov loop

$$\bar{P} = \left\langle \frac{1}{L^3} \sum_{\vec{x}} P_{\vec{x}} \right\rangle, \quad (11.16)$$

the lattice averaged Polyakov loop squared

$$\bar{P}^2 = \left\langle \left(\frac{1}{L^3} \sum_{\vec{x}} P_{\vec{x}} \right)^2 \right\rangle, \quad (11.17)$$

and the sign of the lattice averaged Polyakov loop

$$\text{sign}(\bar{P}) = \left\langle \text{sign} \left(\frac{1}{L^3} \sum_{\vec{x}} P_{\vec{x}} \right) \right\rangle. \quad (11.18)$$

11.2.2 Run parameters and static results

In order to study the acceleration by the multigrid algorithm, we compare the autocorrelations of the nonlocal algorithm with a standard local Creutz heat bath algorithm. Precise measurements of autocorrelation times τ require high statistics simulations with run lengths of at least $1000\tau - 10\,000\tau$. For reasons of computer time we decided to simulate on relatively small lattices. The algorithms are compared on a 8^4 -lattice at $\beta = 2.2, 2.4$ and 2.6 . We started the local heat bath runs from ordered configurations (all link variables set equal to unity) and discarded a suitable number of iterations for equilibration. For the multigrid simulations we used warm starts from already equilibrated configurations. Measurements were taken after each local heat bath sweep.

In order to reduce the computer time needed for gauge fixing, we use 10 sweeps of overrelaxation [54] with overrelaxation parameter $\omega = 1.7$. The degree of maximization of the Coulomb gauge functional G_C (10.15) was found to be about the same as if we used 50 Gauß-Seidel relaxation sweeps.

With these run parameters the computer time needed by our implementation on a CRAY Y-MP for one measurement on the 8^4 -lattice by the multigrid procedure is about a factor of 2.8 larger than the time needed for one measurement by the Creutz heat bath algorithm. This factor could still be lowered by using a multigrid method for gauge fixing [55].

The static results of our runs are given in table 12. The values for the heat bath and for the multigrid algorithm agree within errors. Where a comparison is possible, our results for the Wilson loop observables are consistent with existing data in the literature [59].

Table 12: Comparison of numerical results for various static observables of heat bath (HB) and multigrid (MG) simulations on the 8^4 lattice.

β	2.2		2.4		2.6	
algorithm	HB	MG	HB	MG	HB	MG
statistics	100 000	50 000	100 000	100 000	100 000	100 000
discarded	10 000	equi.	10 000	equi.	10 000	equi.
$W(1, 1)$	0.56922(5)	0.56917(9)	0.63024(3)	0.63026(3)	0.67029(2)	0.67029(2)
$W(2, 2)$	0.13628(7)	0.13625(10)	0.22319(11)	0.22330(13)	0.28875(7)	0.28877(5)
$W(4, 4)$	0.00127(3)	0.00132(4)	0.01371(7)	0.01379(6)	0.03762(8)	0.03770(6)
\bar{P}	0.00006(13)	0.00015(18)	-0.0020(16)	-0.00006(13)	0.008(8)	0.002(6)
\bar{P}^2	0.000584(3)	0.000580(4)	0.00211(5)	0.00202(5)	0.0092(2)	0.0096(2)
$\text{sign}(\bar{P})$	0.0000(2)	0.0002(3)	-0.004(3)	-0.000(2)	0.013(13)	0.003(11)

11.2.3 Autocorrelation times

Table 13: Comparison of the exponential autocorrelation times of heat bath (HB) and multigrid (MG) simulations for different observables on the 8^4 lattice.

β	2.2		2.4		2.6	
algorithm	HB	MG	HB	MG	HB	MG
statistics	100 000	50 000	100 000	100 000	100 000	100 000
discarded	10 000	equi.	10 000	equi.	10 000	equi.
$\tau_{W(1,1)}$	6.9(2.9)	10.3(3.5)	5.7(1.5)	13(9)	1.8(6)	1.9(1.0)
$\tau_{W(2,2)}$	6.9(1.7)	8.0(1.8)	26(6)	35(7)	4.0(1.2)	2.9(6)
$\tau_{W(4,4)}$	≈ 1.3	≈ 1.3	22(3)	26(3)	10.4(1.8)	10.3(2.4)
$\tau_{\bar{P}}$	3.3(5)	3.8(6)	93(13)	67(4)	279(45)	274(33)
$\tau_{\bar{P}^2}$	1.0(3)	≈ 1.3	35(4)	32(6)	48(8)	46(6)
$\tau_{\text{sign}(\bar{P})}$	5.3(1.2)	5.2(1.3)	92(13)	68(6)	275(41)	277(39)

The results for the autocorrelation times are given in table 13. For the observables with the longest autocorrelation times \bar{P} and $\text{sign}(\bar{P})$, we give a comparison of the autocorrelation functions of the multigrid algorithm with the heat bath algorithm for $\beta = 2.2, 2.4$ and 2.6 in figures 21, 22 and 23.

Note that the autocorrelation functions $\rho(t)$ do not in general show a pure exponential decay but exhibit a crossover from a fast mode to a slow mode that eventually governs the asymptotic decay for large t . Therefore the measurement of the integrated autocorrelation time τ_{int} with a self consistent truncation window of $4\tau_{int}$ might not capture the asymptotic

decay of $\rho(t)$ correctly. In the present case we decided to extract a rough estimate of the exponential autocorrelation time τ_{exp} and the corresponding errors by the following procedure: We plotted the $\rho(t)$ with error bars on a logarithmic scale and decided at what value of t the asymptotic exponential behavior started. Then we drew the highest and lowest straight lines that were compatible with the data in the asymptotic regime. The errors are given such that the highest and the lowest value of τ_{exp} lie at the ends of the interval result \pm error.

All our results for the exponential autocorrelation times τ_{exp} of the multigrid and the heat bath algorithm are compatible within errors except from τ_{exp} for \bar{P} and $\text{sign}(\bar{P})$ at $\beta = 2.4$, see also figure 22. In this case the superficial gain of the multigrid algorithm is a factor of 1.4. However the computational overhead of the multigrid method compared to the heat bath algorithm (a factor of 2.8 in our implementation) was not yet taken into account. So there is no net gain in computer time also in the case of $\beta = 2.4$.

11.3 Summary

In this section we studied an implementation of the multigrid Monte Carlo algorithm in four dimensions. We used the time slice blocking method and piecewise constant interpolation with a W-cycle in a recursive multigrid version by updating in $U(1)$ subgroups of $SU(2)$. Simulations with gauge couplings $\beta = 2.2, 2.4$ and 2.6 were performed on an 8^4 -lattice.

Apart from a modest acceleration of Polyakov loop observables at $\beta = 2.4$ by a factor of 1.4, no improvement was found compared to a local heat bath algorithm. Since the nonlocal update procedure has a computational overhead of a factor of 2.8 on the 8^4 -lattice (on a CRAY Y-MP), there is no net gain but even a loss in CPU-time. This factor depends however on the details of the implementation.

Since from the theoretical analysis (section 10) one can not expect a lower dynamical critical exponent z , there is no hope that on larger lattices the method will perform better.

Possible improvements of our nonlocal updating scheme were investigated by Gutbrod [60]. Starting from the Coulomb gauge, he uses an additional smoothing by taking a quadratic approximation to the action and updating in terms of approximate eigenfunctions. The resulting nonlocal updates are performed as (approximately) microcanonical overrelaxation steps. Asymmetric lattices of size L^3T with $T \gg L$ and anisotropic couplings (e.g. $\beta = 4.5$ in the time direction and $\beta = 3.0$ in the space directions) are used. The results indicate a superficial gain of a factor of 1.5 – 3 compared to a local overrelaxation algorithm. However if the (implementation dependent) computational overhead of the nonlocal method is taken into account, the net gain is marginal.

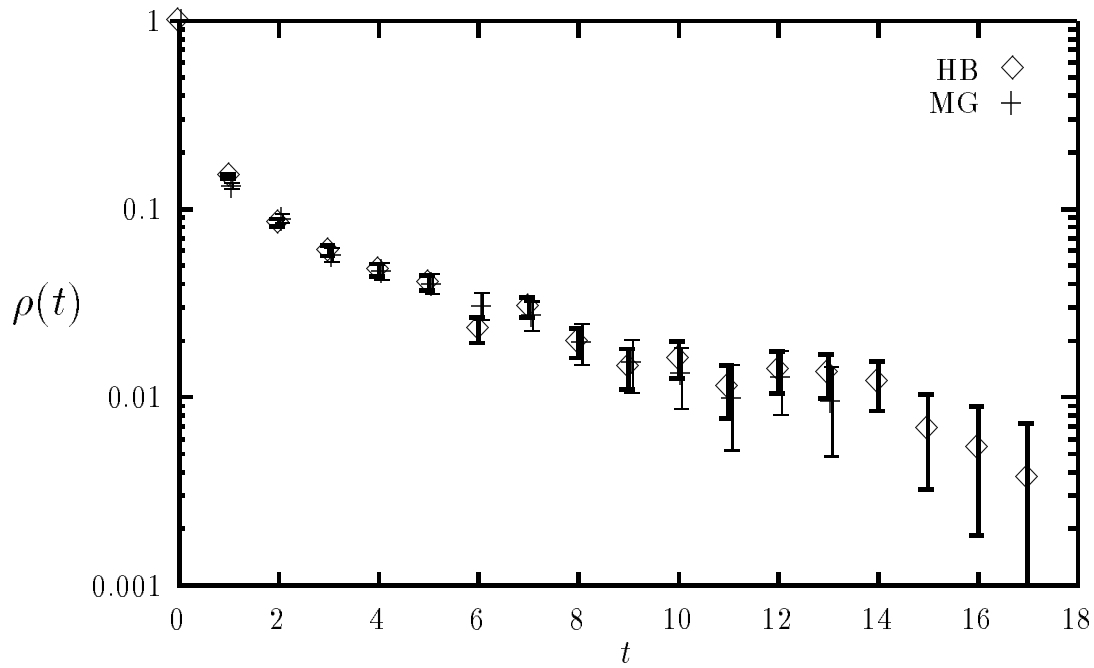
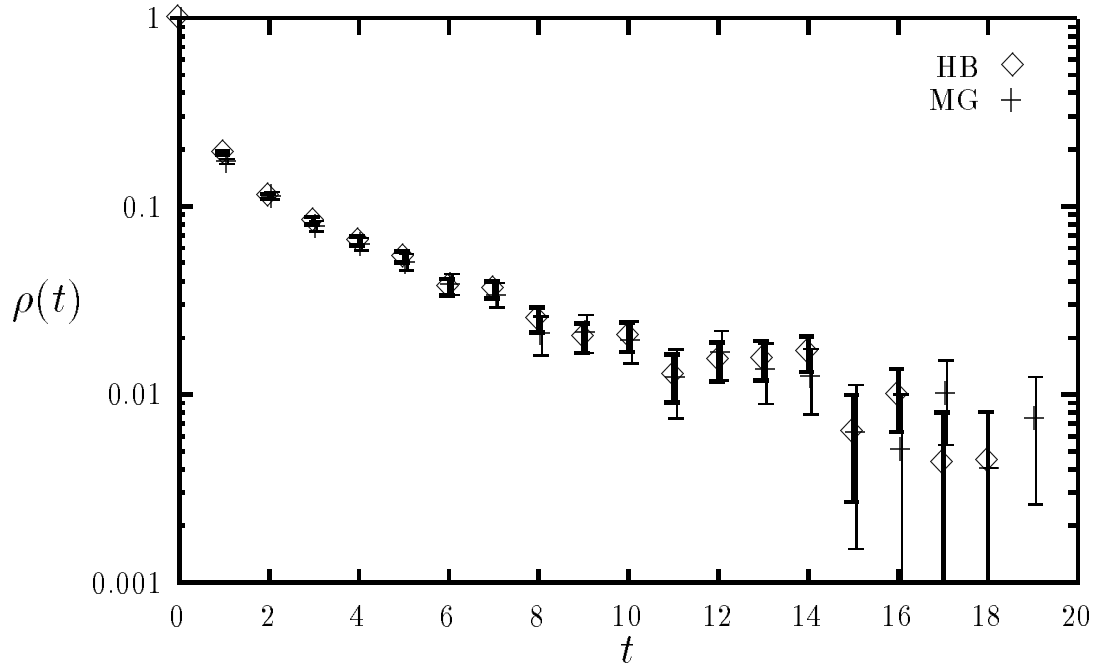


Figure 21: Comparison of the autocorrelation functions $\rho(t)$ for the heat bath (HB) and multigrid (MG) algorithm for $SU(2)$ on the 8^4 -lattice at $\beta = 2.2$. Top: Polyakov loop P , bottom: average sign of Polyakov loop $\text{sign}(\bar{P})$.

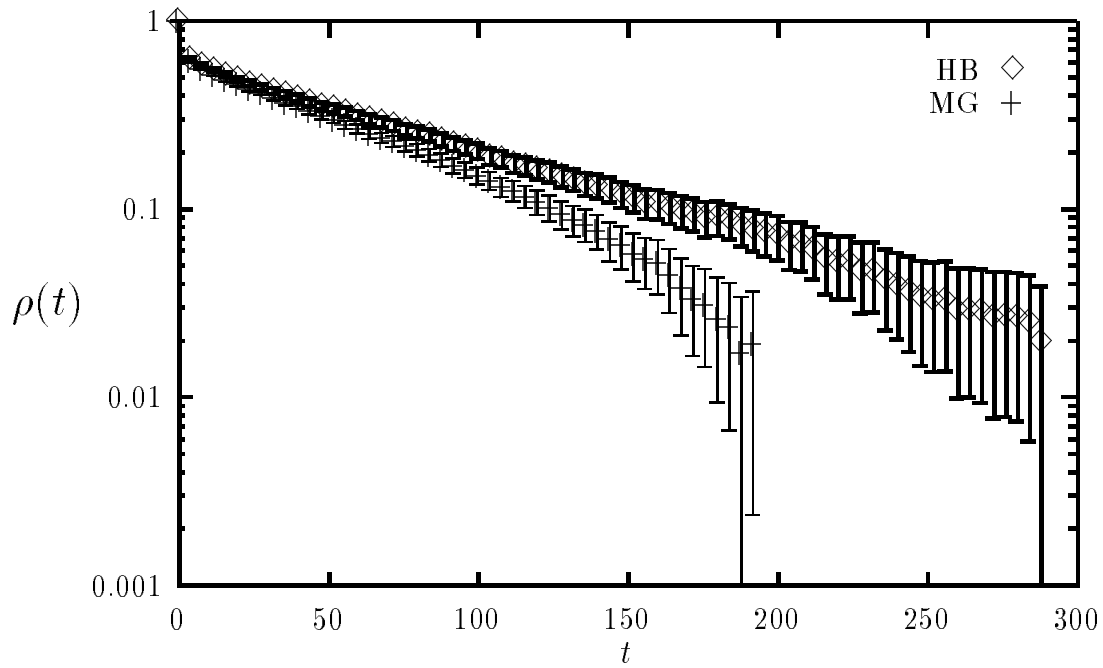
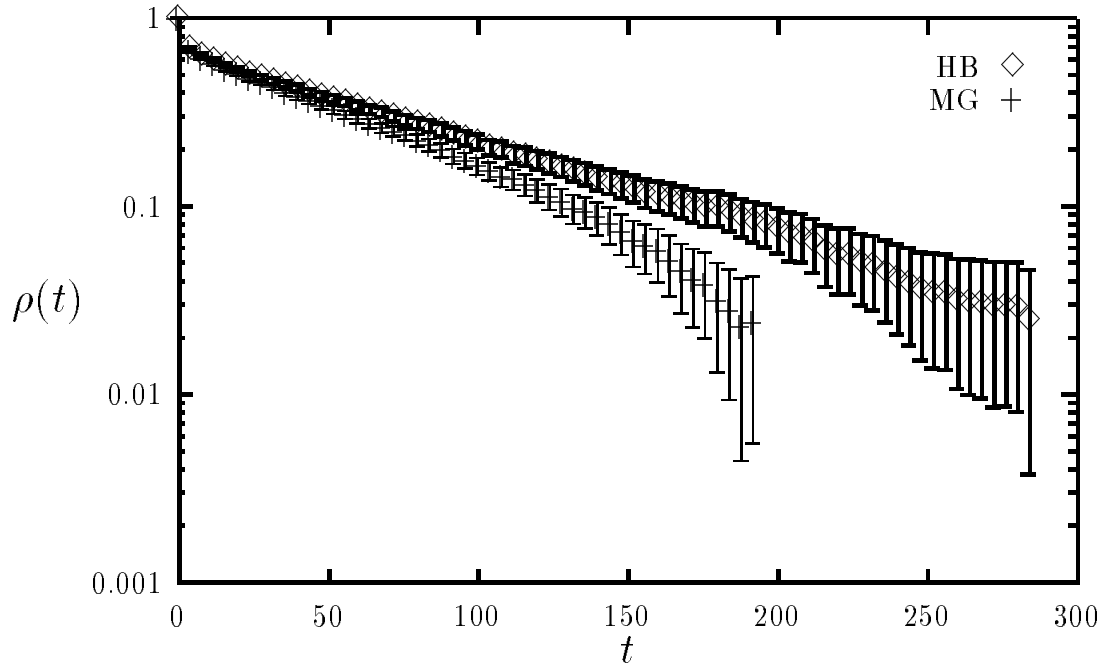


Figure 22: Comparison of the autocorrelation functions $\rho(t)$ for the heat bath (HB) and multigrid (MG) algorithm for $SU(2)$ on the 8^4 -lattice at $\beta = 2.4$. Top: Polyakov loop P , bottom: average sign of Polyakov loop $\text{sign}(\bar{P})$.

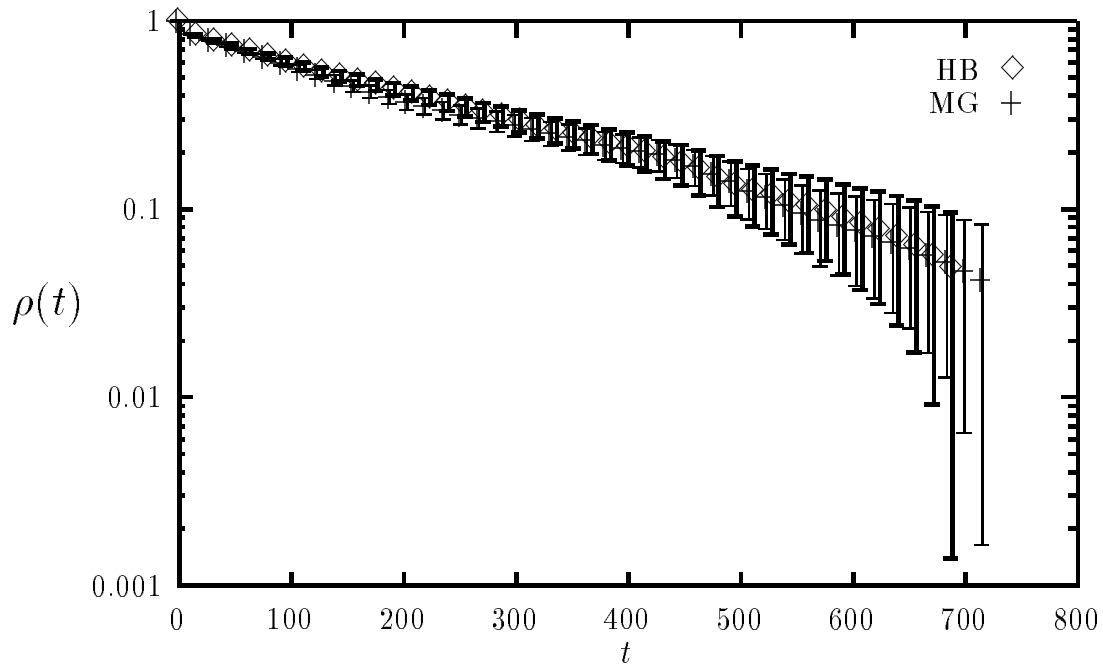
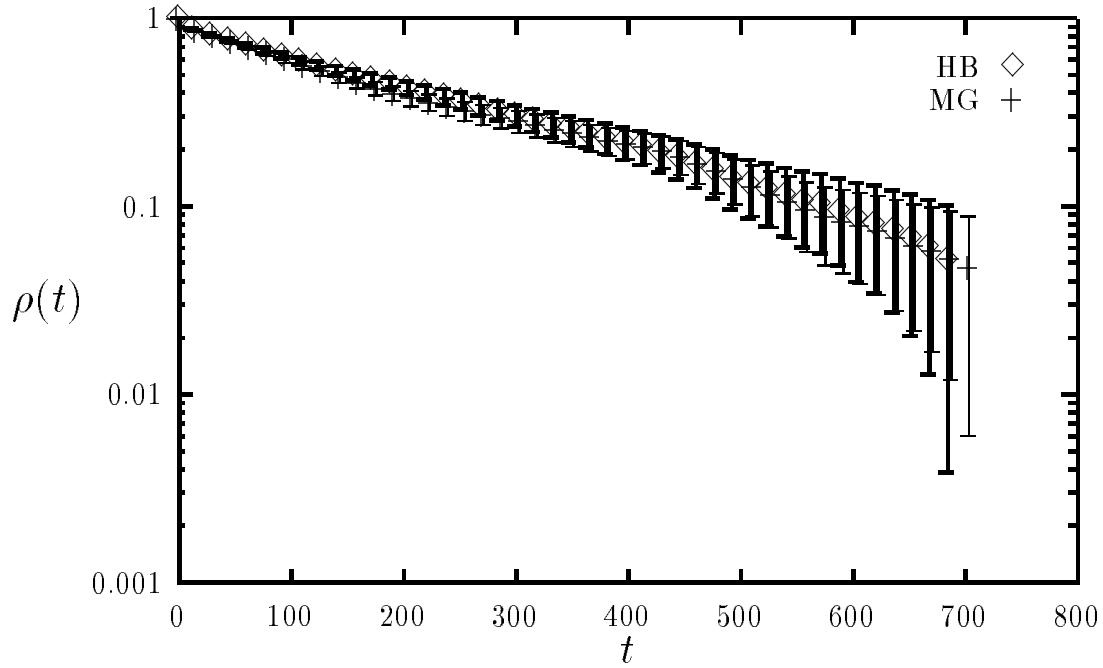


Figure 23: Comparison of the autocorrelation functions $\rho(t)$ for the heat bath (HB) and multigrid (MG) algorithm for $SU(2)$ on the 8^4 -lattice at $\beta = 2.6$. Top: Polyakov-loop P , bottom: average sign of Polyakov loop $\text{sign}(\bar{P})$.

12 Summary and Outlook

We presented a simple yet accurate formula that expresses acceptance rates for nonlocal update algorithms in terms of the average energy change $h_1 = \langle \Delta \mathcal{H} \rangle$ of the proposed move. The quantity h_1 depends only on one local observable (or two in four dimensional $SU(2)$ lattice gauge theory) that is simple to compute, e.g. by Monte Carlo simulations on a small lattice.

With the help of our formula we found that all investigated models fall into two kinematical classes: For Sine Gordon, ϕ^4 theory and $SU(2)$ lattice gauge theory in four dimensions, s had to be rescaled like $1/L_B$ for piecewise constant and for smooth kernels in order to maintain L_B -independent acceptance rates. For massless free field theory, the XY model, the $O(N)$ nonlinear σ -model, the CP^{N-1} model, $U(1)$ lattice gauge theory and $SU(2)$ lattice gauge theory in two dimensions one can achieve $s \sim \text{const}$ by choosing smooth kernels.

The kinematical behavior of multigrid algorithms in interacting models can be related to the dynamical critical behavior. By comparing the behavior of the acceptance rates in interacting models close to a critical point with free field theory, where CSD is known to be eliminated by a multigrid algorithm, we found the following rule: For an interacting model, sufficiently high acceptance rates for a complete elimination of CSD can only be expected if $h_1 = \langle \mathcal{H}(\phi + s\psi) - \mathcal{H}(\phi) \rangle$ contains no algorithmic mass term $\sim s^2 \sum_x \psi_x^2$. To our knowledge, all numerical experiments with multigrid Monte Carlo algorithms that have been performed so far are consistent with this rule. With the help of this criterion it is possible to decide whether a given statistical model is a natural candidate for multigrid Monte Carlo or not.

Heuristically, the meaning of the rule can be stated differently: A piecewise constant update of a nonlocal domain should only have energy costs proportional to the surface of the domain, not energy costs proportional to the volume of the domain.

To check the prediction that too small acceptance rates on large blocks cause CSD, we performed a multigrid Monte Carlo simulation of the Sine-Gordon model in two dimensions. We found $z = 1.9(1)$ with piecewise constant interpolation and a W-cycle. It was studied whether one can compensate for too small update steps on large blocks by accumulating many of these steps randomly. To check this possibility, we simulated the model with a higher cycle with $\gamma = 4$. We found $z = 1.9(1)$ also for this variant of the algorithm.

A multigrid algorithm for nonabelian gauge fields, the time slice blocking, was developed. It is based on the statistical decoupling of adjacent time slices as long as only link variables in the time direction are updated. The kinematical analysis predicted a strong reduction of CSD in a simulation of $SU(2)$ in two dimensions. Almost complete elimination of CSD was indeed observed in numerical experiments on lattice sizes up to 256^2 .

The multigrid Monte Carlo algorithm was generalized from two dimensions to four dimensions. In four dimensions, a nontrivial background field in the bottom of the blocks caused difficulties. We found that this background field generates an algorithmic mass term that suppresses the acceptance rates on large blocks.

We argued that the algorithm will only work well if the algorithmic disorder mass m_D scales like a physical mass, i.e. if m_D decreases exponentially fast with increasing β . However, there is numerical and theoretical evidence that $m_D \sim \text{const}$ for large β . Therefore the expectation is that the proposed algorithm will not have a chance to reduce CSD.

Whether the nonlocal algorithm is at least able to accelerate the local heat bath algorithm by a constant factor was investigated by simulations of $SU(2)$ lattice gauge theory on an 8^4 -lattice. Superficially, a modest acceleration for Polyakov loop observables was found at $\beta = 2.4$, however

when the additional computational work is taken into account, there is no net gain. From the theoretical analysis it can not be expected that on larger lattices the method will perform better. In summary, it is fair to say that for nonabelian pure gauge theory in four dimensions the local overrelaxation algorithm is superior to nonlocal updating schemes up to now.

The kinematical mechanism that leads to a failure of multigrid algorithms is well described by our analysis. As an example, the analysis of the time slice blocking algorithm for nonabelian gauge fields in four dimensions can help to understand the additional difficulties one has to face in four dimensions compared to two dimensions. We hope that a better understanding can lead to improved multigrid algorithms that can overcome kinematical obstructions stemming from an algorithmic mass term.

There are two possible strategies for improved algorithms:

First one could consider the stated rule as a (non rigorous) no-go theorem. Then one can try to avoid kinematical problems beforehand by developing algorithms that do not have energy costs proportional to the volume of a block. A natural way is to take a global symmetry of the model under consideration and to apply the corresponding symmetry transformation locally on blocks.

From this point of view it is clear that updates that are well adapted to the ϕ^4 model (with a discrete Z_2 symmetry of the Hamiltonian) are not continuous, but discrete. In fact, the very efficient cluster algorithm that has been developed for this model is based on the discrete Z_2 symmetry [61]. Another example where discrete updates appear to be more natural than continuous updates is the Sine Gordon model (with a discrete \mathbb{Z} symmetry of the Hamiltonian). Generalizations of the cluster algorithm for the discrete Gaussian model [62] (that has the same symmetry as the Sine Gordon model) seem to be efficient also in this case [63]. The four dimensional nonabelian $SU(N)$ lattice gauge theory has both a global discrete Z_N symmetry and a local $SU(N)$ gauge symmetry (which includes a global $SU(N)$ symmetry as a subgroup). Which symmetry could be used for a fast nonlocal updating algorithm (if there exists any) is an open question.

A second, more ambitious way to deal with kinematical obstructions is not to avoid them but to attempt to overcome them directly. Recently, very efficient methods for the acceleration of tunneling processes in systems close to a first order phase transition have been developed [64]. There, the computational effort could be reduced from an exponential to a polynomial growth with the volume.

Since the mass term problem in models with a discrete symmetry can also be interpreted as slow tunneling between different minima of a conditional coarse grid Hamiltonian, possible combinations of these new developments with multigrid methods might be promising also for reducing CSD. However, since CSD is “only” a polynomial problem, the requirement that the computational work should be proportional to the volume (and not to a power of the volume as in systems close to a first order phase transition) is quite restrictive.

Acknowledgements

First of all, I would like to thank Gerhard Mack for his guidance and his constant support. A better way of supervising a thesis is hard to imagine for me.

This work would have been impossible without Klaus Pinn. During my “sabbatical” in Münster, where we developed the main ideas of this work together, I learned a lot from him. Also during repeated visits from Hamburg, the “Münster-Hamburg-connection” was very motivating and fruitful for me.

Gernot Münster helped to arrange my stay in Münster and was always open for discussions.

I want to thank Bernhard Mikeska for the fruitful collaboration on the simulation of the Sine Gordon model.

During two visits at the Weizmann Institute I profited much from the stimulating atmosphere in the discussions with Achi Brandt.

I am also indebted to Sorin Solomon for his warm hospitality in Jerusalem.

I profited from repeated conversations with Martin Bäker, Hermann Dilger, Hans-Gerd Evertz, Fritz Gutbrod, Martin Hasenbusch, Arjan Hulsebos, Thomas Kalkreuter, Mihai Marcu, Steffen Meyer, Alan Sokal and Ulli Wolff.

Bernhard Mikeska and Klaus Pinn helped me a lot in the discussion and a careful reading of the manuscript.

Financial support by the Deutsche Forschungsgemeinschaft and the German Israeli Foundation is acknowledged.

The numerical computations were performed on the NEC SX-3 in Cologne, the Landesvektorrechner of the RWTH in Aachen, the CRAY Y-MP of the HLRZ in Jülich and on hp 9000/730 RISC workstations at DESY.

A Details of the acceptance analysis for gauge theories

In this appendix we discuss the details of the calculation of $h_1 = \langle \Delta \mathcal{H} \rangle$ for gauge theories.

A.1 Abelian gauge fields

The Wilson action for abelian gauge fields in d dimensions can be written in link angles $\theta_{x,\mu}$

$$\mathcal{H}(\theta) = \beta \sum_{x \in \Lambda_0} \sum_{\mu \neq \tau} [1 - \cos(\theta_{\mu\nu}(x))] \quad , \quad (\text{A.1})$$

with the plaquette angle

$$\theta_{\mu\nu}(x) = \theta_{x,\mu} + \theta_{x+\hat{\mu},\tau} - \theta_{x+\hat{\tau},\mu} - \theta_{x,\tau} \quad . \quad (\text{A.2})$$

All the link angles $\theta_{x,\tau}$ that point from sites x inside the hypercubic block x'_o in the time direction are proposed to be changed simultaneously:

$$\theta_{x,\tau} \rightarrow \theta_{x,\tau} + s\psi_x \quad . \quad (\text{A.3})$$

The associated change of the hamiltonian is

$$\begin{aligned} \Delta \mathcal{H} &= -\beta \sum_{x \in \Lambda_0} \sum_{\mu \neq \tau} \{ \cos(\theta_{\mu\nu}(x) + s(\psi_{x+\hat{\mu}} - \psi_x)) - \cos(\theta_{\mu\nu}(x)) \} \\ &= -\beta \sum_{x \in \Lambda_0} \sum_{\mu \neq \tau} \{ \cos(\theta_{\mu\nu}(x)) [\cos(s(\psi_{x+\hat{\mu}} - \psi_x)) - 1] - \sin(\theta_{\mu\nu}(x)) \sin(s(\psi_{x+\hat{\mu}} - \psi_x)) \} \quad . \quad (\text{A.4}) \end{aligned}$$

Since the transformation $\theta \rightarrow -\theta$ for all link angles is a symmetry of the Hamiltonian, whereas the term $\sin(\theta_{\mu\nu}(x))$ changes its sign under this transformation, the expectation value $\langle \sin(\theta_{\mu\nu}(x)) \rangle$ vanishes. Therefore the average energy change of the nonlocal update (A.3) is

$$h_1 = \beta P \sum_{x \in \Lambda_0} \sum_{\mu \neq \tau} [1 - \cos(s(\psi_{x+\hat{\mu}} - \psi_x))] \quad , \quad (\text{A.5})$$

with $P = \langle \cos(\theta_{\mu\nu}(x)) \rangle = \langle \text{Tr} U_{\mathcal{P}} \rangle$. All expressions for h_1 that are given in section 8 and in section 10 can be obtained from this result by specifying the number of dimensions d and the form of the interpolation kernel ψ .

As an example, let us derive eq. (8.8) for abelian gauge theory in two dimensions: For piecewise constant interpolation on a two dimensional block we have

$$\psi_x^{\text{const}} = \begin{cases} 1 & \text{for } x \in x'_o \\ 0 & \text{for } x \notin x'_o \end{cases} \quad .$$

From eq. (A.5) it is clear that only L_B links at the left boundary and L_B links at the right boundary of the block contribute to the average energy change h_1 . This leads to eq. (8.8):

$$h_1 = 2\beta P L_B [1 - \cos(s)] \quad .$$

A.2 Nonabelian gauge fields

The energy change of a time slice blocking update for $SU(2)$ in d dimensions is

$$\begin{aligned}\Delta\mathcal{H} &= -\frac{\beta}{2} \sum_{\mathcal{P}} \text{Tr}(U'_{\mathcal{P}} - U_{\mathcal{P}}) = -\frac{\beta}{2} \sum_{x \in \Lambda_i^{\tau}} \sum_{\mu \neq \tau} \text{Tr}\{(R_x(g)^* U_{x,\mu} R(g)_{x+\hat{\mu}} - U_{x,\mu}) H_{x,\mu}^*\} \\ &= -\frac{\beta}{2} \sum_{x \in \Lambda_i^{\tau}} \sum_{\mu \neq \tau} \text{Tr}\{(R_x^* U_{x,\mu}^g R_{x+\hat{\mu}} - U_{x,\mu}^g) H_{x,\mu}^{g*}\},\end{aligned}\quad (\text{A.6})$$

with $H_{x,\mu}^* = U_{x+\hat{\mu},\tau} U_{x+\hat{\tau},\mu}^* U_{x,\tau}^*$ and $U_{x,\mu}^g = g_x U_{x,\mu} g_{x+\hat{\mu}}^*$. H^g is defined analogously. ψ denotes a $d-1$ dimensional interpolation kernel, and the rotation matrices $R_x \in SU(2)$ are given by

$$R_x(\vec{n}, s) = \cos(s\psi_x/2) + i \sin(s\psi_x/2) \vec{n} \cdot \vec{\sigma}. \quad (\text{A.7})$$

Therefore we obtain

$$\begin{aligned}\Delta\mathcal{H} &= -\frac{\beta}{2} \sum_{x \in \Lambda_i^{\tau}} \sum_{\mu \neq \tau} \left\{ \text{Tr}(U_{x,\mu}^g H_{x,\mu}^{g*}) [\cos(s\psi_x/2) \cos(s\psi_{x+\hat{\mu}}/2) - 1] \right. \\ &\quad - \text{Tr}(i\vec{n} \cdot \vec{\sigma} U_{x,\mu}^g H_{x,\mu}^{g*}) \sin(s\psi_x/2) \cos(s\psi_{x+\hat{\mu}}/2) \\ &\quad + \text{Tr}(U_{x,\mu}^g i\vec{n} \cdot \vec{\sigma} H_{x,\mu}^{g*}) \cos(s\psi_x/2) \sin(s\psi_{x+\hat{\mu}}/2) \\ &\quad \left. - \text{Tr}(i\vec{n} \cdot \vec{\sigma} U_{x,\mu}^g i\vec{n} \cdot \vec{\sigma} H_{x,\mu}^{g*}) \sin(s\psi_x/2) \sin(s\psi_{x+\hat{\mu}}/2) \right\}. \quad (\text{A.8})\end{aligned}$$

Now we will show that to $h_1 = \langle \Delta\mathcal{H} \rangle$ only terms contribute that are even in s . The point is that all gauge conditions that are used to define the g -matrices specify g only up to a global gauge transformation:

$$g_x \rightarrow h g_x \quad \text{for all } x \in \Lambda_0. \quad (\text{A.9})$$

If we average the expectation value

$$B = \langle \text{Tr}(i\vec{n} \cdot \vec{\sigma} U_{x,\mu}^g H_{x,\mu}^{g*}) \rangle = \langle \text{Tr}(i\vec{n} \cdot \vec{\sigma} g_x U_{x,\mu} H_{x,\mu} g_x^*) \rangle \quad (\text{A.10})$$

over this global symmetry of the Hamiltonian, we get

$$B = \int dh \langle \text{Tr}(i\vec{n} \cdot \vec{\sigma} h g_x U_{x,\mu} H_{x,\mu} g_x^* h^*) \rangle = 0. \quad (\text{A.11})$$

Here we used an identity for $SU(2)$ matrices:

$$\int dh \text{Tr}(A h B h^*) = \frac{1}{2} \text{Tr}(A) \text{Tr}(B), \quad (\text{A.12})$$

and that the Pauli matrices are traceless.

Therefore the studied updating proposal leads to an average energy change

$$\begin{aligned}h_1 &= \beta \sum_{x \in \Lambda_i^{\tau}} \sum_{\mu \neq \tau} \left\{ \left\langle \frac{1}{2} \text{Tr}(U_{x,\mu} H_{x,\mu}^*) \right\rangle [1 - \cos(s\psi_x/2) \cos(s\psi_{x+\hat{\mu}}/2)] \right. \\ &\quad \left. + \left\langle \frac{1}{2} \text{Tr}(i\vec{n} \cdot \vec{\sigma} U_{x,\mu}^g i\vec{n} \cdot \vec{\sigma} H_{x,\mu}^{g*}) \right\rangle \sin(s\psi_x/2) \sin(s\psi_{x+\hat{\mu}}/2) \right\}. \quad (\text{A.13})\end{aligned}$$

All expressions for h_1 that are derived for $SU(2)$ gauge fields in section 8 and section 10 can be obtained from this formula by specifying the number of dimensions d , the choice of the gauge condition that determines the g -matrices, and the form of the interpolation kernel ψ .

As an example, we derive the expression (8.27) for time slice blocking in two dimensions: We assume that the g -matrices are chosen according to the block axial gauge (8.18) and that ψ vanishes outside the block x'_o . Then

$$\frac{1}{2}\text{Tr} \left(i\vec{n} \cdot \vec{\sigma} U_{x,\mu}^g i\vec{n} \cdot \vec{\sigma} H_{x,\mu}^{g*} \right) = -\frac{1}{2}\text{Tr} \left(U_{x,\mu}^g H_{x,\mu}^{g*} \right) , \quad (\text{A.14})$$

since $U_{x,\mu}^g = 1$ within the bottom of the block, and we obtain eq. (8.27):

$$h_1 = \beta P \sum_{x \in \Lambda_t^\tau} \sum_{\mu \neq \tau} [1 - \cos(s(\psi_x - \psi_{x+\hat{\mu}})/2)] .$$

Here $P = \langle \frac{1}{2}\text{Tr}(U_{x,\mu} H_{x,\mu}) \rangle = \langle \frac{1}{2}\text{Tr}(U_{\mathcal{P}}) \rangle$ denotes the plaquette expectation value.

B Exact results for $SU(2)$ lattice gauge theory in two dimensions

Two dimensional $SU(2)$ lattice gauge theory is defined by the partition function

$$Z = \int \prod_{x,\mu} dU_{x,\mu} \exp(-\mathcal{H}(U)). \quad (\text{B.1})$$

The link variables $U_{x,\mu}$ take values in the gauge group $SU(2)$, and dU denotes the corresponding invariant Haar measure. The standard Wilson action $\mathcal{H}(U)$ is given by

$$\mathcal{H}(U) = \beta \sum_{\mathcal{P}} [1 - \frac{1}{2} \text{Tr} U_{\mathcal{P}}] . \quad (\text{B.2})$$

The sum is over all plaquettes in the lattice. Wilson loops are defined by

$$W(C) = \langle \frac{1}{2} \text{Tr}(U(C)) \rangle , \quad (\text{B.3})$$

where $U(C)$ is the parallel transporter around a Wilson loop C of area A . The exact result for $W(C)$ on the infinite lattice is [52]

$$W(C) = \left(\frac{I_2(\beta)}{I_1(\beta)} \right)^A = 1 - \frac{3A}{2\beta} + O\left(\frac{1}{\beta^2}\right) . \quad (\text{B.4})$$

Here, $I_\nu(\beta)$ are the modified Bessel functions. The string tension κ is defined by the asymptotic behavior of the Wilson loop for large A

$$W(C) \underset{A \rightarrow \infty}{\sim} e^{-\kappa A} , \quad (\text{B.5})$$

and has the dimension of a mass squared. Therefore

$$\kappa = -\log \left(\frac{I_2(\beta)}{I_1(\beta)} \right) = \frac{3}{2\beta} + O\left(\frac{1}{\beta^2}\right) . \quad (\text{B.6})$$

The string tension correlation length ξ is given by

$$\xi = \frac{1}{\sqrt{\kappa}} = \left[-\log \left(\frac{I_2(\beta)}{I_1(\beta)} \right) \right]^{-1/2} = \sqrt{\frac{2\beta}{3}} \left[1 + O\left(\frac{1}{\beta}\right) \right] . \quad (\text{B.7})$$

C Gauge conditions on the lattice

In this appendix we discuss the relation of gauge conditions on the lattice that are formulated in terms of parallel transporters $U_{x,\mu}$ with the corresponding gauge conditions given in terms of a gauge potential $A_{x,\mu}$. We follow the presentation of ref. [65].

Our conventions are as follows: A basis of the $SU(N)$ Lie-algebra is given by traceless, anti-hermitean $N \times N$ matrices t^a , normalized to $\text{Tr}(t^a t^b) = -\delta^{ab}/2$, which satisfy $[t^a, t^b] = f^{abc} t^c$, where f^{abc} are the structure constants of the group. In particular for $SU(2)$ we have $t^a = i/2\sigma_a$, where σ_a are the Pauli matrices, and $f^{abc} = \varepsilon^{abc}$.

A gauge potential $A_{x,\mu}$ on the lattice can be defined by

$$A_{x,\mu} = A_{x,\mu}^a t^a = \frac{1}{2}[U_{x,\mu} - U_{x,\mu}^*] - \frac{1}{2N}\text{Tr}[U_{x,\mu} - U_{x,\mu}^*]. \quad (\text{C.1})$$

This definition is motivated by the fact that $U_{x,\mu} = \exp(A_{x,\mu})$ for infinitesimal $A_{x,\mu}$.

C.1 The Landau gauge

The Landau gauge on the lattice is defined by [66]

$$G_L(U, g) = \sum_{x \in \Lambda_0} \sum_{\mu=1}^d \text{Re Tr} \left(g_x U_{x,\mu} g_{x+\mu}^* \right) \stackrel{!}{=} \text{maximal}. \quad (\text{C.2})$$

By performing the gauge transformation $U_{x,\mu} \rightarrow U_{x,\mu}^g = g_x U_{x,\mu} g_{x+\mu}^*$, where g_x is obtained by the absolute maximum of $G_L(U, g)$, the absolute maximum is shifted to $g_x = 1$. The gauge configuration U such that $G_L(U, g)$ for $g = 1$ is in an absolute maximum has the property that the corresponding gauge potential is transverse:

$$\nabla_\mu A_{x,\mu}^a = \sum_{\mu=1}^d \left[A_{x+\mu,\mu}^a - A_{x,\mu}^a \right] = 0. \quad (\text{C.3})$$

$\nabla_\mu A_{x,\mu}^a$ denotes the lattice divergence of $A_{x,\mu}^a$. This can be shown as follows: Consider the one parameter subgroup $g(\tau)$ of the local gauge group defined by

$$g(\tau) = \{g_x(\tau)\} = \{\exp(\tau\omega_x)\}, \quad \omega_x^* = -\omega_x. \quad (\text{C.4})$$

Here, ω_x is an arbitrary element of the local Lie algebra of the form $\omega_x = t^a \omega_x^a$. For fixed ω and U , let $U(\tau)$ be the one parameter curve on the gauge orbit through U defined by

$$U_{x,\mu}(\tau) = g_x(\tau) U_{x,\mu} g_{x+\mu}^*(\tau). \quad (\text{C.5})$$

Let $G(\tau)$ be defined by

$$G(\tau) = G_L(U, g(\tau)) = \sum_{x \in \Lambda_0} \sum_{\mu=1}^d \text{Re Tr} \left(\exp(\tau\omega_x) U_{x,\mu} \exp(-\tau\omega_{x+\mu}) \right). \quad (\text{C.6})$$

We have

$$\frac{dG(\tau)}{d\tau} = G'(\tau) = \sum_{x \in \Lambda_0} \sum_{\mu=1}^d \text{Re Tr} \left[(\omega_x - \omega_{x+\mu}) U_{x,\mu}(\tau) \right]$$

$$= \sum_{x \in \Lambda_0} \sum_{\mu=1}^d \text{Re Tr} [\omega_x (U_{x,\mu}(\tau) - U_{x-\mu,\mu}(\tau))] .$$

Now we use the fact that $\text{Re Tr}(\omega_x U_{x,\mu}(\tau)) = -\text{Re Tr}(\omega_x U_{x,\mu}^*(\tau))$ and get

$$G'(\tau) = \frac{1}{2} \sum_{x \in \Lambda_0} \sum_{\mu=1}^d \text{Re Tr} [\omega_x (U_{x,\mu}(\tau) - U_{x,\mu}^*(\tau) - U_{x-\mu,\mu}(\tau) + U_{x-\mu,\mu}^*(\tau))] .$$

With the definition (C.1) of the gauge potential and taking into account that ω_x is traceless, we obtain

$$G'(\tau) = \sum_{x \in \Lambda_0} \sum_{\mu=1}^d \text{Re Tr} [\omega_x (A_{x,\mu}(\tau) - A_{x-\mu,\mu}(\tau))] = -\frac{1}{2} \sum_{x \in \Lambda_0} \omega_{x-\mu}^a \sum_{\mu=1}^d (A_{x+\mu,\mu}^a(\tau) - A_{x,\mu}^a(\tau)) .$$

The τ -dependence of A is induced by the τ -dependence of U . Finally, $G'(\tau)$ can be expressed by the lattice divergence (C.3) of the gauge potential:

$$G'(\tau) = -\frac{1}{2} \sum_{x \in \Lambda_0} \omega_{x-\mu}^a \nabla_\mu A_{x,\mu}^a(\tau) . \quad (\text{C.7})$$

If U is a stationary point of the gauge functional $G_L(U, g)$ at $g = 1$, we have $G'(0) = 0$ for all ω_x^a , which implies

$$\nabla_\mu A_{x,\mu}^a = 0 . \quad (\text{C.8})$$

Therefore, the transversality of the gauge potential A is the condition for the functional $G_L(U, g)$ to be stationary at $g = 1$.

C.2 The Coulomb gauge

The Coulomb gauge condition is

$$G_C(U, g) = \sum_{x \in \Lambda_0} \sum_{\mu=1}^{d-1} \text{Re Tr} (g_x U_{x,\mu} g_{x+\mu}^*) \stackrel{!}{=} \text{maximal} . \quad (\text{C.9})$$

Note that now only spatial link variables enter in the gauge functional. A similar argumentation as above shows that this gauge condition leads to a transversality condition for the spatial components of the gauge potential

$$\vec{\nabla}_\mu \vec{A}_x^a = \sum_{\mu=1}^{d-1} [A_{x+\mu,\mu}^a - A_{x,\mu}^a] = 0 . \quad (\text{C.10})$$

Here, $\vec{\nabla}_\mu \vec{A}_x^a$ denotes the $d - 1$ dimensional lattice divergence of the spatial components $\vec{A}_x^a = (A_{x,1}^a, \dots, A_{x,d-1}^a)^T$ of the gauge potential.

C.3 An alternative formulation of the Landau gauge condition

The Landau gauge condition can also be formulated as a minimization of a quadratic form

$$Q(U, g) = (g^*, -\Delta g^*) \stackrel{!}{=} \text{minimal} , \quad (\text{C.11})$$

under the constraint that the g_x are elements of the gauge group. Here Δ denotes the gauge covariant Laplacian

$$(\Delta\phi)_x = \sum_{\mu=1}^d [U_{x,\mu}\phi_{x+\mu} + U_{x-\mu,\mu}^*\phi_{x-\mu} - 2\phi_x] , \quad (\text{C.12})$$

and the scalar product is defined by

$$(\phi, \psi) = \sum_{x \in \Lambda_0} \frac{1}{N} \text{Re Tr}(\phi_x^* \psi_x) . \quad (\text{C.13})$$

The subtraction of a constant of the form

$$const = 2 \sum_{x \in \Lambda_0} \frac{1}{N} \text{Re Tr}(g_x g_x^*) \quad (\text{C.14})$$

from $Q(U, g)$ will not alter the solution of the minimization problem. Using this, it is simple to check that the gauge conditions (C.2) and (C.11) are equivalent.

References

- [1] K. Binder, ed., *Monte Carlo Methods in Statistical Physics* (Springer, Berlin, 1986).
- [2] C. Rebbi, ed., *Lattice Gauge Theory and Monte Carlo Simulations* (World Scientific, Singapore, 1983).
- [3] S.L. Adler, Phys. Rev. D 23 (1988) 458;
H. Neuberger, Phys. Rev. Lett. 59 (1987) 1877;
for a recent review see
U. Wolff, in: *Proceedings of the 31. IUKT, Schladming, Austria, February 1992*, H. Gaus-
terer, C.B. Lang, eds., (Springer, Berlin, 1992).
- [4] A.D. Kennedy, B. Pendleton, in: *Lattice '90*, Proceedings of the International Symposium,
Tallahassee, USA, 1990, U.M. Heller, A.D. Kennedy, S. Sanielevici, eds., [Nucl. Phys. B
(Proc. Suppl.) 20 (1991) 118];
S. Gupta, in: *Lattice '90*, Proceedings of the International Symposium, Tsukuba, Japan,
M. Fukugita *et al.*, eds., [Nucl. Phys. B (Proc. Suppl.) 26 (1992) 617].
- [5] R.H. Swendsen, J.S. Wang, Phys. Rev. Lett. 58 (1987) 86.
- [6] U. Wolff, Phys. Rev. Lett. 62 (1989) 361.
- [7] M. Hasenbusch, Nucl. Phys. B 333 (1990) 581.
- [8] U. Wolff, in: *Workshop on Fermion Algorithms*, HLRZ, KFA Jülich, April 1992, H.J. Herr-
mann, F. Karsch, eds., (World Scientific, Singapore, 1991).
- [9] S. Caracciolo, R.G. Edwards, A. Pelissetto, A.D. Sokal, Nucl. Phys. B 403 (1993) 475. For
a discussion of common features of multigrid and cluster algorithms see section 5.
- [10] Pioneering papers are
A. Brandt, in: *Lecture Notes in Physics 18*, (Springer, Berlin, 1973);
A. Brandt, Math. Comp. 31 (1977) 333.
- [11] For a review see
K. Stüben, U. Trottenberg, in: *Multigrid Methods*, Proceedings, Köln-Porz, 1981, W. Hack-
busch *et al.*, eds., (Springer, Berlin, 1982).
- [12] G. Parisi, in: *Progress in Gauge Field Theory*, Proceedings of the Cargèse Summer Insti-
tute, Cargèse, France, 1983, G. 't Hooft *et al.*, eds., (Plenum, New York, 1984).
- [13] H. Meyer-Ortmanns, Z. Phys. C 27 (1985) 553.
- [14] J. Goodman, A.D. Sokal, Phys. Rev. Lett. 56 (1986) 1015.
- [15] G. Mack, in: *Nonperturbative Quantum Field Theory*, Proceedings, Cargèse, France, 1987,
G. 't Hooft *et al.*, eds., (Plenum, New York, 1988).
- [16] M. Hasenbusch, S. Meyer, Phys. Rev. Lett. 68 (1992) 435.

- [17] M. Hasenbusch, G. Mack, S. Meyer, in: *Lattice '90*, Proceedings of the International Symposium, Tallahassee, USA, 1990, U.M. Heller, A.D. Kennedy, S. Sanielevici, eds., [Nucl. Phys. B (Proc. Suppl.) 20 (1991) 110].
- [18] M.L. Laursen, J. Smit, J.C. Vink, Phys. Lett. B 262 (1991) 467.
- [19] R.G. Edwards, S.J. Ferreira, J. Goodman, A.D. Sokal, Nucl. Phys. B 380 (1992) 621.
- [20] J. Linn, diploma thesis, Kaiserslautern 1991.
- [21] QCD-TARO collaboration, K. Akemi *et al.*, preprint FUP-93-02, December 1993, to appear in: *Lattice '93*, Proceedings of the International Symposium for Lattice Field Theory, Dallas, USA, October 1993.
- [22] M. Creutz, Phys. Rev. D 36 (1987) 515;
F.R. Brown, T.J. Woch, Phys. Rev. Lett. 58 (1987) 2394;
for a review, see, e.g.
S.L. Adler, in: *Lattice '88*, Proceedings of the International Symposium, Batavia, USA, 1988, A.S. Kronfeld, P.B. Mackenzie, eds., [Nucl. Phys. B (Proc. Suppl.) 9 (1989) 437].
- [23] M. Lüscher, R. Sommer, U. Wolff, P. Weisz, Nucl. Phys. B 380 (1992) 621.
- [24] R. Ben-Av, H.G. Evertz, M. Marcu, S. Solomon, Phys. Rev. D 44 (1991) 2953.
- [25] R. Sinclair, Phys. Rev. D 45 (1992) 2098.
- [26] M.L. Laursen, J.C. Vink, Nucl. Phys. B 401 (1993) 745.
- [27] G. Bhanot, S.L. Adler, Phys. Rev. Lett. 66 (1991) 1806;
G. Bhanot, S.L. Adler, T. Lippert, K. Schilling, P. Ueberholz, Nucl. Phys. B 368 (1992) 745.
- [28] M. Grabenstein, K. Pinn, Phys. Rev. D 45 (1992) 4372.
- [29] M. Grabenstein, K. Pinn, J. Stat. Phys. 71 (1993) 607.
- [30] M. Grabenstein, K. Pinn, in: *Lattice '92*, Proceedings of the International Symposium, Amsterdam, Netherlands, 1992, J. Smit, P. van Baal, eds., [Nucl. Phys. B (Proc. Suppl.) 30 (1993) 265].
- [31] M. Grabenstein, B. Mikeska, Phys. Rev. D 47 (1993) 3101.
- [32] M. Grabenstein, B. Mikeska, preprint hep-lat 9311021, to appear in: *Lattice '93*, Proceedings of the International Symposium for Lattice Field Theory, Dallas, USA, October 1993.
- [33] A. Brandt, in: *Lattice '91*, Proceedings of the International Symposium, Tsukuba, Japan, M. Fukugita *et al.*, eds., [Nucl. Phys. B (Proc. Suppl.) 26 (1992) 137].
- [34] J. Goodman, A.D. Sokal, Phys. Rev. D 40 (1989) 2035.
- [35] S. Gupta, A. Irbäck, F. Karsch, B. Petersson, Phys. Lett. B 242 (1990) 437.

- [36] K. Gawędzki, A. Kupiainen, *Comm. Math. Phys.* 77 (1980) 31;
K. Gawędzki, A. Kupiainen, *Comm. Math. Phys.* 99 (1985) 197 and references cited therein.
- [37] G. Mack, S. Meyer, in: *Lattice '89*, Proceedings of the International Symposium, Capri, Italy, 1989, R. Petronzio *et al.*, eds., [*Nucl. Phys. B (Proc. Suppl.)* 17 (1990) 293].
- [38] T. Kalkreuter, *Nucl. Phys. B* 376 (1992) 637.
- [39] See section 8 of [34] in combination with the results of
W. Hackbusch, *Multi-Grid Methods and Applications*, (Springer, Berlin, 1985);
J. Mandel, S.F. McCormick, R. Bank, in: *Multigrid Methods*, S.F. McCormick, ed., (SIAM, Philadelphia, 1987).
- [40] J. Goodman, A.D. Sokal, unpublished.
- [41] B. Mikeska, diploma thesis, Heidelberg 1992.
- [42] B. Mikeska, private communication.
- [43] G. Mack, T. Kalkreuter, G. Palma, M. Speh, in: *Proceedings of the 31. IUKT, Schladming, Austria, February 1992*, H. Gausterer, C.B. Lang, eds., (Springer, Berlin, 1992).
- [44] See, for example, section 3.3 of G. Forgacs, R. Lipowsky, Th. M. Nieuwenhuizen, in: *Phase Transitions and Critical Phenomena*, Vol. 14, C. Domb, J. L. Lebowitz, eds., (Academic Press, London, 1991).
- [45] M. Hasenbusch, M. Marcu, K. Pinn, in: *Lattice '91*, Proceedings of the International Symposium, Tsukuba, Japan, M. Fukugita *et al.*, eds., [*Nucl. Phys. B (Proc. Suppl.)* 26 (1992) 598] and in preparation.
- [46] R.G. Edwards, J. Goodman, A.D. Sokal, *Nucl. Phys. B* 354 (1991) 289;
A. Hulsebos, J. Smit, J.C. Vink, *Nucl. Phys. B* 356 (1991) 775.
- [47] The cluster algorithm for the Sine Gordon model was developed by M. Hasenbusch and K. Pinn. Their program was used for comparison.
- [48] N. Madras, A. D. Sokal, *J. Stat. Phys.* 50, (1988) 109, Appendix C.
- [49] T. Hattori, H. Nakajima, preprint UTUP-95, hep-lat 9210016, October 1992.
- [50] A. Kennedy, B. Pendleton, *Phys. Lett. B* 156 (1985) 393.
- [51] K. Fredenhagen, M. Marcu, *Phys. Lett. B* 193 (1987) 486.
- [52] R. Balian, J.M. Drouffe, C. Itzykson, *Phys. Rev. D* 10 (1974) 3376;
D.J. Gross, E. Witten, *Phys. Rev. D* 21 (1980) 446.
- [53] J. Jersak, T. Neuhaus, P.M. Zerwas, *Phys. Lett. B* 133 (1983) 103;
V. Azcoiti, G. di Carlo, A.F. Grillo, *Phys. Lett. B* 268 (1991) 101.
- [54] J.E. Mandula, M. Ogilvie, *Phys. Lett. B* 248 (1990) 156.

- [55] A. Hulsebos, M.L. Laursen, J. Smit, A.J. van der Sijs, in: *Lattice '90*, Proceedings of the International Symposium, Tallahassee, USA, 1990, U.M. Heller, A.D. Kennedy, S. Sanielevici, eds., [Nucl. Phys. B (Proc. Suppl.) 20 (1991) 110];
A. Hulsebos, J. Smit, J.C. Vink, Phys. Lett. B 291 (1992) 431.
- [56] C. Michael, M. Teper, Phys. Lett. B 199 (1987) 95.
- [57] M. Creutz, *Quarks, Gluons and Lattices*, (Cambridge University Press, Cambridge, 1983).
- [58] A.S. Kronfeld, M.L. Laursen, G. Schierholz, U.-J. Wiese, Phys. Lett. B 198 (1987) 516.
- [59] B. Berg, J. Stehr, Z. Phys. C 9 (1981) 333.
- [60] F. Gutbrod, preprint DESY 92-185, December 1992.
- [61] R.C. Brower P. Tamayo, Phys. Rev. Lett. 62 (1989) 1087.
- [62] H. G. Evertz, M. Hasenbusch, M. Marcu, K. Pinn, S. Solomon, Phys. Lett. B 254, (1991) 185.
- [63] A simple generalization of the cluster algorithm for the discrete Gaussian model [62] seems to eliminate CSD in the simulation of the Sine Gordon model, M. Hasenbusch, K. Pinn, private communication.
- [64] B. Berg, T. Neuhaus, Phys. Lett. B 267 (1991) 249; Phys. Rev. Lett. 68 (1992) 9;
E. Marinari, G. Parisi, Europhys. Lett. 19 (1992) 451.
- [65] D. Zwanziger, Nucl. Phys. B 378 (1992) 525.
- [66] K.G. Wilson, in: *Recent Developments in Gauge Theories*, Proceedings of the Cargèse Summer Institute, Cargèse, France, 1980, G. 't Hooft *et al.*, eds., (Plenum, New York, 1980).